In presenting the dissertation as a partial fulfillment of the requirements for an advanced degree from the Georgia Institute of Technology, I agree that the Library of the Institute shall make it available for inspection and circulation in accordance with its regulations governing materials of this type. I agree that permission to copy from, or to publish from, this dissertation may be granted by the professor under whose direction it was written, or, in his absence, by the Dean of the Graduate Division when such copying or publication is solely for scholarly purposes and does not involve potential financial gain. It is understood that any copying from, or publication of, this dissertation which involves potential financial gain will not be allowed without written permission.

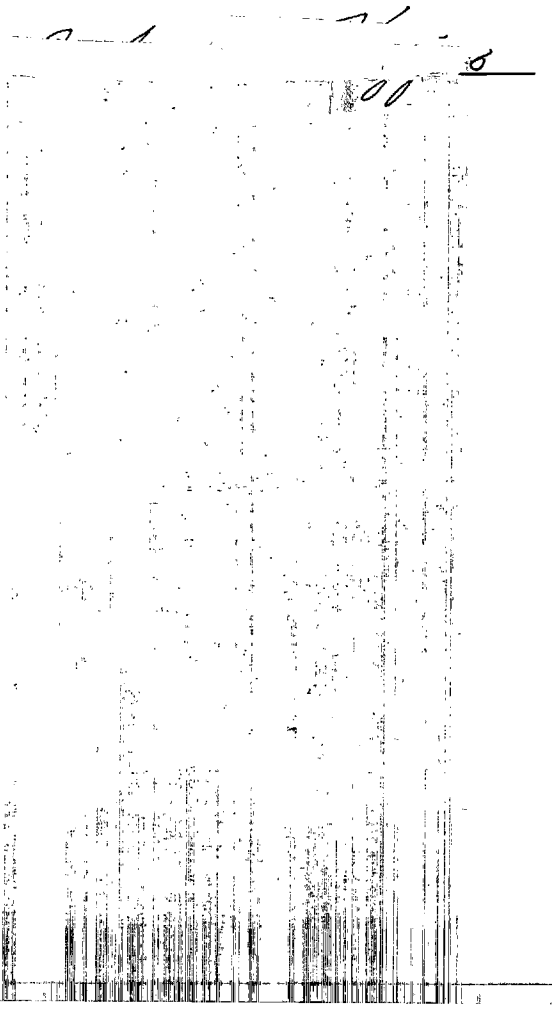

3/17/65
b

CAUSES OF THE POLAROGRAPHIC IRREVERSIBILITY IN THE COPPER(II)-PYROPHOSPHATE SYSTEM

A THESIS

Presented to

The Faculty of the Graduate Division

by

Gibson Watley Higgins

In Partial Fulfillment

of the Requirements for the Degree

Doctor of Philosophy

in the School of Chemistry

Georgia Institute of Technology

November, 1966

CAUSES OF THE POLAROGRAPHIC IRREVERSIBILITY IN THE COPPER(II)-PYROPHOSPHATE SYSTEM

Approved:

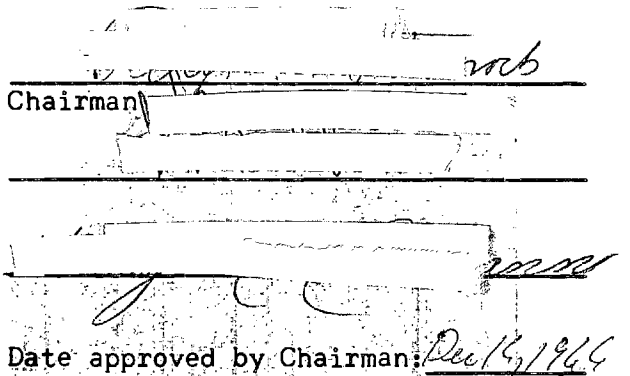

Chairman

Date approved by Chairman: Dec 14, 1964

ACKNOWLEDGMENTS

I wish to thank my preceptor, Dr. P. E. Sturrock, for the sincere friendship, encouragement, guidance, and tolerance, without which this project would never have reached its conclusion. Dr. H. A. Flaschka and Dr. H. M. Neumann were quite generous of their time during the preparation of the manuscript. Dr. W. M. Spicer, Chairman, School of Chemistry, was often most helpful during my residence.

The work was performed under a grant from the Petroleum Research Fund. This support is gratefully acknowledged.

I wish also to express gratitude to the many friends here who made my four years in Atlanta a most enjoyable and profitable personal experience.

TABLE OF CONTENTS

LIST OF TABLES

LIST OF FIGURES

Figure Page

Figure | Page

SUMMARY

The polarographic waves of a number of complex ion systems are known to be irreversible in alkaline solution. One such system is the copper(II) pyrophosphate system. Below pH 6 a reversible polarographic wave is obtained as the pH approaches 9, the wave becomes split into two parts, and the normal diffusion current is not attained until the electrode potential is at least -1.3 volts versus S.C.E. In addition to the varying behavior of the reduction wave, its appearance is influenced by the concentration of the supporting electrolyte, through the influence of the latter upon the electrical double layer.

Both relaxation and steady -state techniques were used to study the combined effects of pH and supporting electrolyte (potassium nitrate) concentration. Techniques employed include the potential step method, chronocoulometry, triangular sweep voltammetry, electrocapillary measurements, and conventional and A.C. polarography. Hanging drop and dropping mercury and dropping amalgam electrodes were used exclusively. Self-constructed apparatus included an electronic potentiostat and a time synchronizing controller.

Since it was initially hypothesized that perhaps adsorption was the cause of the irreversibility, double layer capacity measurements were obtained from triangular sweep voltammetry of the sodium nitrate-sodium pyrophosphate system. No adsorption of pyrophosphate was detected using this method, or by searching for the Esin and Markov effect for pyrophosphate. During the course of the investigation, evidence

supporting the existence of the specific adsorption of the nitrate ion was published, and subsequent correlation with data taken in the present study proved that nitrate is adsorbed at mercury electrodes. The value of the ECM in 1 F potassium nitrate was found to b e -0.519 volts. In pyrophosphate solution the ECM shifted to slightly more anodic values with concentration, but was still only -0.427 volts at 25 degrees in 0.2 F solution.

Chronocoulometry, selective for the detection of adsorption of electroactive species, was employed to determine whether any of the copper(II) pyrophosphate complex is adsorbed. The greatest possible amount of adsorption was found to be only about 0.5×10^{-10} Moles $cm.^{-2}$, not enough to constitute blocking of the reaction, even in relaxation experiments.

Previous reports, plus evidence found in the present study, indicate that, in alkaline solution, the rate of the overall reaction is controlled by the rate of the dissociation of the 2:1 complex to form the reducible species $Cu(P_2O_7)^{-2}$. By employing relaxation techniques, it was possible to measure the parameters of the electrochemical reduction step in both acid and alkaline solution. The values found for a 1 F solution of potassium nitrate of pH 9.34 are the following: $i_a^o = 0.596 \times 10^{-3}$ amp. $cm.^{-2}$, $k_a^o = 0.38 \times 10^{-2}$ cm. $sec.^{-1}$, and $\alpha = 0.4$. These apparent values tended generally to increase with decreasing nitrate concentration and pH. Double layer corrections applied to the apparent values yielded the following "true" values: $i_t^o = 1.21 \times 10^{-6}$ amp. $cm.^{-2}$, $k_t^o = 6.7 \times 10^{-6}$ cm. $sec.^{-1}$, $\alpha = 0.5$ at pH 9.34. At pH 3.0 the values are the following: $i_t^o = 1.07 \times 10^{-2}$ amp. $cm.^{-2}$,

$k_t^o = 5.94 \times 10^{-2}$ cm. sec.$^{-1}$, $\alpha = 0.5$. From a plot of log i_a^o versus pH, the reaction order with respect to H^+ is found to be two at pH 9, and nearly zero at pH 3. The values at pH 3 agree with the published values for the reduction of copper (II) in 1 F nitrate, and thus it is thought that the complex is weak in acid solution, particularly in the presence of 1 F nitrate. This conclusion is strengthened by the results obtained for the ionic charge z on the reducible species. At pH 9, z = -2, while at Ph 3, z = +1. This is the result of the presence of the excess of alkali cations, known to form complexes with pyrophosphate.

The Gierst analysis of polarograms of the alkaline solutions gave the results $\alpha n = 0.43$, $z = -1.2$, $v^o = 8.0 \times 10^{-4}$ cm. sec.$^{-1}$ for the potential region of positive electrode charge, and $\alpha n = 0.10$, $z = -0.32$, and $v^o = 8.7 \times 10^{-4}$ cm. sec.$^{-1}$ for the potential region of negative electrode charge. In the region of positive electrode charge, the apparent rate is nearly independent of φ', and only the 1:1 complex is reduced, after being formed from the 2:1 complex by the dissociation of either a pyrophosphate or a potassium pyrophosphate ion. In the region of negative electrode charge both complex species undergo reduction, accounting for the unusually low value of z. The low value of α accounts for the diminished influence of φ' at moderately negative potentials. From the average v^o, a value of 0.10 was obtained for the product $K\vec{v}$ of the preceding chemical reaction. Although not directly comparable with concentration-independent published values for this quantity, it still is of the same magnitude. Specific adsorption of nitrate complicated the interpretation by shifting the effective potential of the electrode by varying amounts.

An equation for studying preceding chemical reactions by

chronocoulometry is given, along with the results of its application to the determination of $K\vec{v}$. Only approximate agreement was obtained with the polarographic results for identical solutions. Chronocoulometry was also applied to the determination of k_a^o and α, and reasonable agreement was found for k_a^o between the potential step and chronocoulometric results. Because of this, it is thought that achievement of diffusion control for study by chronocoulometry is difficult in kinetic cases, and a new approach is needed, due to variations of the value of the term $\exp y^2$ erfc y.

CHAPTER I

INTRODUCTION

Cathodic polarographic waves are reversible when the current is controlled by the rate of diffusion of the reducible species to the electrode surface. If any other factor controls the current the wave is not reversible. Among the factors capable of causing irreversibility are the following: adsorption phenomena at the electrode surface, a slow electron transfer step, a slow preceding chemical reaction, and effects of the diffuse double layer. If any one of these effects alone is the cause of the irreversibility the explanation of the irreversibility is usually straightforward. However, if several of these effects simultaneously influence the polarographic current, a complete explanation of the polarogram is quite complex. The latter is the case with the copper-pyrophosphate system.

The present study involves the polarographic irreversibility of the reduction of the copper(II) pyrophosphate complex. Sturrock (57) has shown that the relative abundance of various complex species existing in a solution of copper and pyrophosphate is a function of the pH. With increasing pH the following species become, in turn, predominant: $Cu(H_2P_2O_7)^{2-}$, $Cu(H_2P_2O_7)(HP_2O_7)^{3-}$, $Cu(HP_2O_7)_2^{4-}$, $Cu(HP_2O_7)(P_2O_7)^{5-}$, $Cu(P_2O_7)^{6-}$, with the last named species being essentially the only one present above about pH nine. The degree of irreversibility closely parallels the concentration of $Cu(P_2O_7)_2^{6-}$, although some irreversibility

is noted prior to the formation of that species (53). This complex is not reversibly reducible at the electrode. The change from reversible to irreversible behavior with changing pH occurs in several complex systems, including many complexes of citrate and of EDTA (48, 38).

Various authors (37, 22, 34) have shown that alkali metal cations form complexes with pyrophosphate. The study of Sturrock (57) was made with solutions in which all of the alkali cations had been replaced by tetramethylammonium ions. This conditions obviates the necessity for considering the association of the pyrophosphate ligand with the alkali metal ions. However, it is known (22) that tetramethylammonium ions are adsorbed at the surface of mercury electrodes. It is also known (48) that adsorption changes the electrochemical parameters of the electrode reaction. Consideration of these two facts disallowed the use of alkylammonium cations in the present study, and alkali metals had to be employed.

Under these conditions the reaction of ion-pair formation between pyrophosphate ligands and alkali metal cations must be considered. Ion pair formation reduces the net ionic charge on the complex. This charge reduction must be accounted for in the consideration of the effects of the electrical double layer on the reaction. Charge reduction must also be considered when writing equations for the reactions occurring during electrolysis. Nonetheless ion-pair formation is considered to be less of a problem than is adsorption at the electrode.

Several other studies have been made of the copper-pyrophosphate system. Schupp, Sturrock, and Watters (53) measured the stability constants of copper hydrogen pyrophosphate complexes of the type

$$CuH_i(P_2O_7)_j^{v-} \qquad (1\text{-}1)$$

Laitinen and Onstott (36) polarographically investigated copper-pyrophosphate in alkaline medium; they found two waves and explained their occurrence as being due to the reduction of two species in sluggish equilibrium with each other. Rogers and Reynolds (50) also studied the system in alkaline solution, and found two waves. The first wave was attributed to a reduction of copper(II) to copper(I). The second was attributed to the direct reduction of copper(II) to metallic copper.

Furlani and Guiliani (23) studied the system with oscillographic polarography, and observed two reduction peaks. The first peak occurs at about -0.05 volts at pH 2, and shifts cathodically with increasing pH. The second peak occurs at about -1.3 volts at pH 9 and shifts anodically with decreasing pH. This same qualitative behavior was observed in the present work.

In a chronopotentiometric study of the system, Foster (22) showed that the electrode reaction is irreversible in alkaline solution because of a slow preceding chemical reaction in which a pyrophosphate ligand dissociates from the complex prior to its reduction. Such type of reaction may be represented as

$$Y \rightleftharpoons Z + Ox \qquad (2a)$$

$$Ox + ne \rightleftharpoons Red \qquad (2b) \qquad (1\text{-}2)$$

where Y and Z are not reduced at potentials at which Ox is reduced. Foster showed that the dissociation of Y is the rate determining step of the reaction. He also showed that, in the presence of alkali metal cations, at least one such cation is associated with each pyrophosphate

ligand. Considering this association, the complete reaction for the reduction of the copper-pyrophosphate complex in alkaline medium may be written as

$$Cu(MP_2O_7)_2^{4-} \rightleftarrows MP_2O_7^{3-} + Cu(MP_2O_7)^{1-} \qquad (3a)$$

$$Cu(MP_2O_7)^{1-} + 2e^- \rightleftarrows Cu(0) + MP_2O_7^{3-} \qquad (3b) \qquad (1\text{-}3)$$

where M is the alkali metal cation.

In the present work copper nitrate furnished the copper(II), sodium pyrophosphate furnished the pyrophosphate ligand, and potassium nitrate was the supporting electrolyte. Thus an excess of alkali metal cations was always available to associate with the pyrophosphate ligand. In alkaline solution above pH 9 reaction 1-3 is the overall reaction. As already indicated, at lower pH values the complex associates with one or more protons, and the reversibility of the electrode reaction increases.

During the course of the present investigation, Payne (44) published evidence proving that the nitrate ion is specifically adsorbed at the surface of mercury electrodes. Since the nitrate ion had already been employed in many experiments, use of it was continued and Payne's results were correlated with the results of similar experiments of our own. Since the ionic charges of the copper complexes are high, studies were made of the effect of the supporting electrolyte, potassium nitrate, on the reduction of the complex. These effects are known as double layer effects, and were evaluated with the aid of the Gouy-Chapman Theory (30, 3) as modified by Stern (56). Knowledge of the existence of the specific

adsorption of nitrate allowed a more complete explanation of the double layer effects on the electrode reaction.

The initial phase of the present study, performed at a time prior to the availability of Payne's report (44), was concerned with determining which, if any, of the species present in solution were specifically adsorbed. Triangular sweep voltammetry and A. C. polarography were used, and it was found that none of the pyrophosphate species is adsorbed. The Esin-Markov effect and the data of Payne were used to confirm the adsorption of nitrate. Chronocoulometry was used to prove that none of the reducible species, that is, any of the copper pyrophosphate complexes, is adsorbed. These results are presented in Chapter IV.

Examination of Reaction 1-3 shows that there are several features which need independent investigation. The electrochemical parameters of the reduction reaction should be determined under conditions where that reaction is the rate-determining step. These determinations were made with the potential step method. The results of these experiments are presented in Chapter V.

The kinetics of a chemical reaction that precedes the electroreduction should be determined under conditions where that reaction is the rate-determining step. When the electrode potential is at least 0.1 volt more cathodic than the equilibrium potential, the rate of the reduction reaction is so fast that the chemical reaction is the rate-determining step. The kinetics of the chemical reaction were studied by polarography. Results of this study are presented in Chapter VI.

The results of all experiments contain the contribution due to the electrical double layer. Methods are available for correcting results for

double layer effects. Experimentally, the double layer effects are studied by vary ing the concentrations of the ions which determine the characteristics of the double layer. In the present work potassium and nitrate ions were in excess and thus determined the characteristics of the double layer. Experiments were performed in 1.0 F, 0.5 F, 0.1 F, and 0.05 F potassium nitrate solutions. The corrected electrochemical parameters are presented in Chapter V, and the corrected chemical kinetic parameters are presented in Chapter VI. The latter chapter also contains an interpretation of the polarograms of the system in alkaline solution based on the Gierst analysis (28), in terms of Reaction 1-3 and the influence of the double layer. An attempt to correct the polarographic results for the specific adsorption of nitrate is also explained in Chapter VI.

Since the electrochemical behavior of the system is a function of the pH, experiments were performed at different pH values. The three values normally used were three, six, and nine. At pH 3, completely reversible behavior is noted for the reduction. At pH 5.8 some irreversibility began to appear. At this pH value the species $Cu(HP_2O_7)_2^{4-}$ and $CuH(P_2O_7)_2^{5-}$ are present in approximately equal concentrations. Removal of a proton from the latter of these species results in $Cu(P_2O_7)_2^{6-}$, the species which is not reversibly reduced. This pH value also corresponds to the third pK value of pyrophosphoric acid. At pH 9 and above essentially all of the complex is in the unprotonated form, and the reaction is totally irreversible. Plots of particular parameters versus pH allowed the pH dependence of the parameters to be established.

By separation whenever possible of the different effects on the polarization curve, a fairly complete explanation of the polarographic

irreversibility was attained. The effects investigated were the following: specific adsorption, pH effects, double layer effects, ion-pair formation, chemical kinetics, and electrochemical kinetics. There are interactions between some of these effects, and in the obvious cases an attempt has been made to account for these interactions.

CHAPTER II

EXPERIMENTAL METHODS

Potentiostatic Techniques

Potential Step Method

Theory. The theoretical and experimental aspects of the use of a potential step in the study of electrode reactions were first described by Gerischer and Vielstich (27). A theoretical treatment was also given by Delahay (9), whose ideas are embodied here. The potential step method is a relaxation technique in which the controlled electrode potential E is the perturbed variable while the transient current I is studied as a function of time. The electrode reaction studied is of the following general type:

$$Ox + ne^- \underset{\overleftarrow{k}}{\overset{\vec{k}}{\rightleftarrows}} Red \qquad (2\text{-}1)$$

where Ox signifies a species reducible at the electrode and Red the reduced species. The reaction can be described by forward and reverse heterogeneous rate constants $\vec{k}$ and $\overleftarrow{k}$, that are measures of the velocity of reaction at a particular potential. When the concentrations of Ox and Red are equal and the electrode potential is such that no net current flows, $\vec{k}$ and $\overleftarrow{k}$ are equal, and the value thus attained is referred to as k_a^o, the apparent standard heterogeneous rate constant. This constant has the units of cm sec^{-1} and is a measure of the rate of penetration

through the energy barrier at the electrode-solution interface by the electron (9). This quantity, together with i_a^o and α, characterize the electrode reaction. The apparent exchange current density, i_a^o, is the amount of current per unit area which flows in either direction when the net current flow is zero. The transfer coefficient α is a measure of the symmetry of the energy barrier of the reaction 2-1. Potential measurements are referred to the formal equilibrium potential E_e, at which no net current flows.

In this work a dropping copper amalgam electrode furnished the reduced species. Using the time delay circuit and the potentiostat (vide infra) at a known time in the life of a drop, a potential step is applied to the electrode, originally held at E_e. Assuming that the current due to charging of the double layer does not affect the Faradaic current, an expression for the Faradaic current which flows per unit area may be written as follows:

$$i = i_a^o [\exp(-\alpha n f \eta) - \exp(1-\alpha)(n f \eta)] \exp y^2 \operatorname{erfc} y \qquad (2\text{-}2)$$

Here the number of electrons is n, and f is defined as

$$f = \frac{F}{RT} \qquad (2\text{-}3)$$

where F, R, and T are Faraday's Constant, gas constant, and absolute temperature, respectively. The overvoltage, η, is defined as

$$\eta = E - E_e \qquad (2\text{-}4)$$

The parameter y is

$$y = \lambda t^{1/2} \tag{2-5}$$

and λ, having the units of $sec^{-1/2}$, is given by

$$\lambda = \frac{i_a^o}{nF} \frac{\exp(-\alpha nF\eta)}{C_{Ox} D_{Ox}^{1/2}} + \frac{\exp (1-\alpha)(nF\eta)}{C_{Red} D_{Red}^{1/2}} \tag{2-6}$$

The quantity t is time (in seconds) and D is the diffusion coefficient, in cm^2 sec^{-1}, of the species indicated by the appropriate subscript.

The function exp y^2 erfc y is depicted in Figure 1 versus its argument.

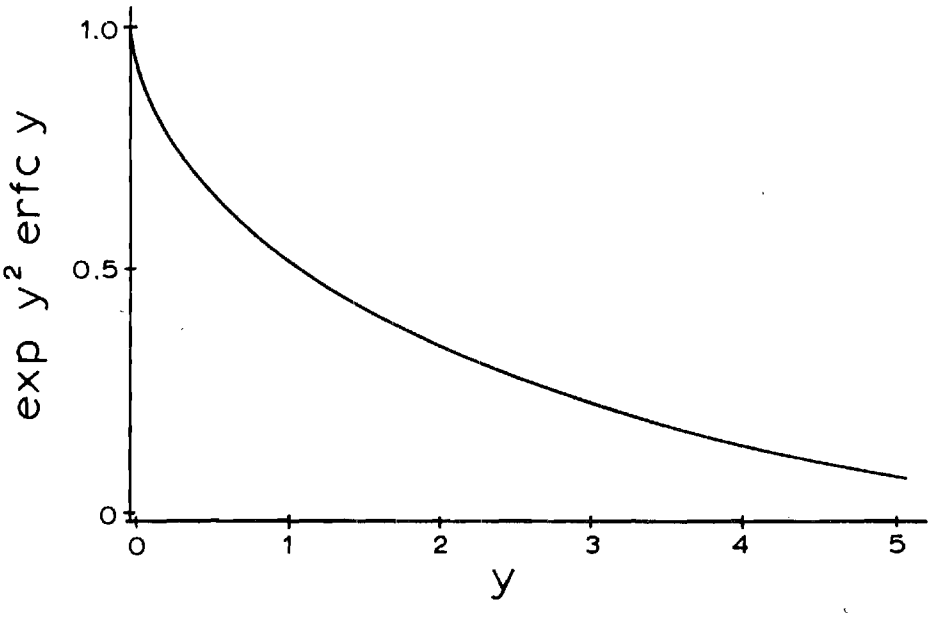

Figure 1. The Function exp y^2 erfc y Versus Its Argument y.

Except for this function in Equation 2-2 the current density at any potential would be constant. The term is related to the formation of a concentration gradient at the electrode and the change of current control from the kinetics of the electrode reaction to mass transfer of the reactants. Since it is desired to study the kinetics of the reaction, measurements must be made at times before the development of an appreciable concentration gradient. The normally accepted criterion (9,42) for this condition, that

$$y \leq 0.1 \tag{2-7}$$

is based on the function $\exp y^2 \operatorname{erfc} y$ being close to unity. For a value of y of this magnitude, the function simplifies to

$$\exp y^2 \operatorname{erfc} y \simeq 1 - \frac{2y}{t^{1/2}} = 1 - \frac{2\lambda t^{1/2}}{\pi^{1/2}} \tag{2-8}$$

The current I is now plotted versus $t^{1/2}$ and extrapolation to $t^{1/2} = 0$ is made. Equation (2-2) may be written as

$$i = i_o \exp y^2 \operatorname{erfc} y \tag{2-9}$$

where

$$i_o = i_a^o [\exp(-\alpha n f \eta) - \exp(1-\alpha)(n f \eta)] \tag{2-10}$$

and i_o is the current at $t^{1/2} = 0$.

Unfortunately there are several invalid assumptions in making an I versus $t^{1/2}$ plot and extrapolating it to get i_o. The electrical double layer at the electrode-solution interface acts as a capacitor, and

changing the potential across the interface requires that a current flow to charge the capacitor to the new potential. The time required for this charging is approximately three times the product of capacitance times solution resistance. Typical values of this product are

$$[(2 \times 10^{-7} \text{ farads})(5 \times 10 \text{ ohms}) = 10^{-5} \text{ seconds}]$$

that is, 10 μ seconds. Since most measurements are of millisecond duration the double layer charging is not interfering, but must be remembered. Delahay (17) has contended that equations for the current derived without considering the charging of the double layer are potentially in error. The accuracy of available data for the double-layer charge as a function of potential is sufficiently low to justify writing the current density equation without consideration of the double layer charge.

The condition set forth in Equation (2-7) implies that, considering equation (2-9), the condition

$$\frac{i}{i_o} \geq 0.9 \qquad (2\text{-}11)$$

must be met in order for the extrapolation to $t^{1/2} = 0$ to be valid (42). As pointed out by Oldham and Osteryoung (42) extrapolations have been performed with data not satisfying this criterion; consequently some reported k_a^o and i^o values are considerably in error. There are two methods (42, 26) for obviating these difficulties; both allow easier calculation of the intercepts and also tell immediately whether the data

contain enough kinetic information to warrant their inclusion. Both methods assume that i_x is less than i_o. The i_x is the intercept at $t = 0$ when condition (2-11) is not satisfied.

In the first method tangents are drawn to the i versus $t^{1/2}$ curve and extrapolated to $t^{1/2} = 0$. Differentiation of Equation (2-9) with respect to $y = \lambda t^{1/2}$ and evaluation at $t^{1/2} = 0$ gives

$$\frac{i_x}{i_o} = (1 - 2\lambda^2 t)\,\frac{i}{i_o} + 2\lambda\,(\frac{t}{\pi})^{1/2} \qquad (2\text{-}12)$$

Use of Equations (2-9) and (2-12) allows the plot of i_x/i_o versus i/i_x to be constructed. This plot is shown in Figure 2. The ratio of i/i_x, i being the point at which the tangent is drawn, is used in conjunction with the graph to find i_x/i_o, and then i_o.

In the second method tangents are drawn to the original i-t traces. Differentiation of Equation (2-9) with respect to $y^2 = \lambda^2 t$ and evaluation at $t = 0$ yields

$$\frac{i_y}{i_o} = (1 - \lambda^2 t)\,\frac{i}{i_o} + \lambda(\frac{t}{\pi})^{1/2} \qquad (2\text{-}13)$$

The ratio of i/i_y, i being the point at which the tangent was drawn and i_y being the $t = 0$ intercept, is used with Figure 2 to find i_y/i_o, and then i_o. The advantages of the second method are: time is saved, the original curve is more precise than the transcription, and the validity of the data can immediately be determined.

After i_o is determined, the exchange current density i^o must be found. This is done by rearranging Equations (2-10) to the form

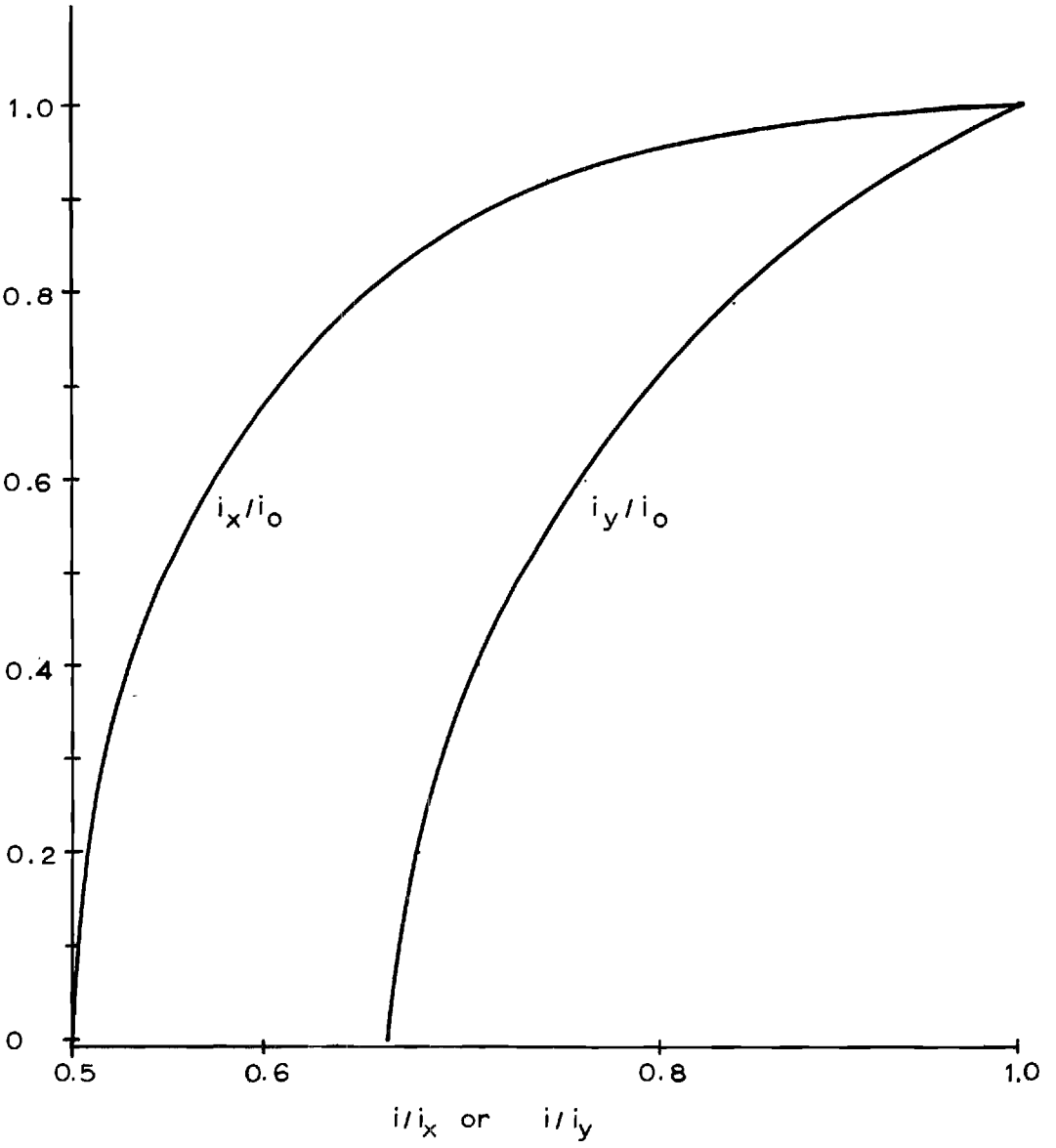

Figure 2. Working Curves for Potential Step Extrapolations.

$$\frac{i_o}{1 - \exp(nf\eta)} = i_a^o \exp(-\alpha nf\eta) \qquad (2\text{-}14)$$

and rewriting as

$$B = 2.303 \log \frac{i_o}{1 - \exp(nf\eta)} = 2.303 \log i_a^o - \alpha nf\eta \qquad (2\text{-}15)$$

A plot of B versus η yields i_a^o at the $\eta = 0$ intercept, and the slope of the plot yields the value of the transfer coefficient α. Tabulated values of $nf\eta$, $e^{nf\eta}$, and $1-e^{nf\eta}$ for the η values used allowed easy calculation of B. The value of η was always less than 50 millivolts, in multiples of 5 millivolts, and was normally made just large enough to get a measurable current.

The above calculation of i_a^o and α does not include a correction for double layer effects, that is, for the potential drop ϕ across the double layer (an explanation of ϕ_o is given in the section on double layer theory on page 30). A ϕ_o correction is mathematically straightforward. There should actually be a term in ϕ_o in the original and all subsequent i-η equations. Inclusion of this term would result in Equation (2-14) being written according to Delahay (14). The new equation is

$$i_o \frac{\exp(zf\phi_o)}{1 - \exp(+nf\eta)} = i_t^o \exp[\alpha nf(\phi_o - \eta)] \qquad (2\text{-}16)$$

where i_t^o is the true exchange current density. Rearranging, Equation (2-16) yields

$$2.303 \log \frac{i_o}{1 - \exp(+nf\eta)} + zf\phi_o = 2.303 \log i_t^o + \alpha nf(\phi_o - \eta) \qquad (2\text{-}17)$$

A plot of the left side of the equation versus $(\psi_o - \eta)$ should yield the true α and i^o, which may be appreciably different from the apparent ones, calculated by ignoring double-layer effects.

Four techniques were used to calculate the electrochemical parameters. At first the data were treated by plotting i versus $t^{1/2}$, selecting the linear section and extrapolating the best straight line through these points to $t^{1/2} = 0$. Then a computer program was written (see Appendix) to take the points from the supposedly linear sections, fit a least-squares straight line to them, and calculate the intercept. The program allowed calculation of i_a^o and α by the previously outlined procedure, and found k_a^o from

$$i_a^o = nFAk_a^o C_{Ox}^{1-\alpha} C_{Red}^{\alpha} \qquad (2\text{-}18)$$

where the C's are concentrations of the species Ox and Red. Later the methods of Oldham and Osteryoung became available in the literature and were found to be much more accurate. The fourth calculation involved application of double layer corrections to the parameters as determined from the Oldham-Osteryoung intercepts.

Experimental Technique. An operational amplifier potentiostat, a time delay generator, and a dual trace oscilloscope constituted the instrumentation used. The dropping copper amalgam electrode was the working, that is, test electrode. Its area was pre-determined for each time that could be selected with the time delay generator for applying a potential step. A particular solution was placed in a thermostated cell and deaerated with nitrogen saturated with water vapor from a salt solution having approximately the same vapor pressure as the test solution.

Nitrogen was allowed to flow over the solution during the experiment. A time as late as possible in the normal drop life was selected with the time delay generator, and a calibrated potential step was applied to the electrode by means of the potentiostat adjusted for optimum rise-time. The oscilloscope was set to be triggered a very short time (0.2 millisecond) before application of the step, giving a single sweep in which the depicted step, defining zero time, and the transient current were displayed. A series of traces was made at overvoltages of both signs and one trace of each overvoltage was photographed. Figure 3 displays a typical trace.

Chronocoulometry

Theory of Single Step Chronocoulometry. The considerations of this section are primarily an extension of those involved in the potential step method. The reaction considered is

$$Ox + ne^- \xrightarrow{k_a^o} Red \qquad (2\text{-}19)$$

Chronocoulometry is a relaxation process in which the quantities measured are time and the number of coulombs which flow upon the application of a potential step. The potential step is applied to the electrode by an electronic potentiostat, the potential being stepped from a value at which no current flows to one at which the current is diffusion controlled. The expression derived by Christie, Lauer, and Osteryoung (4) for the current which flows upon application of a potential step is

$$I = K \exp y^2 \operatorname{erfc} y \qquad (2\text{-}20)$$

where K is given by

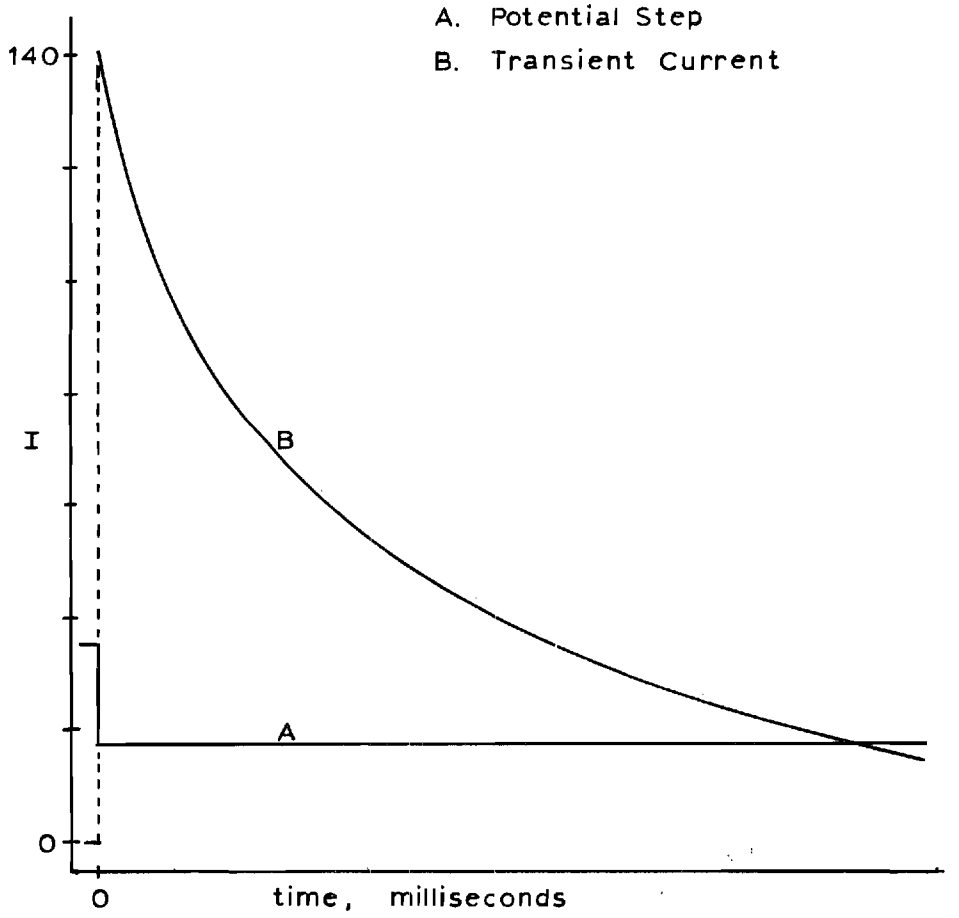

Figure 3. Theoretical Oscilloscopic Trace in a Potential Step Experiment.

$$K = n F A k_a^o [C_{Ox} \exp(-\alpha n f \eta) - C_{Red} \exp (1-\alpha)(n f \eta)] \qquad (2\text{-}21)$$

The parameter y is again given by

$$y = \lambda t^{1/2} \qquad (2\text{-}22)$$

and λ is given by

$$\lambda = k_a^o \left[\frac{\exp(\alpha n f \eta)}{D_{Ox}^{1/2}} + \frac{\exp(1-\alpha)(n f \eta)}{D_{Red}^{1/2}} \right] \qquad (2\text{-}23)$$

The other symbols are the same as given in the previous section. Christie *et al.* (4) assumed C_{Red} to be zero initially, an assumption which relaxes the experimental requirements but does not simplify the derivation. Since an equation for the number of coulombs is needed, Equation (2-20), is integrated with respect to time,

$$Q = \int_o^t I dt = \int_o^t K \exp y^2 \operatorname{erfc} y \qquad (2\text{-}24)$$

The result of the integration gives

$$Q = \frac{K}{\lambda^2} \left(\exp y^2 \operatorname{erfc} y + \frac{2y}{\pi^{1/2}} - 1 \right) \qquad (2\text{-}25)$$

where Q is the charge in coulombs. Since $\exp y^2 \operatorname{erfc} y$ contains t, y must be assumed to be either very small or very large so that the function will be nearly constant. The potential step method makes measurements for conditions such that $y \leq 0.1$, corresponding to kinetic control of the current. Chronocoulometry makes measurements for conditions such that

$$y \geq 5 \tag{2-26}$$

which corresponds to a current controlled by diffusion. Condition (2-26) allows (2-25) to be simplified to

$$Q = \frac{2K}{\lambda\pi^{1/2}} t^{1/2} - \frac{K}{\lambda^2} \tag{2-27}$$

Then, for $y \geq 5$, a plot of Q versus $t^{1/2}$ should be linear. The slope of this plot may be expressed as

$$\frac{\partial Q}{\partial t^{1/2}} = \frac{\partial K}{\lambda\pi^{1/2}} \tag{2-28}$$

The plot has an intercept $t_i^{1/2}$ at Q = 0 such that

$$\lambda = \frac{\pi^{1/2}}{2t_i^{1/2}} \tag{2-29}$$

The nature of the intercept $t_i^{1/2}$ is such that it increases with increasing values of the potential step, exhibits a maximum at $E = E_e$, and decreases as E becomes greater than E_e, meaning that there are optimum values of η which should be used to calculate λ. Since λ contains the parameters k_a^o and α, Equation (2-23) may be written as

$$\log \lambda = \log k_a^o - \frac{1}{2} \log D_{Ox} - \frac{1}{2.303} \alpha n f\eta \tag{2-30}$$

where the term containing $(1 - \alpha)$ may be omitted if η is sufficiently large (η = 0.1 volt for n = 2). Then a plot of log λ versus η allows the determination of k_a^o from the intercept at $\eta = 0$ and the determination

of α from the slope. The value of D_{Ox} may be determined as suggested by Christie et al. (4) from

$$\frac{\partial Q}{\partial t^{1/2}} = \frac{\partial}{\pi^{1/2}} n F A D_{Ox}^{1/2} C_{Ox} \qquad (2\text{-}31)$$

This is the equation for the potential-independent limiting slope of the plot corresponding to a large η.

The effect of the double layer capacity has been ignored in the foregoing treatment. Every change of potential requires a current to flow into the double layer. Thus the measured values of Q will exceed the real values by a constant amount for a given step. If no specific adsorption occurs, blank curves in the absence of reactant may be run at each step used and these values of the charge subtracted from the measured values.

For a sufficiently large η, the corrected $t_i^{1/2}$ intercept is very nearly zero. Since, however, the uncorrected Q versus $t^{1/2}$ plot contains a contribution due to the double layer effect, a backward extrapolation gives an intercept Q_i on the Q axis at $t^{1/2} = 0$. This intercept will thus give the amount of charge $Q_{d.l.}$ required to change the potential of the electrode between the initial and final values. If $Q_{d.l.}$, for a fixed initial and final potential, varies with the concentration of a reactant or product, this is an indication and a sensitive measure of adsorption of that species (1). For specific adsorption the following equation is applicable

$$Q = \frac{2}{\pi^{1/2}} n F A C D^{1/2} t^{1/2} + Q_{d.l.} + nF A\Gamma \qquad (2\text{-}32)$$

where $Q_{d.l.}$ is the number of coulombs required to charge the double layer, and Γ is the surface excess in moles cm^{-2}.

Theory of Double Step Chronocoulometry. In this method the potential of the electrode is suddenly changed to a new value at which current flows, and then is suddenly changed back to the original value after a time τ. The total current-time integral, Q, is measured (1), beginning with the application of the first step. This procedure is particularly useful in testing for adsorption of any reactant or product of an electrochemical system. The equation for Q for times greater than τ has been given by Anson (1). The equation is

$$Q(t > \tau) = \frac{2}{\pi^{1/2}} n F A C D^{1/2} [t^{1/2} - (t - \tau)^{1/2}] \qquad (2\text{-}33)$$

A plot of $Q\ (t > \tau)$ versus $[t^{1/2} - (t - \tau)^{1/2}]$ should give a zero-zero intercept if neither reactants nor products are adsorbed. This intercept value would result if no adsorption occurred because then the $Q_{d.l.}$ values for the two steps would be equal but of opposite sign, and would thus cancel.

Another expression for Q may also be written. For this purpose $Q(t > \tau)$ is measured with respect to Q_τ, the value of Q at t equal τ. Then Q_r is defined by

$$Q_r = Q_\tau - Q(t > \tau) \qquad (2\text{-}34)$$

Because Q_τ is given by

$$Q_\tau = \frac{2}{\pi^{1/2}} n F A C D^{1/2} \tau^{1/2} + Q_{d.l.} \qquad (2\text{-}35)$$

it follows that Q_r is

$$Q_r = \frac{2}{\pi^{1/2}} n F A C D^{1/2} [\tau^{1/2} + (t - \tau)^{1/2}] + Q_{d.l.} \qquad (2\text{-}36)$$

The absolute value of $Q_{d.l.}$ should be the same for the two steps, and therefore a plot of Q ($t > \tau$) versus $t^{1/2}$ and of Q_r versus $[\tau^{1/2} + (t - \tau)^{1/2} - t^{1/2}]$ on the same graph should have the same Q intercepts if no adsorption occurs. Any difference between the values of $Q_{d.l.}$ is an indication of and its magnitude a measure of adsorption. A term for the amount adsorbed then appears in (2-35) or (2-36) in the form of $n F A \Gamma$.

Experimental Technique. The instrumentation and procedure were the same as in the potential step method, except that an operational amplifier integrator was used to integrate the output of the current follower. The integrator was calibrated by integrating known currents with the same RC values of the integrator as used in the experiments. The oscilloscope was triggered and the integrator switched on just prior to the application of the potential step. The dual trace oscilloscope gave a simultaneous indication of both the potential step and the number of coulombs (see Figure 4). In double step experiments, the delay time for the reverse step was adjusted to a convenient value, usually half of the time of the oscilloscope tracing, and a double step was applied to the electrode (Figure 5) at a point late in the drop life to minimize area change. The maximum total time used for a given step was 100 milliseconds, corresponding to an electrode area change of two per cent with the particular electrode used. This is also the maximum allowable time in avoiding the onset of spherical diffusion.

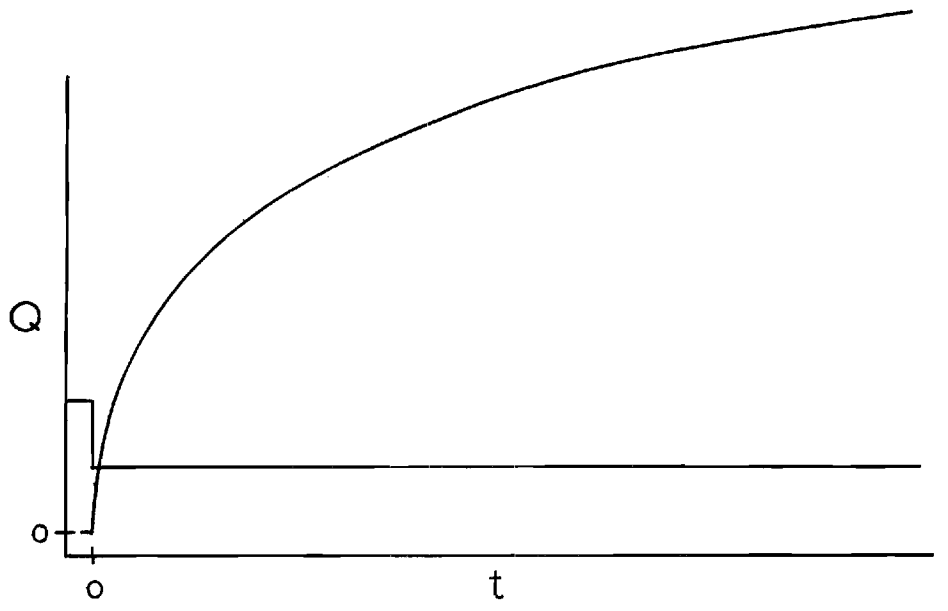

Figure 4. Theoretical Chronocoulometric Trace.

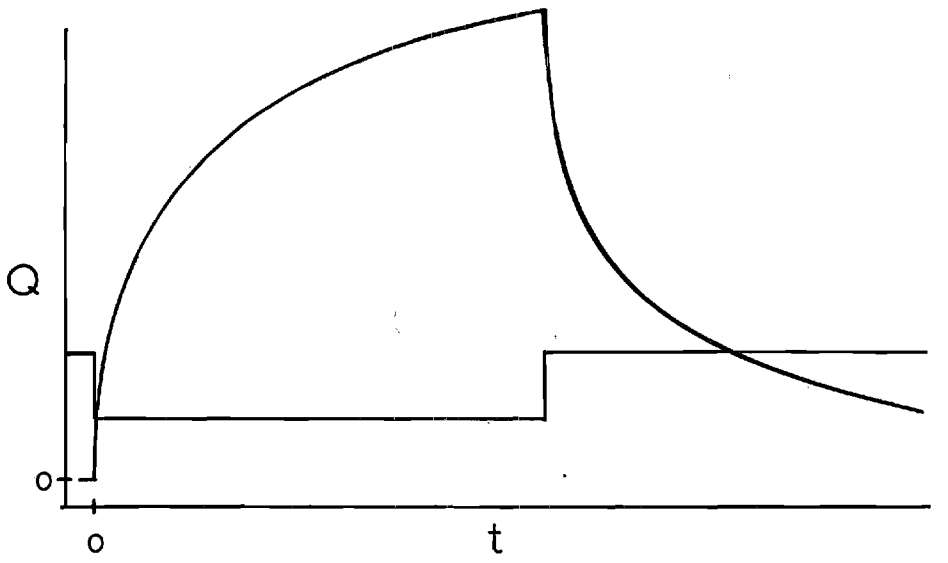

Figure 5. Theoretical Double-Step Chronocoulometric Trace.

Triangular Sweep Voltammetry

This method involves changing the potential of the electrode linearly with time, according to Figure 6a.

For $0 < t < 1/2\ t'$ $\quad E = E_i - wt$ (2-37)

and for $1/2\ t' < t < t'$ $\quad E = E_i - w(t' - t)$

with w being the rate of change of the potential and t' being the time for one cycle. Sevcik (55) and Delahay (7) have given the derivation of the equation for linear diffusion in the case of irreversibility due to a slow electron transfer step. It is possible to measure α from the peak current

$$i_p = 3.01 \times 10^5\ n(n\alpha)^{1/2}\ AD_{Ox}^{1/2} C_{Ox}\ w^{1/2} \qquad (2\text{-}38)$$

A major use of triangular sweep voltammetry is for the determination of the differential double-layer capacity, defined by

$$L = -\frac{dQ}{dE} \qquad (2\text{-}39)$$

From Equation (2-37) one obtains

$$\frac{dE}{dt} = -w \qquad (2\text{-}40)$$

and since

$$\frac{dQ}{dt} = I \qquad (2\text{-}41)$$

it follows that

$$I_c = \frac{L\,w}{A} \qquad (2\text{-}42)$$

where i_c is the capacity current density. Equation (2-42) allows the calculation of the double layer capacity directly from a triangular sweep experiment. Since an oscilloscopic readout was used (see Figure 6b for a typical trace) values of the current at different potentials were read from the trace and divided by the drop area and the sweep rate to obtain the capacity per unit area. Either hanging drop electrodes were used to give constant area electrodes, or a rapid potential sweep was made on a dropping electrode.

The chief drawback of the triangular sweep method for determination of double layer capacity resides in the fact that it is the least accurate of the methods commonly used. Hence its use is limited primarily to survey purposes.

If an anodic sweep follows the cathodic sweep a mirror image of the capacity curve should result. If an electrode reaction takes place cathodic and anodic peaks, corresponding to reduction and reoxidation, respectively, occur. The mathematical formulation for a "completely reversible" couple was given by Delahay (7) as

$$E_{p,\text{anodic}} - E_{p,\text{cathodic}} = \frac{0.059}{n} \text{ volts} \qquad (2\text{-}43)$$

The degree of separation of the peak potentials is then a measure of the degree of reversibility of the couple.

A.C. Polarography and Tensammetry

A.C. polarography involves superimposition of a small sinusoidal

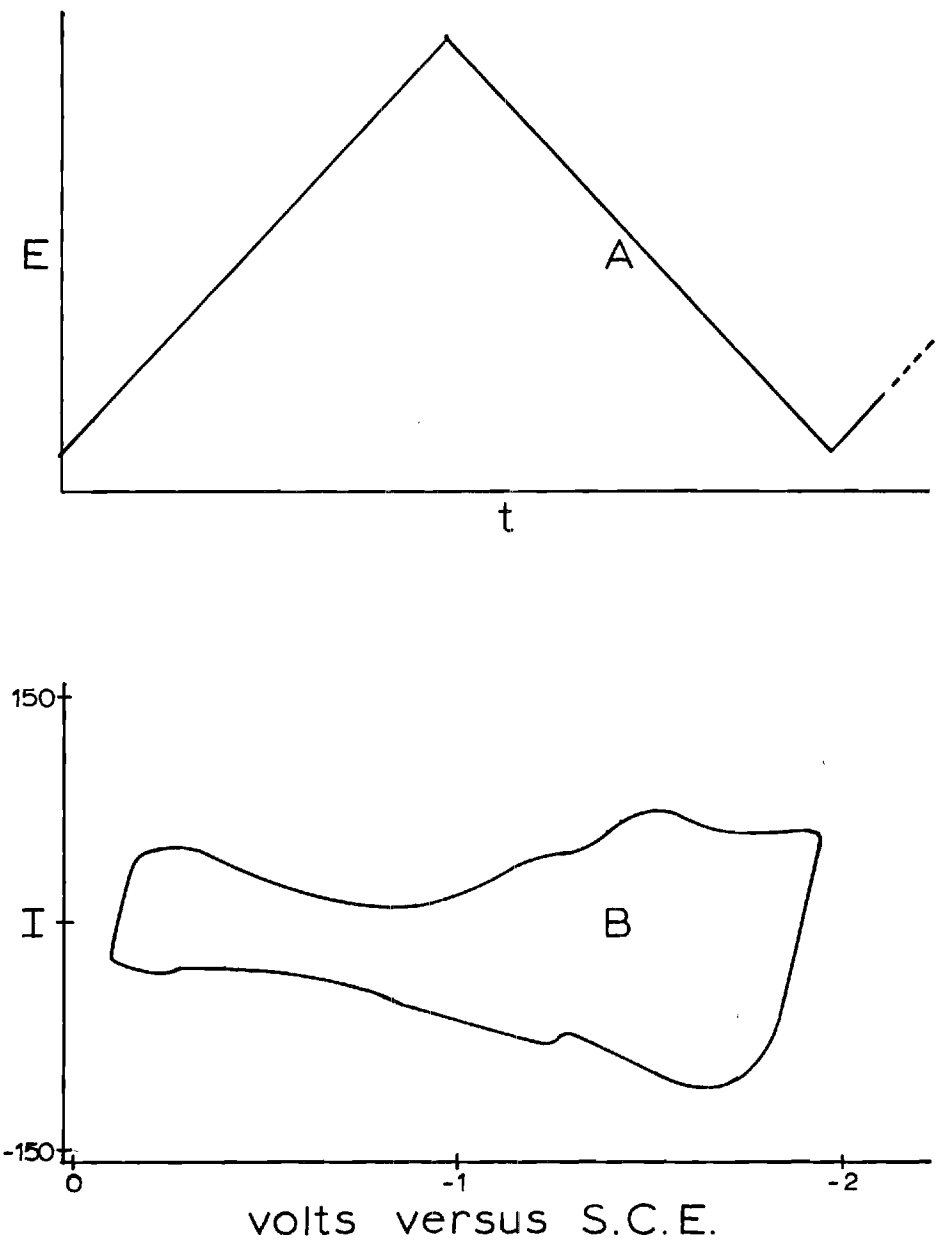

Figure 6. Triangular Sweep Voltammetry.
A. Potential-Time Relationship.
B. Typical Capacitance Curve Display.

component of fairly low frequency on the ramp voltage used in ordinary polarography. The resulting alternating current in the simplest case is separated from the D.C. current, amplified, rectified, and recorded on an X-Y or strip chart recorder. The method is more valuable when millivolt range alternating voltages are used. As a survey tool the method allows the showing of the presence of reversible reactions to the extent that the alternating component is small, for example 10 millivolts alternating would only give an A.C. wave if the couple were reversible in the classic sense. The method also allows demonstration of the presence of adsorption by giving so-called tensammetric waves at certain potentials on either side of the electrocapillary maximum. As the electrode potential is increased, adsorption occurs at some potential, giving a tensammetric peak. As the electrode potential increases further and passes through the electrocapillary maximum, adsorption continues until some desorption potential beyond the electrocapillary maximum is reached. At this point desorption occurs and another tensammetric peak is obtained.

Used in conjunction with D.C. polarographic waves, A.C. polarography is a useful diagnostic tool for the prediction of reaction irreversibility and possible reaction blocking because of adsorption.

Electrocapillary Phenomena

Aspects of Double Layer Theory

The quantitative study of electrode processes involves consideration of the effects of the electrical double layer at the electrode (31). The structure of this double layer is that depicted in the profile of Figure 7. The inner and outer Helmholtz planes, a and b, are referred

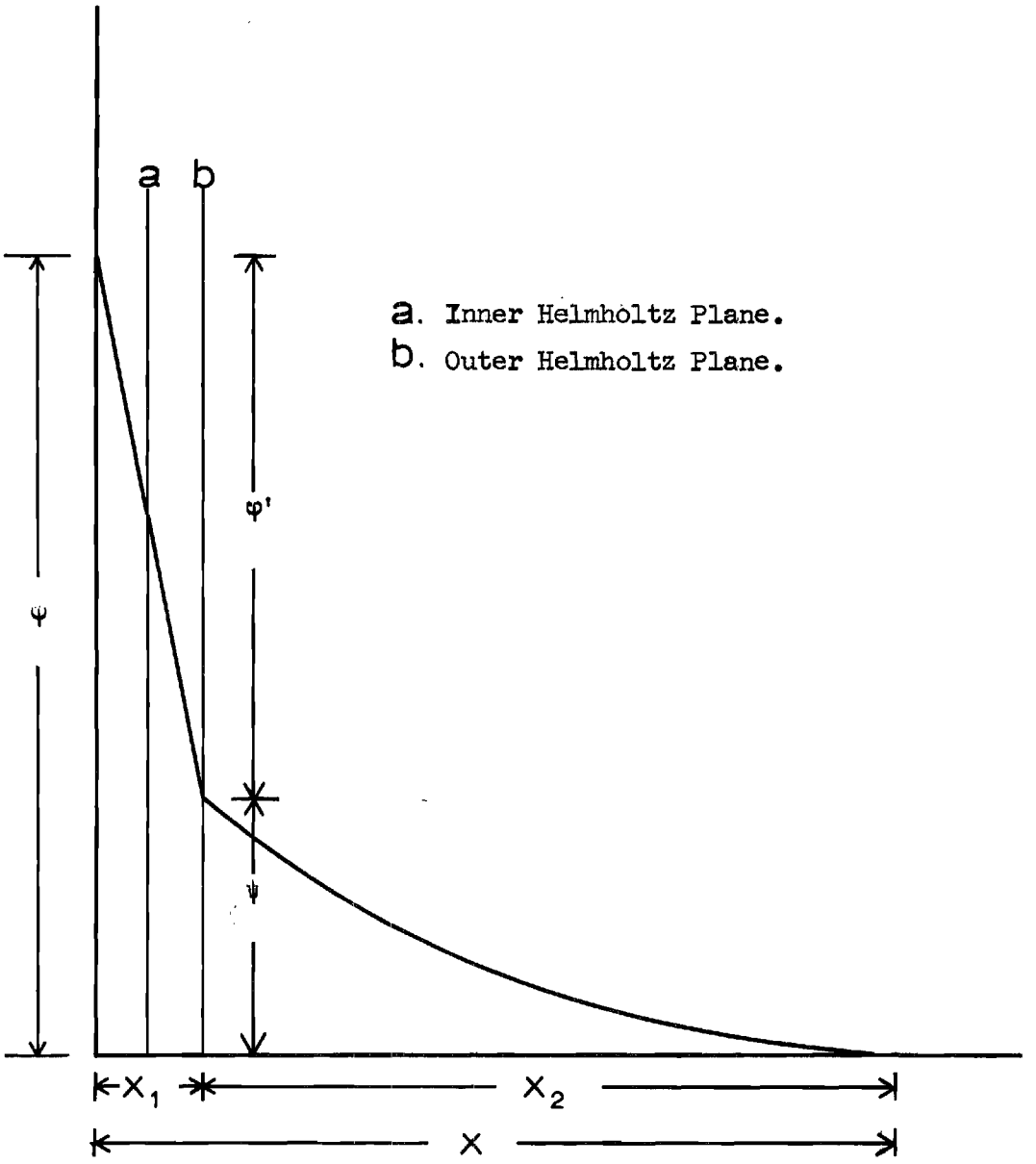

Figure 7. The Electrical Double Layer. A Profile of the Potential as a Function of Distance.

to as planes of closest approach of non-hydrated and hydrated ions, respectively. The two layers are present whenever the electrode is completely or partially polarized. An electrode reaction normally occurs at the outer Helmholtz plane, and it is thus φ', the potential drop between the electrode and this point, that is the primary driving force of the electrode reaction, although the value of ψ_o is also a factor, as will be indicated. The quantity x represents the distance from the electrode surface. The total potential drop across the double layer is φ. The potential drop across the compact double layer, composed of the inner and outer planes of closest approach, is φ', and that across x_2, the diffuse double layer, is ψ_o.

$$\varphi = \varphi' + \psi_o \qquad (2\text{-}44)$$

In discussing these phenomena, potentials are referred to a potential known as the zero charge potential, or electrocapillary maximum potential. This is the spontaneous open-circuit potential which the electrode would assume in a solution. The value of the ECM potential is normally about one-half volt negative with respect to the saturated calomel electrode. At this potential the electrode is not electrically charged, and no double layer exists. If the potential is changed from this value, the electrode must assume a charge, and an array of charges will also appear on the solution side of the interface. This array of charges constitutes the double layer. Such an array of charges acts as a capacitance, which is called the integral capacitance K, and is defined by

$$K = -\frac{Q}{\varphi} \qquad (2\text{-}45)$$

where Q is the electrode charge, and φ the rational potential. It is seen that at $\varphi = 0$ the charge Q is zero.

Further, the surface tension ν of the electrode-solution interface is a function of potential, because of the array of charges surrounding the electrode at all potentials other than $\varphi = 0$. The surface tension decreases proportionally to the charge density on the electrode, as expressed by

$$q = - \frac{d\nu}{dE} \qquad (2\text{-}46)$$

The quantity q is different from Q only in that the former is a charge density and the latter simply a charge. The potential E may be measured against any reference electrode, since only the potential change is of interest. The potential at which the surface tension at the interface is at its maximum is the potential at which the electrode is uncharged, and that potential is the electrocapillary maximum potential. Consequently all these quantities are interrelated.

A second kind of double layer capacity known as the differential capacity is defined by

$$L = - \frac{dQ}{dE} \qquad (2\text{-}47)$$

The differential capacity may be measured with any reference electrode, and is also more conveniently measured experimentally than the integral capacity.

By comparing Equations (2-45) through (2-47) it may be seen that by a single differentiation of the surface tension versus potential curve the electrode charge results. A second differentiation yields an

expression for the double layer capacity. Conversely, Q and v may be obtained by a single or double integration, respectively, of the equation for the differential capacity.

The original Gouy-Chapman theory (30, 3) assumed that the ions were point charges. By assuming that the ions in the diffuse double layer are of finite size, as was done by Stern (56), the potential at the outer Helmholtz plane may be calculated from

$$\psi_o = \left(\frac{2}{fz}\right) \sinh^{-1} \left(\frac{q}{\partial A}\right) \qquad (2\text{-}48)$$

where

$$A = \left(\frac{R\,T\,\varepsilon\,C_s}{2\pi}\right)^{1/2} \qquad (2\text{-}49)$$

and where ε is the dielectric constant. The potential-distance relationship is depicted in Figure 7. Equation (2-48) reduces to

$$\psi_o = \left(\frac{2}{38.935}\right) \sinh^{-1} \left(\frac{q}{11.74\,C_s^{1/2}}\right) \qquad (2\text{-}50)$$

for univalent electrolytes whose concentration is C_s moles liter^{-1}, and for a temperature of 25°C.

Streaming Electrode Potentials

Grahame (32) pointed out that the potential of a streaming mercury electrode, for solutions containing no reducible species is a function of the head of mercury above the electrode until a sufficiently large head exists, after which the potential becomes essentially independent of the head, and depends only on the type of ions in the solution. This

phenomenon was used to measure the electrocapillary maximum potential (ECM) of a mercury electrode in a solution of non-reducible ions.

The existence of the Esin and Markov effect (21, 10) was also conveniently tested for by using the ECM potentials thus measured. This effect is the variation of the ECM with the electrolyte activity, and may be mathematically formulated as

$$E_r = E \pm \frac{1}{|z|f} \ln a + \text{constant} \qquad (2\text{-}51)$$

It signifies the existence of specific adsorption of electrolyte, and may be applied to any electrolyte.

The precision of the method of streaming potentials is ± 3 millivolts, as compared to ± 1 millivolt or even less for other methods. The former precision is commensurate with that of other potential measurements in this work.

A Beckman Research pH Meter was used to measure the potential of the streaming electrode against the same calomel reference electrodes used in the other experiments. It was found that the potential measurement was extremely sensitive to traces of dissolved oxygen, and best results were obtained by vigorous deaeration of the solution with nitrogen during the course of the measurement. In every case the height of the mercury head was constant and greater than one meter. With these precautions the potentials were reproducible to within one half a millivolt.

Calculation of the Potential Drop Across the Diffuse Double Layer

Electrocapillary Curves by the Drop-Time Method. It has been

shown (6) that under very carefully controlled conditions the variation of the drop time of a dropping mercury electrode with potential is proportional to the variation of the interfacial tension at the electrode with potential. This is a convenient way of determination of the ECM and of the charge on the electrode, given by Equation (2-46). By plotting drop time versus potential an electrocapillary curve is obtained. This curve has the shape of a distorted parabola, the maximum of which occurs at the ECM potential.

Considering Equation (2-46), if drop time is proportional to interfacial tension the equation for the resulting curve may be given as

$$q = -k \left(\frac{dt}{d\varphi}\right) \tag{2-52}$$

where

$$dv = k\,dt \tag{2-53}$$

Here k is a proportionality constant.

In order to determine the electrode charge q the constant k must be evaluated. The value of 420 dynes $cm.^{-1}$ was taken as the interfacial tension (12). The ordinate of the maximum of the curve was taken as the maximum drop time, and k was then calculated. A series of electrocapillary curves was made at different salt concentrations. Since the value of ψ_o ultimately obtained depends on the salt concentration, the same values were chosen as those used in other experiments whose results it was desired to correct for double layer effects. For each curve, the charge q was determined at various potentials by measuring the slope of the tangent to the curve at those potentials and multiplying that slope, dt/dE,

by k to get q.

Use of the Gouy-Chapman Equation. Equation (2-50) allows the calculation of ψ_o from q for a given salt concentration C_s. Since q is known as a function of φ, ψ_o will then be known as a function of φ, and this will allow the use of ψ_o to make double layer corrections on data taken at any potential. With the values of q versus φ at different salt concentrations a complete set of ψ_o versus φ values may be obtained.

Polarography

Irreversible Waves

The theory of irreversible polarographic waves is well known (16). The equation for the current in a completely irreversible system of the type of equation (2-1) is

$$I = n F A C_{Ox} \vec{k} \exp y'^2 \operatorname{erfc} y' \qquad (2\text{-}54)$$

where

$$y' = \overleftarrow{k} \left(\frac{t}{D_{Ox}}\right)^{1/2} \qquad (2\text{-}55)$$

t being the drop time in seconds. Even if the system is not totally irreversible, $\overleftarrow{k}$ is so small as to be negligible as long as η is greater than 0.1 volt. By dividing Equation (2-54) by the equation for a diffusion-controlled current we obtain

$$\frac{I}{I_d} = \pi^{1/2} y' \exp y'^2 \operatorname{erfc} y' \qquad (2\text{-}56)$$

Values of the parameter y' versus the fraction I/I_d were derived and

listed by Koutecky (35). A plot of y' versus I/I_d is given in Figure 8. The value of $\vec{k}$ is thus directly calculable from I/I_d.

The value of $\vec{k}_a^o$ may be determined from

$$\vec{k} = k_a^o \exp(-\alpha n f \eta) \tag{2-57}$$

if the electrochemical reaction is rate-controlling. This will be true if λ' (given by Equation (2-55) as $\vec{k}/D_{Ox}^{1/2}$) is less than 0.25, corresponding to low values of I/I_d. At intermediate points there is mixed control by electrode kinetics and diffusion.

Kinetic Waves

If a homogeneous chemical reaction precedes the electrochemical reduction, as

$$Y \underset{\overleftarrow{v}}{\overset{\vec{v}}{\rightleftharpoons}} Z + Ox \xrightarrow{ne} Red \tag{2-58}$$

the resulting polarographic wave is referred to as a kinetic one. The example given here is of a first order - second order reaction, and the symbols $\vec{v}$ and $\overleftarrow{v}$ refer to chemical rate constants of the appropriate units. The analogous equation for I/I_d is (30)

$$I/I_d = \pi^{1/2} \lambda \exp y''^2 \operatorname{erfc} y'' \tag{2-54}$$

where y", K, and K' are given by

$$y'' = (\vec{v} K t)^{1/2} \tag{2-60}$$

$$K = \frac{K'}{C} \tag{2-61}$$

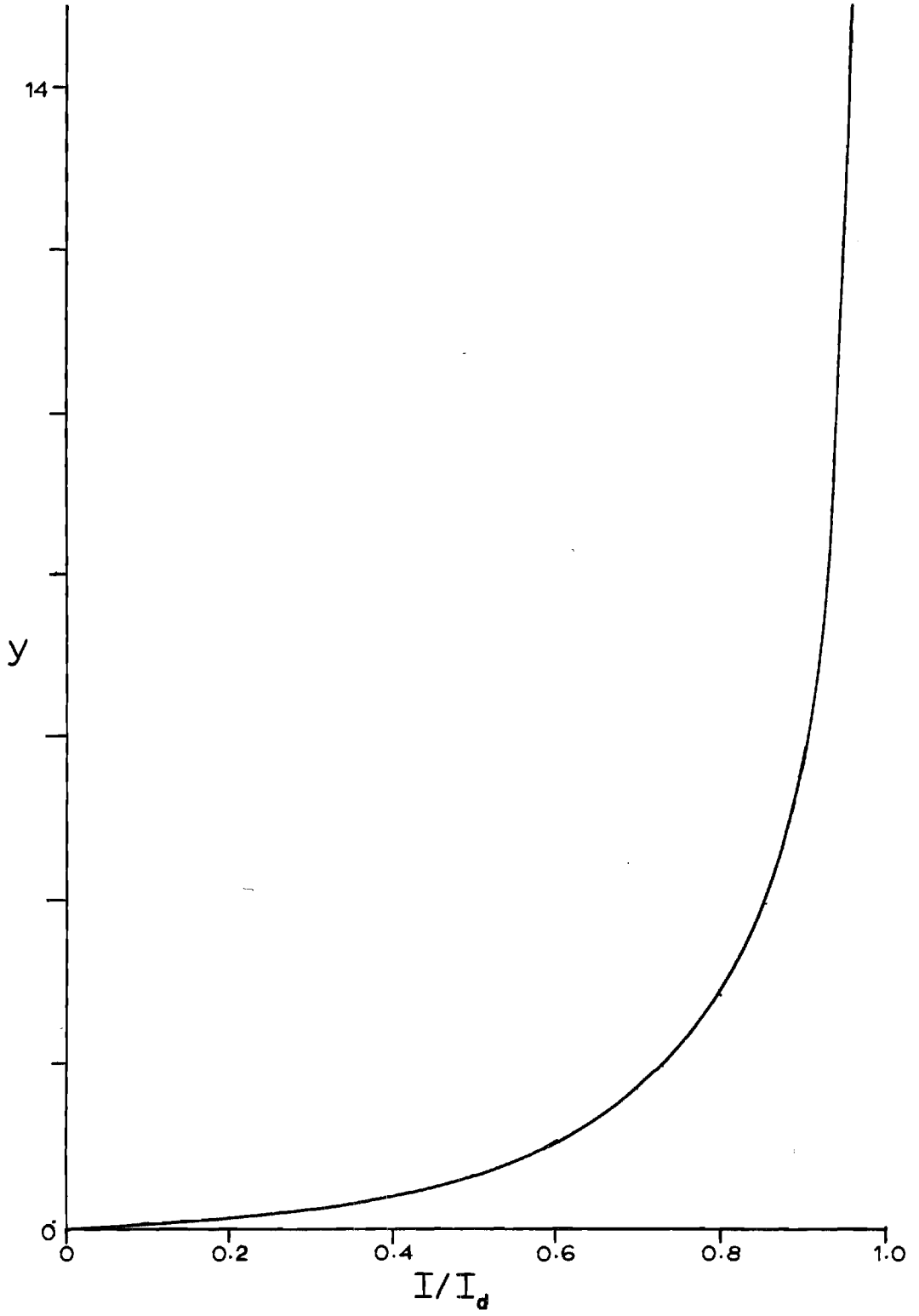

Figure 8. The Quantity y Versus I/I_d .

$$K' = \frac{C\, C_{Ox}}{C_y} \tag{2-62}$$

$$K' = \frac{\vec{v}}{\overleftarrow{v}} \tag{2-63}$$

If no other than the kinetic effect controls the current, $\vec{v}$ may be calculated using Figure 8 and Equation (2-60). Knowledge of K' allows calculation of $\overleftarrow{v}$.

Double Layer Effects - The Gierst Analysis

In polarographic experiments the results are influenced by the characteristics of the electrical double layer at the electrode-solution interface. The degree of influence increases with the dilution of the electrolyte which determines those characteristics. This additional effect makes interpretation of the shape of the curves more difficult. The total potential drop between the electrode and the solution may be split into two parts, one between the electrode and the outer Helmholtz plane, and the other between the latter and the "bulk" of the solution. The expression for the total potential drop is

$$\varphi = \varphi' + \psi_o \tag{2-64}$$

where φ' is the former quantity and ψ_o the latter. The value of ψ_o can only be calculated from theoretical considerations and is not measurable. For potentials away from the ECM and at salt concentrations less than 0.1 F the value of ψ_o can readily exceed 0.1 volt (see Equation (2-48) this chapter). Attempts have been made (49) to correct results for the effects of ψ_o. A treatment for a very general

case has been given by Gierst (28). The treatment, which considers irreversible reactions and kinetic processes, is based upon the Frumkin equation (24). This equation is

$$V^* = V^o[\exp(-\alpha n f \varphi')] \exp(-zf\psi_o) \qquad (2\text{-}65)$$

where v^* is an apparent rate constant, in cm.sec.$^{-1}$, and v^o is the value of v^* at $\varphi = 0$, that is, where no double layer effects are operative. The Gierst analysis allows separate study of the effects of φ' and of ψ_o, and allows a mechanism diagnosis at the end of the analysis.

A series of polarograms is run at different electrolyte concentrations. The apparent rate constant v^* is calculated from Equation (2-55) where v^* replaces $\vec{k}$

$$y' = v^* \left(\frac{t}{D_{Ox}}\right)^{1/2} \qquad (2\text{-}66)$$

and y' is given in Figure 8 as a function of I/I_d.
Rearranging Equation (2-55) gives

$$\frac{2.303}{f} \log v^* = \frac{2.303}{f} \log v^o - \alpha n \varphi' - z\psi_o \qquad (2\text{-}67)$$

A plot of $2.303/f \log v^*$ versus φ, the rational potential, is made and on the same paper at the same scale a plot of ψ_o versus φ is made, ψ_o being calculated as indicated earlier. Drawing of constant φ' and ψ_o lines on the v^* plot allows separation of effects, and the determination of αn and z. The value of v^o is found from the line

$$\frac{2.303}{f} \log v^* = F(\varphi) \qquad (2\text{-}68)$$

extrapolated to $\varphi = 0$. This value is used for correlation with k_a^o, the apparent standard heterogeneous rate constant at the equilibrium potential. The term "apparent" standard rate constant means that no double layer correction was applied to its determination, and therefore perfect correlation may not be expected between v^o and k_a^o, but rather between v^o and k_t^o, the true value of k^o, by the relation

$$v^o = k_t^o \exp(-\alpha n f \eta) \tag{2-69}$$

If a kinetic process is rate-controlling, the quantities v^*, and therefore v^o, have different meanings. The treatment for kinetic control (28, 29) involves knowing the function

$$v^* = F(v^o, \psi_o, \ldots) \tag{2-70}$$

where by definition

$$v^o = (K \vec{v} D_{Ox})^{1/2} \tag{2-71}$$

Therefore v^* is calculated as before, and the entire Gierst plot is constructed. The value of v^o is then found, and from this the value of $\vec{v}$ K is obtained; αn and z may be determined as before but in this case their interpretation is different, as is explained in Chapter VI.

CHAPTER III

CHEMICALS, EQUIPMENT, AND INSTRUMENTATION

Electrodes and Cell

All work was done with mercury electrodes. The hanging mercury drop, the dropping mercury, and the dropping amalgam electrodes were employed.

The hanging mercury drop electrode was a Metrohm Number 410 electrode. Area calibrations were performed on this electrode in the same manner as on the dropping electrodes, and the measured values for each turn of the micrometer dial were found to be within ± 0.02 mm.^{2} of the values given by the manufacturers. Some initial work with a hanging drop electrode was done with a mercury-coated platinum wire electrode sealed in the end of a 6-mm. glass tube. The exposed end of the wire was cleaned in perchloric acid (19) and electroplated with a layer of mercury. A plastic spoon was used to catch mercury drops from a dropping electrode and attach them to the stationary electrode. Uniform detachment of the hanging drop was assured by having mercury in the spoon in excess over the amount capable of being held by the Pt wire. The drop area was calculated from the mass of the drop, assuming sphericity and negligible contact area with the Pt wire.

A standard dropping mercury electrode was constructed of 6 mm. Pyrex-glass tubing, a Pyrex reservoir, and Tygon tubing. One half of a Sargent 5-10 second polarographic capillary was used. The capillary

was rinsed carefully with distilled water after every experiment and prior to interruption of mercury flow, and was maintained in air between experiments.

A dropping amalgam electrode (57) was constructed of Pyrex glass. It had been found (57) that copper amalgams change composition when in contact with Tygon tubing, so an all-glass construction was used. The electrode consisted of a 150 ml. amalgam reservoir atop a jacketed column of about 20 cm. length. Below the jacket a 2 mm. stopcock, a through-glass platinum electrical connection, and a standard external 10/30 glass joint were included. One half of a Sargent 5-10 second capillary was sealed with Varno cement into a 1 cm. glass tubing which had a diameter slightly larger than that of the capillary. The glass tubing was joined to a standard internal 10/30 glass joint. With such an arrangement, the capillary could be replaced without draining the mercury and exposing the entire amalgam to the atmosphere. The electrode was readied for use by adding amalgam to the upper portion and attaching the capillary assembly filled with pure mercury. With the capillary tip in a small beaker of pure mercury, a vacuum pump was employed to remove most of the air dissolved in the amalgam, the contents of the reservoir having been already protected by a covering of Nujol. Afterwards, the electrode was allowed to drain until all of the pure mercury had been displaced by the amalgam and the concentration of the emerging amalgam had become constant. The tip of the capillary was maintained in a 10 ml. beaker of mercury and was only exposed to the atmosphere or to a solution when flowing. In this way air oxidation of the amalgam in the capillary was avoided and the electrode was stable

for as long as used.

For each type of dropping electrode, the surface area of the drops was determined in the following manner: 50 drops were collected and the time measured. The mercury thus collected was washed with deionized water, rinsed with reagent grade acetone, warmed in a drying oven for 5 minutes, cooled and weighed. Assuming sphericity and negligible contact area, the surface area was then calculated from

$$A = (3V)^{2/3} (4\pi)^{1/3} \qquad (3\text{-}1)$$

where V is the volume in cubic centimeters, given by

$$V = \frac{mt}{d} \qquad (3\text{-}2)$$

with m being the flow rate in grams second^{-1}, t the time in seconds, and d the density in grams centimeter^{-3}. The assumption of negligible contact area is more valid with the Sargent capillaries than for either of the hanging drop electrodes because the bore of the Sargent capillary has a cross-sectional area smaller than that of the Metrohm electrode or of the platinum wire.

For measurement of electrocapillary maximum potentials (32) a streaming mercury electrode was constructed. The construction was quite similar to that of the dropping mercury electrode, a 1.1 meter length of heavy-walled 3mm. glass tubing was used. This tubing was mounted to a meter stick secured by clamps to a ringstand. A glass-T, a 2-cm. stopcock, and a through-glass Pt electrical connection were located at the lower end of the glass tubing. Tygon tubing connected this element to a 150 ml. glass mercury reservoir, and the reservoir

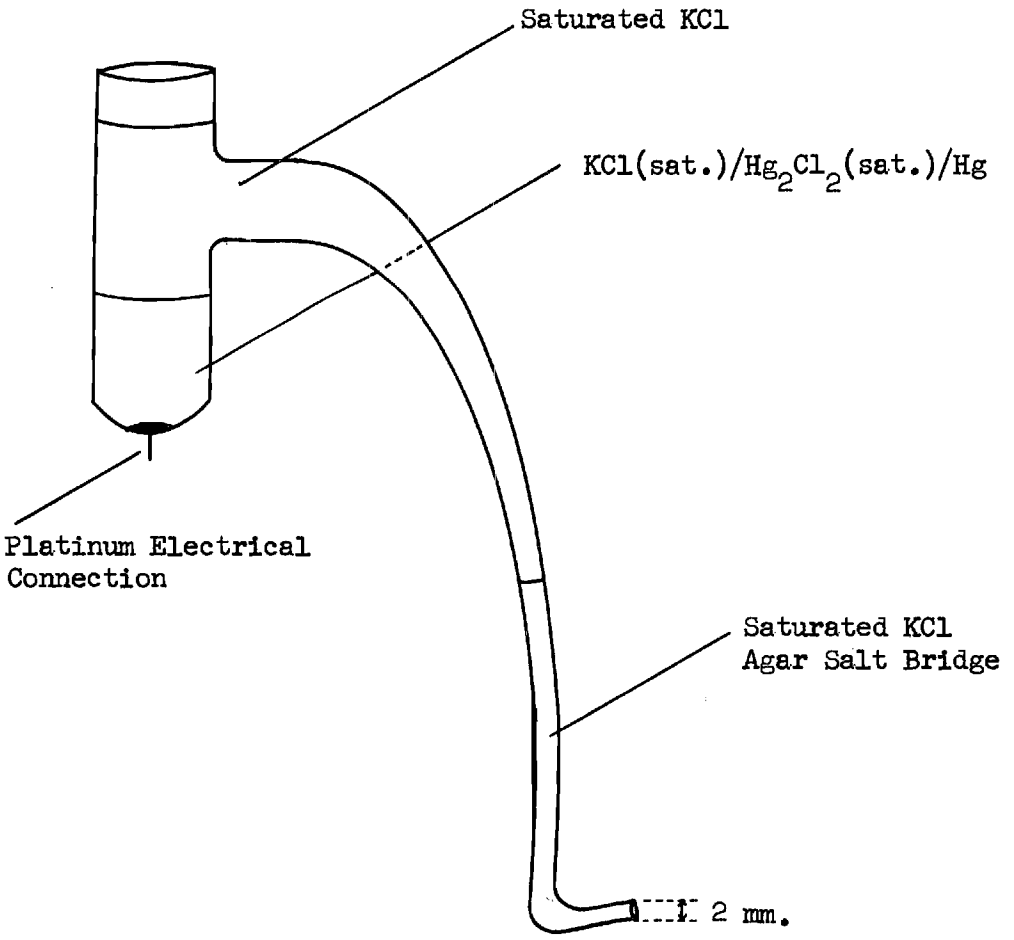

Figure 9. Diagram of the Saturated Calomel Reference Electrode Used.

to a stopcock arrangement to allow N_2 pressure and aspirator vacuum to be used to regulate the mercury head. A 5-cm. piece of Pyrex tubing having a 1-mm. bore was drawn to a tip of vanishingly small inner diameter and attached to the head tubing above by a 10/30 ground-glass joint. For mercury heads greater than 15 cm., a very fine stream of mercury was obtained when the stopcock was opened.

A number of commercial reference electrodes were employed when measuring potentials. These units had varying lifetimes before ceasing to function properly. Therefore, electrodes were made according to Figure 9, based on a design by Wilson (60). The saturated calomel half cell was employed, together with a saturated potassium chloride agar salt bridge junction. When maintained in thermostated saturated potassium chloride solution, these electrodes were trouble free and reproducible throughout the investigation. The small electrode-solution interface area facilitated placement of the electrode close to the test electrode.

The cell consisted of a 100-ml. Berzelius beaker with a No. 10 rubber stopper drilled to accommodate a fritted glass deaerator, the test electrode, the reference electrode, and another fritted glass deaerator, in which was placed a large platinum wire to serve as the counter electrode. To have the counter electrode shielded by the deaerator prevented any oxygen generated at that electrode from getting to the solution.

Controlled Potential Polarograph

The controlled potential polarograph used as the central instrument in this investigation was constructed largely on the basis of a

circuit by Enke. The circuit was obtained by private communication, but was later published by its designer (20). The basic circuit is shown in Figure 10. A commercial version, model EUW-401, is now available from Heath Company, Benton Harbor, Michigan. A brief description of the operating principles will be given, followed by an account of the modifications made to render the instrument more suitable to specific requirements of the intended work.

The operational amplifiers needed were available in a Heath model EUW-19A unit, which consists of four amplifiers, a current booster, and regulated positive and negative 300-volt power supplies. The controlled potential circuit was constructed on a Heath model EUA-19-1 five-socket plug-on module matching the EUW-19A. The elements of the instrument are the potentiostat, the sweep generator, the initial potential source, the cell, and the current measuring section. The cell is a three-electrode cell. The electrodes are designated T, R, and C, corresponding to test, reference, and counter electrodes, respectively. The potentiostat controls the electrode potential via continuous comparison of all the potentials received at S, the summing point, with the potential of the test electrode. The comparison is made by means of the reference electrode and VF, the voltage follower. Regulation of the electrode potential is then achieved by passing current through the cell at the counter electrode. Since essentially no current can pass through the reference electrode-voltage follower combination, with a total resistance of 10^8 ohms, essentially all cell current must pass through the test electrode, connected to the current follower CF, which then produces a voltage proportional to the input current. An RC network allows

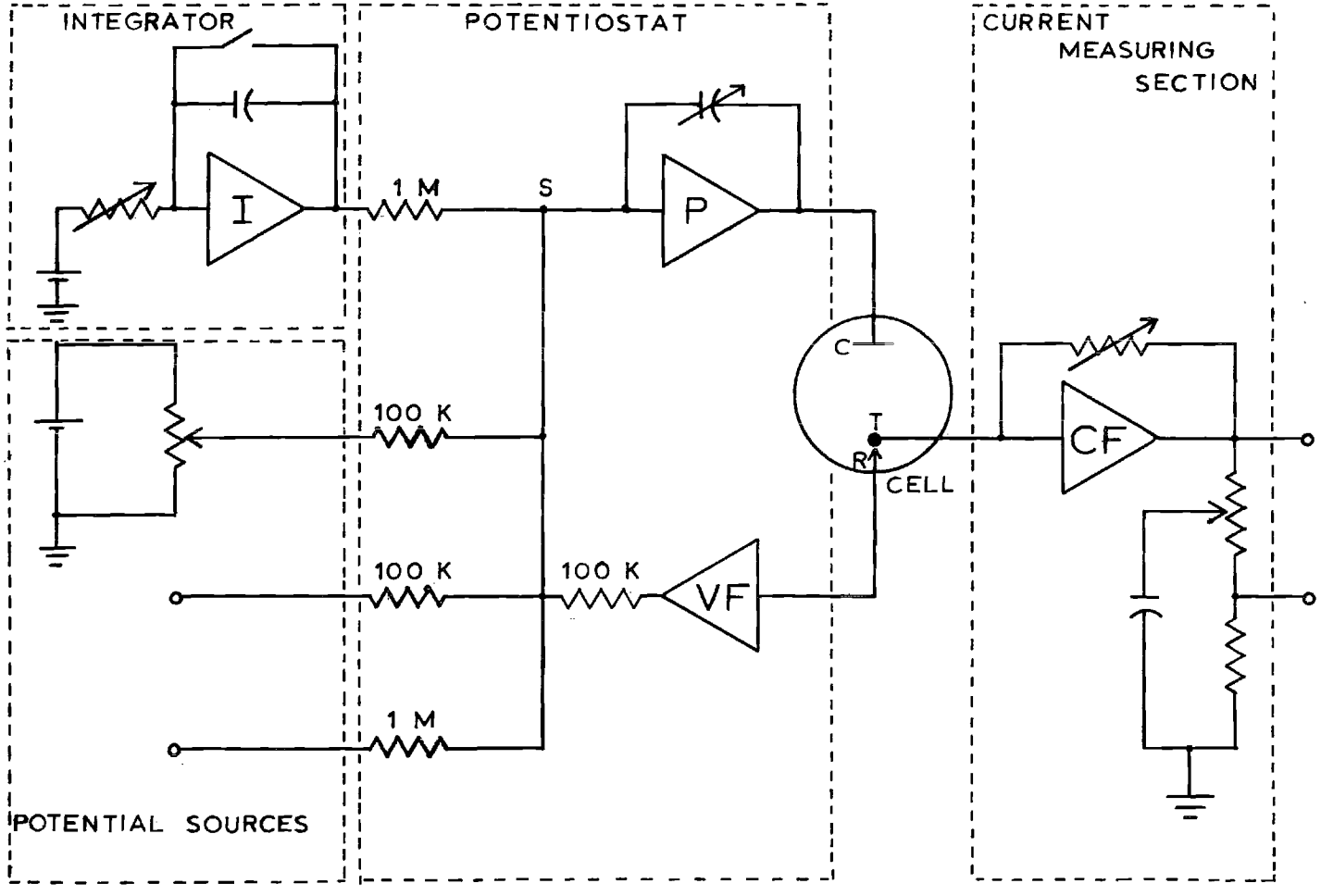

Figure 10. Controlled Potential Polarograph.

damping of the current signal at the attenuated output of the current follower. The integrator, consisting of amplifier I and its elements, furnishes a voltage which is attenuated 10-fold to reduce the effect of drift. The "initial potential" control allows the adjustment of the initial electrode potential over the entire range of interest, that is, -2 to +2 volts. A function switch, now shown, allows individual balancing of amplifiers by disconnecting the cell from the circuit. Certain features of Enke's instrument, including the constant current and linear current compensators, were excluded from this instrument.

A number of modifications was made to render the instrument more suitable to the type of experiments to be performed. Booster amplifiers were used with the potentiostat amplifier and the current follower to increase the allowable cell current by a factor of 10, so that 20 milliamperes could be drawn. The capacitor across the potentiostat amplifier was changed from fixed 100 pf to values variable from 25 to 225 pf to allow adjustment of the potentiostat for optimum risetime. With the cell arrangement used, the potentiostat risetime was typically 40 μ sec. without oscillation or overshoot. Potential steps used for these tests were as great as several tenths of a volt, which is higher than any potential steps used in the actual experiments.

Because of the desire for better drift control, Philbrick K2-PA chopper stabilizers were utilized (see Fig. 11 for circuitry). The stabilizer amplifiers were mounted on a separate chassis and received their power from an EUW-19A power supply. Shorting phone jacks were mounted in the chassis and connection was made between the operational amplifiers and the stabilizers by phone plugs and shielded

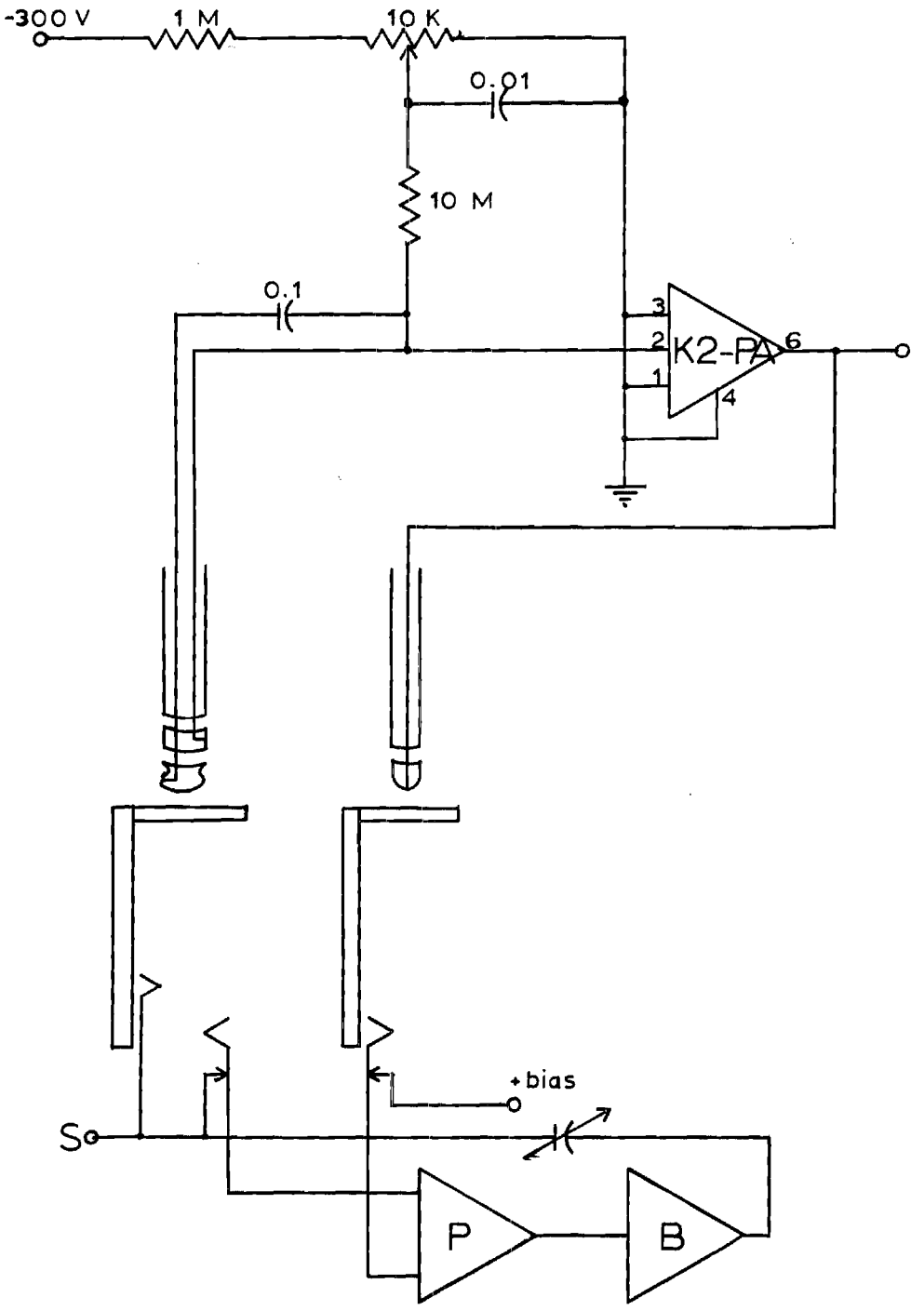

Figure 11. Schematic Diagram for Connection of Chopper Stabilizers.

cables. All amplifiers except the voltage follower were wired in this manner, allowing use of the amplifiers either with or without stabilization. It was found that stabilization resulted in drifts typically less than one millivolt/day.

Chronocoulometry requires the measurement of the current-time integral. Measurements are conveniently obtained by using an operational amplifier integrator. In order to function as such the ramp generator was converted by switching its input to the output of the current follower and its output to an external connection. Values of the resistance and capacitance of the integrating circuit were adjusted to have reasonable time constants. The previously mentioned chopper stabilizer was quite useful to prevent error being introduced into the integrator signal. Any offset would result in an ever-increasing integrator output, even in the absence of input signal. The type of stabilizer circuit used reduces offset to so nearly zero as to be negligible. Testing the stabilized integrator over periods much longer than ever encountered in actual chronocoulometric experiments showed no output signal at zero input voltage. The integrator was calibrated by applying a known voltage to a precision resistor in place of the cell and integrating the resulting current. The integrator output was observed directly with an oscilloscope. For chronocoulometry the operation of the integrator was controlled by a mercury relay. The "initial potential" circuit was modified by installation of a ten-turn control and a fine adjustment control to allow more precise adjustment of potential.

Time Delay Generator

For the purpose of making transient measurements with the three-electrode cell, an electronic controller was desired to facilitate operation of the controlled potential apparatus with respect to performing a number of closely spaced, synchronized operations. The instrument constructed consists of logic-type circuits and mercury relays. See Figure 12a for the elements of the circuit, designated by upper case letters. See Figure 12b for a non-linear time plot indicating the behavior of the various units of Figure 12a. These units in Figure 12a are designated by corresponding letters in Figure 12b. Since the electrode used was a dropping mercury electrode, all operations necessarily had to be predicated on its drop time. Therefore the functions of the generator are all initiated by a relaxation oscillator, that controls a solenoid for detaching the drop from the electrode. An internal resistor is provided by simple switching to replace the external solenoid. The relaxation oscillator is essentially a device which gives a sawtooth voltage, used here to trigger monostable vibrator B. The switching of the monostable vibrator B is indicated by line B, in Figure 12b. Line A is the oscillator period as seen by the solenoid. Line C represents the switching of a bistable oscillator used to control the relay coil. The bistable is triggered by B to activate the relay. It may be triggered in the reverse direction by A or by an external signal, as desired. Associated with relay 1 is a ten-turn potentiometer which may be used to adjust, between zero and ± one volt, the value of the potential step provided by relay 1. Line D indicates the appearance of the potential step relative to activation of the relay coil. The quantity of time d

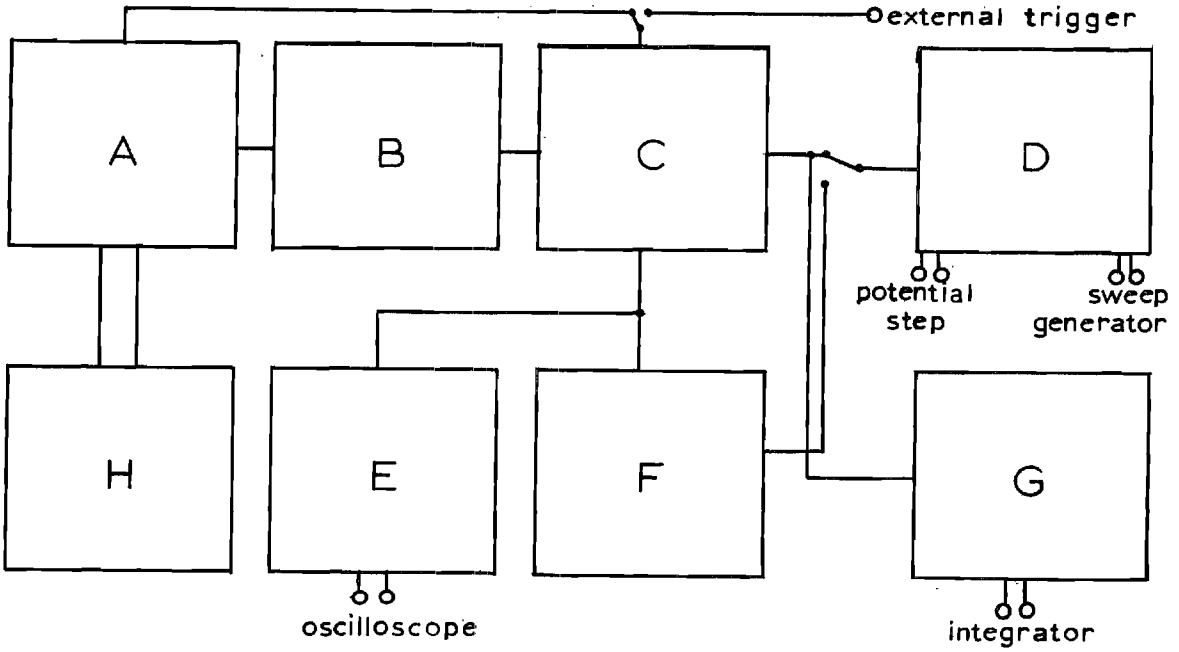

A. Adjustable Oscillator; Relaxation Oscillator.

B. Variable Time Delay; Monostable Vibrator.

C. Relay Controller; Bistable Multivibrator.

D. Relay 1; Single (D) or Double Potential Step (D'), Single-Sweep Operation of External Function Generator.

E. Variable Delay Oscilloscope Trigger; Monostable Vibrator.

F. Relay Controller; Monostable Multivibrator.

G. Relay 2; Operating Switch for Integrator.

H. Drop Detaching Mechanism.

Figure 12a. Polyfunctional Time Delay Generator. Block Diagram.

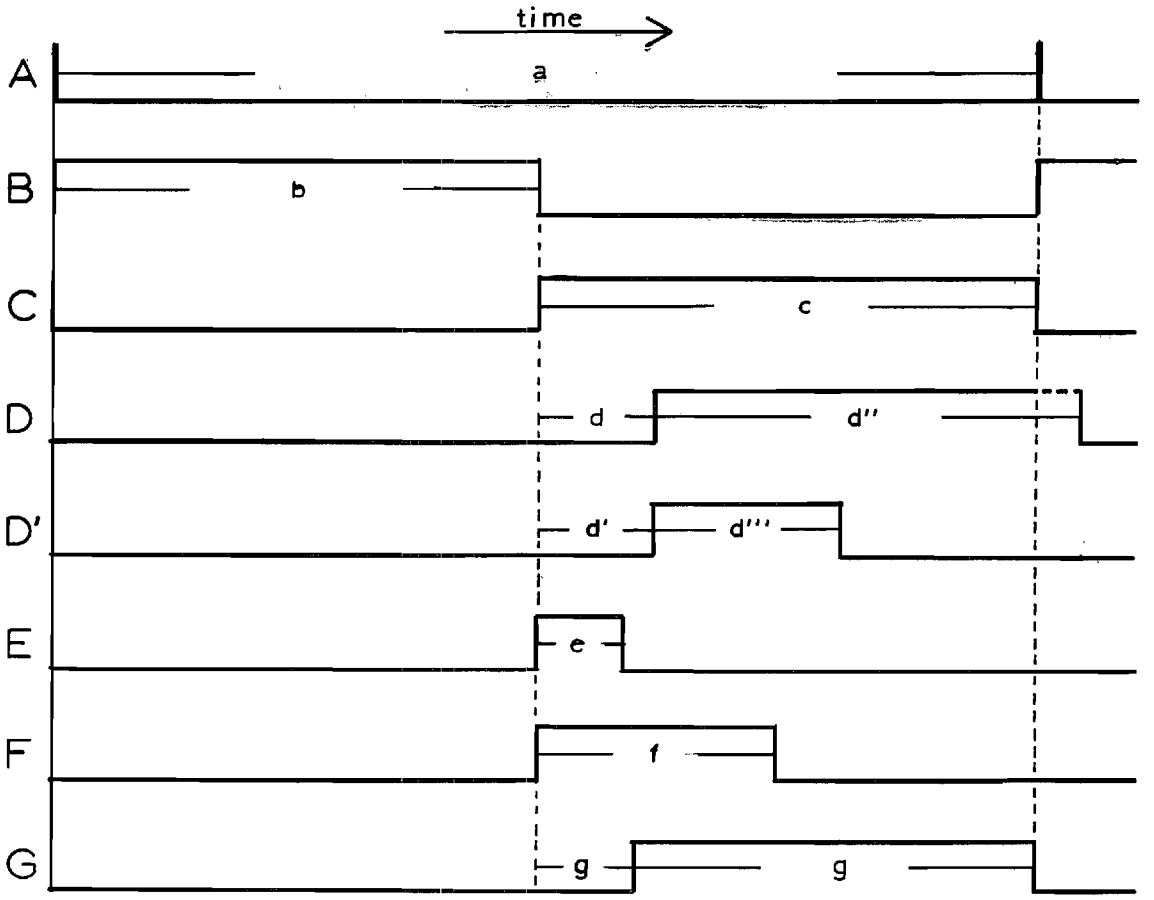

a. Oscillator Period. Variable Between 0.308 and 6.2 Seconds.

b. Initial Delay Time. Variable Between 0.26 and 5.1 Seconds.

c. Relay Controller 1 State Two. $c = a - b$.

d. Hysteresis in Relay 1. About 7 milliseconds.

d'' Duration of Single Potential Step. $d'' = c - d$.

d'. Hysteresis in Relay 1 During Double Step Operation. $d' = d$.

d''' Amount of Time Between the Forward and Reverse Potential Steps. Adjustable Between 0 and 250 Milliseconds.

e. Amount of Oscilloscope Trigger Delay. Adjustable, Set so that $e < d$ or $e < d'$.

f. Same as d''', Except That $f = d''' + d$.

g. Hysteresis in Relay 2. Fixed so that $g > d$, $g > d'$.

g'. Function Time of Integrator

Figure 12b. Polyfunctional Time Delay Generator. Plot of Functions.

is the amount of hysteresis between activation of the coil and appearance of the potential step. The oscilloscope used as a readout device must be triggered during this time interval. Since the times, after actual application of the potential step, when measurements were taken are 50 per cent less than the relay hysteresis time of seven milliseconds, monostable E was used to trigger the oscilloscope. The delay time e of monostable E is adjustable so that $e < d$. Relay 2 functions as a shorting switch that controls the electronic integrator used in chronocoulometry. The hysteresis of relay 2 was fixed to be less than d or d' so that the integrator would be on before any potential step was applied. In some applications a double potential step between fixed limits was desired and relay 1 may thus be switched to be controlled by the monostable vibrator F. Monostable F is triggered by the bistable C. The switching action of F is indicated by line F. The appearance of the double potential step is indicated by line D', with d'" being variable between about 3 and 250 milliseconds. Relay 1 may also be used to turn on the triangular sweep generator described herein. A voltage pulse from the sweep generator as it starts the second half of its cycle turns off the relay, thus allowing the generation of a single triangular wave. The same function of relay 1 may be used to activate a chronopotentiometer for doing single current reversal experiments. In each case the only limitation on frequency is the speed at which the relay can operate. The entire assembly was constructed of solid state components and is powered by a 12-volt lead accumulator. The circuits were all mounted in a metal cabinet to minimize noise pickup.

Triangular Sweep Generator and A.C. Polarograph

In initial phases of the present project survey work was done with A.C. polarography, and differential capacitance was studied with triangular sweep voltammetry. A dual purpose instrument was constructed with Heath EUW-19A Operational amplifiers and the Heath EUA-19-1 five-socket plug-in Blank Chassis. The chassis contained both an adapter for doing A.C. polarography and a triangular sweep generator. Each required only two operational amplifiers.

The A.C. polarographic section, based on ideas of Underkofler and Shain (58), contains two high gain amplification stages, a half wave diode rectifier, and a variable RC damping circuit. The input of the A.C. adapter was taken directly from the high level current output of the polarograph. A simplified circuit is presented in Figure 13, together with a calibration curve of the instrument. It was found that the output was proportional to the input as long as the output was greater than one volt.

The triangular sweep generator constructed was designed to give known constant rates of potential changes as required by triangular sweep voltammetry. A simplified diagram of the circuit is shown in Figure 14. A bistable multivibrator is used to generate a constant voltage. This voltage is integrated by an operational amplifier integrator to give a voltage ramp. The integrator may be adjusted to give different dE/dt values by adjusting the RC product. The bistable is triggered by the integrator output, thus reversing the slope of the ramp voltage and resulting in a triangular wave output. The voltage limit of the ramp is determined by an adjustable feedback to the bistable

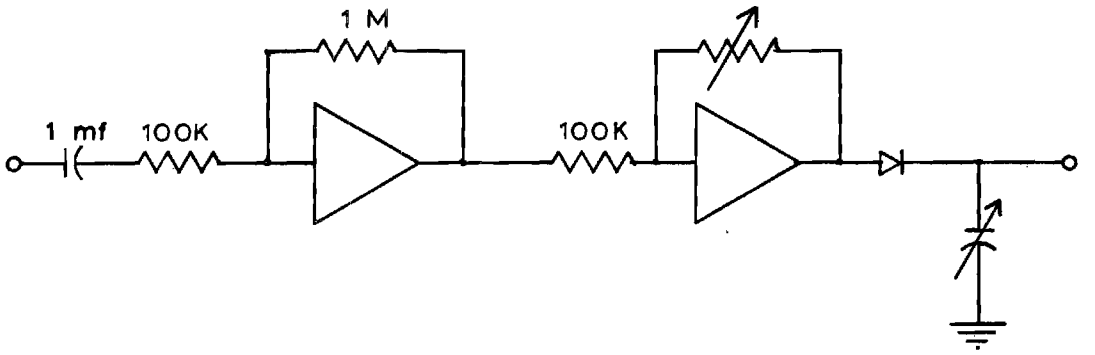

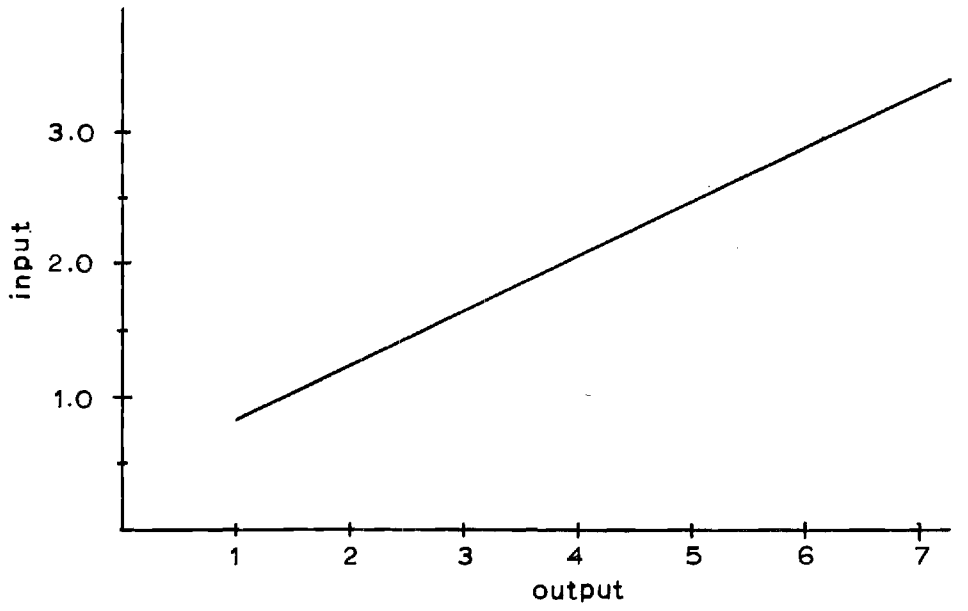

Figure 13. Schematic Diagram and Calibration Curve for A.C. Polarographic Module.

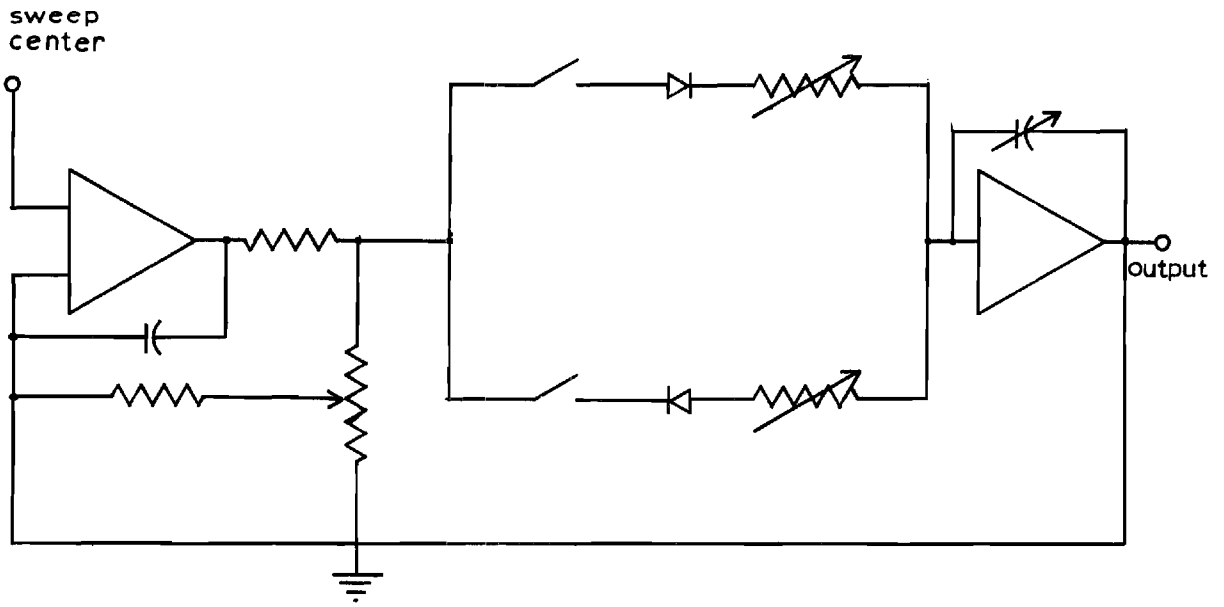

Figure 14. Triangular Sweep Generator.

amplifier, which allows any potential range between 0 and 20 volts to be selected. An additional feature of the circuit allows independent variation of the sweep rates in both directions. A total of 7 1/2 orders of magnitude of sweep rates is available. The range is from 5×10^{-2} volts sec^{-1} to 1×10^{5} volts sec^{-1}, more than normally used in any triangular sweep work. The sweep rates are attenuated by a factor of ten when presented to the input of the potentiostat of the controlled potential instrument.

Commercial Equipment

In addition to the self-constructed instrumentation, a number of commercial units were used in the investigation.

A Houston Instrument HR 96 T Time-Base and XY recorder was used for recording triangular sweep voltammograms, D.C. and A.C. polarograms, and A.C. current-time curves. It was also used for locating the equilibrium potential in cases where both halves of a metal couple were present. The precision of this unit is ± 0.25% of full scale, and since it was used ordinarily at the 0.1 volt $inch^{-1}$ sensitivity, the potential reading was precise to ± 2.5 millivolts.

A Tektronix 561A Oscilloscope was employed for current time curve measurement, for transient measurements in relaxation experiments, and for triangular sweep voltammetry where sweep rates were too large for an XY recorder. In the latter case a pair of 2A60 plug-in-amplifiers was used. These units have calibrated voltage ranges from 50 millivolts $division^{-1}$ to 100 volts $division^{-1}$ and a reliability of ± 3 per cent. For work involving a function of time, a 2B67 plug-in Time Base was used.

This unit has calibrated sweep rates from five seconds division^{-1} to 200 nanoseconds division^{-1}. Periodic recalibration of the Time Base Amplifier was performed to insure maximum accuracy. A 3A72 dual trace amplifier, modified to increase the chopping frequency, was used in the potentiostatic relaxation experiments to allow simultaneous observation of both the potential step and the resulting current transient. This unit has calibrated voltage ranges from 10 millivolts division^{-1} to 20 volts division^{-1}, and a reliability of ±3 per cent. A Tektronix C-12 oscilloscope camera with a Polaroid back was used to photograph traces. Polaroid 3000 speed roll film was used with this camera.

A Beckman model 1019 Research pH Meter was employed to measure pH and as a standard for all potentials generated by other circuits in the set-up. It is capable of measuring potentials to the nearest 0.2 millivolt without introduction of appreciable IR drop.

Chemicals

All chemicals employed were reagent grade material and used without further treatment. J. T. Baker "Analyzed" Reagent Grade potassium nitrate, potassium chloride, potassium hydroxide, nitric acid, sodium pyrophosphate, copper nitrate, mercuric nitrate, mercurous chloride, and triple-distilled mercury were used. Bethlehem Instruments triple-distilled pure mercury was also used on occasion. Difco Laboratories agar was employed for salt bridges.

A 2.0 F stock solution of potassium nitrate was prepared and diluted as needed. The maximum concentration employed in experiments was 1 F.

Saturated potassium chloride solution was prepared in small

quantities and used for making and refilling calomel reference electrodes.

1 F Potassium hydroxide and nitric acid solutions were prepared and kept in dropping bottles for pH adjustment.

A 0.2 F stock solution of sodium pyrophosphate was prepared and diluted as needed. Rose (51) has shown that pyrophosphate solutions are stable when stored in the alkaline form, as was done here. The rate of hydrolysis increases rapidly with increasing acidity. Low pH values were avoided until just prior to making measurements in acid solutions.

Agar salt bridges were prepared according to Meites (40) by dissolving 4 grams in 90 grams of water, heating gently until solution was effected, and adding 30 grams of potassium chloride to the agar solution. The reference electrodes were filled with an agar plug by placing them in the solution and allowing it to cool and thus solidify.

Copper amalgam for the amalgam electrodes was prepared by electrolytically reducing measured quantities of Cu (II) nitrate solution into known volumes of mercury. The amalgam finally used in measurements was 7.39×10^{-4} F in Cu (0). This concentration was determined from the polarographic anodic diffusion current found with the dropping amalgam electrode. The diffusion coefficient of Cu(0) in the amalgam was assumed equal to that of the aquo copper (II) ion.

Eastman tetramethylammonium chloride was used in some of the preliminary experiments.

American Cryogenics dry nitrogen was used to remove dissolved oxygen from the test solutions. The nitrogen was saturated with water vapor by passing it through a 1 F solution of potassium nitrate.

Kimax Class A pipettes and Exax volumetric glassware were used.

Water

Doubly deionized water was used for all solutions and for rinsing. It is known that adsorption of certain organic species such as ion exchange resin is a source of error in many electrochemical experiments. Distilled water was available, and it was tested for adsorbable impurities, as was water distilled from alkaline permanganate solution. The method of testing used was the observation of the double layer capacity change with time, as evidenced by a decreasing value of an AC current-time curve. This was done at different potentials. Measurements made with dropping electrodes were always performed within five seconds after the initial formation of the drop. Within this time there was no appreciable decrease in capacity at a new-formed hanging mercury drop electrode, regardless of which water was used to prepare the solution. With greater time periods the capacity decreases occurred in each solution, with not much difference being observed among the solutions. At least 120 seconds was required for equilibrium to be reached at a hanging drop electrode. Similar tests run with the organic surfactants octyl alcohol and alkanox showed much lower values of the capacitance per unit area. It was therefore concluded that even the worst cases of ion exchange resin adsorption did not correspond to film formation or blocking of the electrode reaction.

CHAPTER IV

REACTION INHIBITION BY ADSORPTION

A.C. Polarography and Tensammetry

In the initial phase of the project it was hypothesized that a possible cause of the anomalous characteristics of the polarographic wave of the alkaline copper pyrophosphate system was blocking of the electrode reaction by specific adsorption of some species of the system (18, 48). A.C. Polarography gives so-called tensammetric peaks (2) at potentials at which substances are adsorbed or desorbed, and was chosen as a survey tool for this study.

A.C. Polarograms were run for several systems in which no reducible species was present. The principal contention was to prove whether or not a species of the pyrophosphate ligand is adsorbed. Both the hanging drop and dropping electrodes were used for these experiments. The dropping electrode has only the lifetime of a drop to reach adsorption equilibrium, while the hanging drop has the entire experimental time (15 minutes or longer). Although such times are not important polarographically, they were used to see if any adsorption did exist.

In solutions containing sodium pyrophosphate along or in mixture with potassium nitrate or tetramethylammonium chloride, no tensammetric peaks were observed at potentials where the reduction of copper(II) occurs. Some non-reproducible peaks were observed at potentials greater than zero versus the S.C.E., but in this region no reduction occurs, and

any adsorption would be a problem only if it interfered with the oxidation of the copper amalgam. It is known (57) that no such interference occurs. If specific adsorption of pyrophosphate had occurred as possibly indicated by one of the small peaks mentioned above, it is extremely likely that also a desorption peak would appear at a potential not very negative of the electrocapillary maximum, since the ion has a large negative charge in alkaline solution and would soon be repelled by the electrode, also negatively charged at such potentials. However, no such desorption peak appeared.

The principal purpose for using tetramethylammonium ion was to achieve a connection between this and previous work on the system (57). It is known that the tetramethylammonium ion is adsorbed when the electrode is negatively charged. If adsorption of tetramethylammonium ion is appreciable tensammetric peaks should appear at some potential. The potential range covered was between one half volt positive and two and one half volts negative versus the S.C.E. No difference was noted between the results for system containing tetramethylammonium ion and those free of it. This disproves the possibility that the copper pyrophosphate D.C. polarograms showing anamalous behavior do so because of electrode blocking by adsorption of the tetramethylammonium ion.

If any tensammetric wave should have occurred due to nitrate adsorption at potentials greater than the electrocapillary maximum potential (44) the conclusion must be drawn that the peak was obscured due to mercury dissolution or some other effect. It has been shown (44) that there is a competing adsorption equilibrium between nitrate ion and water dipoles at these potentials. Such an adsorption, however, would

most likely manifest itself rather via double layer effects on reaction rate than by a blocking of the reaction. The same reasoning may be applied to the tetramethylammonium ion but at more negative potentials.

The Mercury (II)-Pyrophosphate complex is reduced at potentials more negative than zero volts versus the S.C.E. (59). The diffusion of this complex to the electrode would cause an enhanced concentration of pyrophosphate molecules at the electrode upon reduction, and therefore faster achievement of a possible slow adsorption equilibrium could be obtained. Upon addition of mercury (II) ion to some of the test solutions, no effect on the A.C. polarographic behavior was noted, meaning that transport or more ligand to the electrode surface did not produce any detectable increase in either the amount of adsorption or rate of adsorption, the latter being proportional to concentration.

Copper (II) ion was added in some cases to see whether an A.C. wave, corresponding to reversible D.C. polarographic behavior, would occur. It was expected that, in the copper-pyrophosphate systems, an A.C. wave would be obtained at either about -0.1 volt or about -1.3 volts versus the S.C.E. At these potentials the D.C. polarogram shows definite rises. No A.C. waves were noted with copper (II) present, indicating that "normal" polarographic reversibility is not achieved in this case.

Triangular Sweep Voltammetry

Qualitative Observations

A series of triangular sweep experiments was performed with sodium pyrophosphate solutions. The concentration of these solutions ranged between 0.1 F and 0.001 F. The influence of the variation of pH was

studied to a small extent but the principal investigation employed alkaline solutions of reasonably constant pH. In addition, a series of experiments was performed in 1 F potassium nitrate with the concentration of pyrophosphate varying between zero and 0.1 F. Various types of studies involved both the hanging drop and dropping electrodes. The goal of these experiments was to determine whether or not any adsorption could be detected.

The general appearance of the double layer capacity curve is that given by Figure 15. The cathodic capacity peak occurs at -1.35 volts versus the S.C.E. This peak is in the general region where peaks resulting from the desorption of some species occur. The behavior of the capacity at the peak potential and at other points was studied vs. time. Adsorption lowers the capacity, and a significant lowering at any potential could be used to confirm adsorption at this potential.

A series of experiments was also performed with mercury (II) ion in solution in order to study the enhancement effect discussed in the previous section.

Results

Using the hanging drop electrode, a series of experiments was performed with 0.1 F pyrophosphate. The electrode potential was held at -0.20 volts between the application of single triangular sweeps at known times. If any adsorption had occurred, the capacity should have decreased at potentials below that of the peak and the value at the peak should have increased. Such behavior was found, as shown in Table 1. Adsorption is therefore indicated. However, the apparent time for adsorption equilibrium, more than 200 seconds, is not compatible with

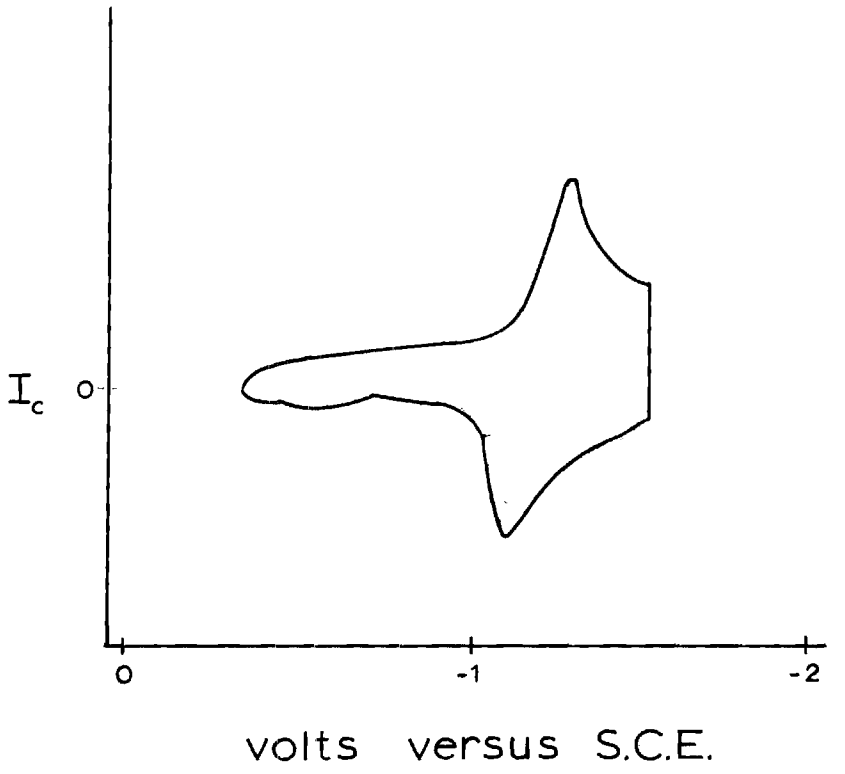

Figure 15. Differential Capacity Curve for Sodium Pyrophosphate.

the amount of material present if pyrophosphate ion is the species adsorbed. The time for attainment of a kinetically controlled adsorption equilibrium would be small for 0.1 F solution. For a diffusion controlled adsorption process equilibrium would be reached almost instantaneously.

In a series of experiments the capacity of a dropping electrode in 0.1 F sodium pyrophosphate was measured as a function of the time during the life of a drop. Prior to sweep initiation the electrode potential was held at different values in different sets of experiments. The results are given in Table 2. The most reliable results are those with an initial electrode potential of -0.36 volt, but in each case there is clearly no decrease in the capacity values. An increase in the peak value would possibly indicate some adsorption, but only the increase in the last column is at all significant.

As a further test, the values of the capacity at -0.80 volt were tabulated from the same determinations. The results are given in Table 3. Slight decreases are observed in the first and last cases. However, no definite trend can be established. The estimated error in reading the scale on the oscilloscope is at least ± 3 per cent of full scale, the possible error on the reading approaches 40 per cent. However, changes are still plainly visible in the curves. Their best explanation is that the capacity of the electrode is essentially unaffected by any species in the solutions. See Figure 16. The sets of data with the electrode initially at -0.20 and -0.65 volts represents nearly isotension points on the electrocapillary curve* in 0.1 F pyrophosphate, and

*Isotension points on an electrocapillary curve are potentials at which the surface tension of the interface at the electrode is the same.

Table 1. Values in $\mu f. cm.^{-2}$ of the Capacitance per Unit Area of a Hanging Mercury Drop Electrode in 0.1 F Sodium Pyrophosphate Solution

Age of Drop, sec.	Potential volts	Capacity per unit area	Peak Potential volts	Capacity per unit area
4	-0.60	16.5	-1.31	74
65	-0.60	11	-1.32	78
120	-0.60	10	-1.33	85
190	-0.60	9	-1.33	87

Table 2. Values in $\mu f. cm.^{-2}$ of the Capacitance per Unit Area at the Potential of the Capacity Peak of the Dropping Mercury Electrode in 0.1 F Sodium Pyrophosphate

	Potential Prior to Initiation of the Sweep		
Age of Drop	-0.20 volt	-0.36 volt	-0.65 volt
1 second	28.7	----	----
2 second	28.3	31.9	22.4
3 second	29.7	33	26.9
4 second	27.4	33	28.3
5 second	25.4	32	29.7
6 second	33	33	32.6
7 second	32.3	34	34.5

Table 3. Values in $\mu f. cm.^{-2}$ of the Capacitance per Unit Area of the Dropping Mercury Electrode in 0.1 F Sodium Pyrophosphate at a Potential of -0.80 Volts Versus S.C.E.

	Potential Prior to Initiation of the Sweep		
Age of Drop	-0.20 volt	-0.36 volt	-0.65 volt
1 second	20.7	----	----
2 second	18.8	17.4	15.2
3 second	18.7	17.3	14.3
4 second	18.3	16.4	13.7
5 second	16.8	17.2	13.7
6 second	18.1	17.4	13.5
7 second	17.9	17.6	13.2

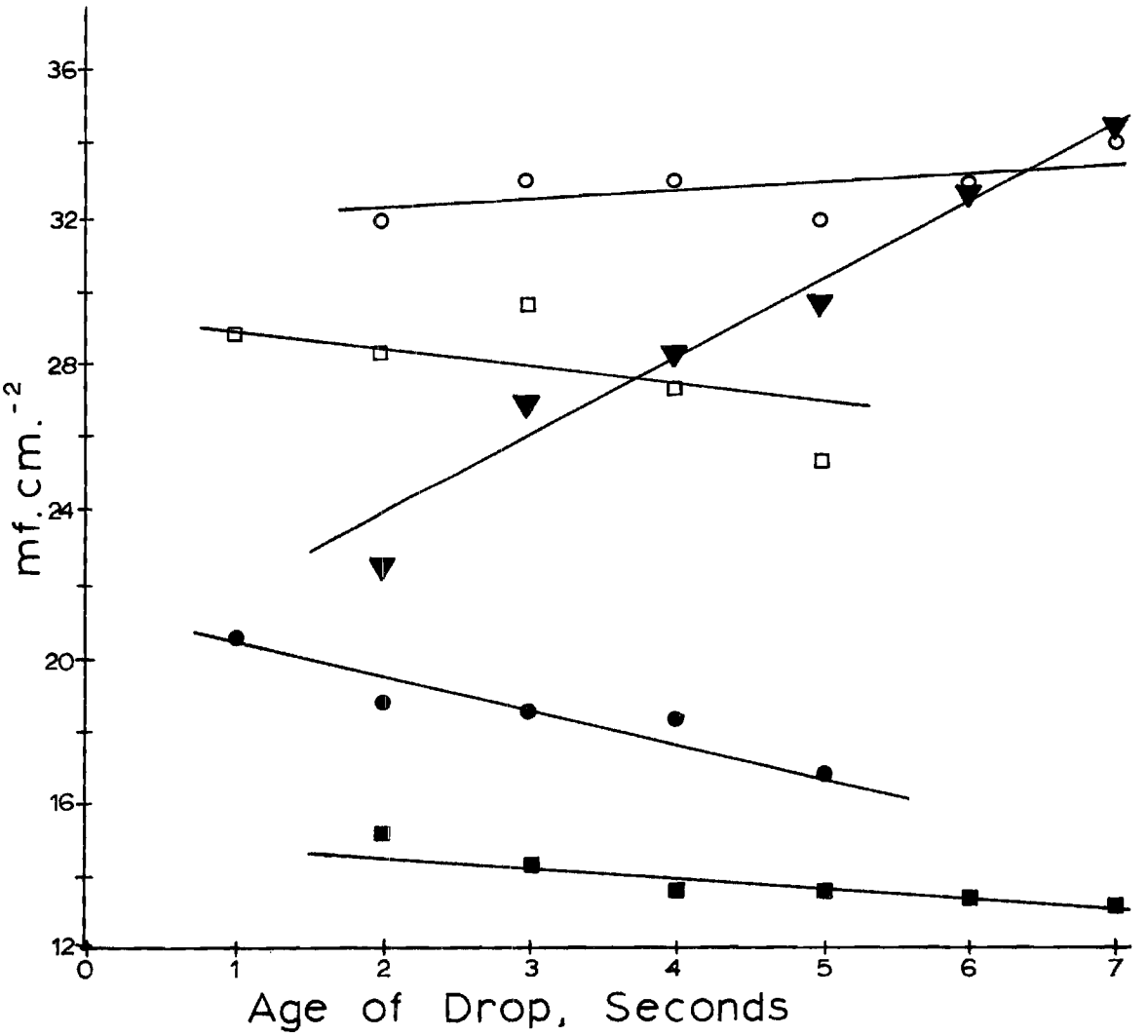

○ E_i = -0.36 ; E_{dl} = -1.3

□ E_i = -0.20 ; E_{dl} = -1.3

▼ E_i = -0.65 ; E_{dl} = -1.3

● E_i = -0.20 ; E_{dl} = -0.80

■ E_i = -0.65 ; E_{dl} = -0.80

Figure 16. Capacitance per Unit Area of a Dropping Electrode in 0.1 F Sodium Pyrophosphate.

adsorption of a neutral species would be approximately the same at either potential. If an adsorbed species were ionic, it would be adsorbed more on the side of the electrocapillary curve where the electrode has a charge sign opposite that of the ion. If the adsorbed species were pyrophosphate ion, it should be expected to show less adsorption on the negative side. If the species were a neutral substance such as an ion exchange resin particle, maximum adsorption should occur near the electrocapillary maximum.

Another series of experiments employed the hanging drop electrode and different concentrations of pyrophosphate. In all cases the potential of the electrode was held at -0.36 volt between sweeps. The increase with time of the capacitance peak was followed for long periods. The results are listed in Table 4 and plotted in Figure 17. Again no definite trend can be established, but the data seem to indicate that the decrease of slope corresponding to the approach of adsorption equilibrium is not a function of the pyrophosphate concentration.

In experiments in which mercury (II) ion was added to pyrophosphate solution to test for additional and faster lowering of the capacity corresponding to an increasing surface concentration of pyrophosphate, the hanging drop electrode was used and the experiment performed as previously. In this case the measured current also contained a Faradiac component resulting from the reduction of mercury. The latter component was reasonably constant at potentials more cathodic than -0.3 volt. Plots of the capacitance peak versus drop age did not show perfect consistency, but their general shape was nearly the same as that of Figure 17, and there seemed to be no difference between curves obtained with

Figure 4. Capacitance per Unit Area in $\mu f.cm.^{-2}$ of a Hanging Drop Electrode at -1.30 Volts as a Function of Pyrophosphate Concentration and Electrode Age.

Age of Drop in seconds	Pyrophosphate Concentration 0.1F	0.01F	0.001F
15	31	--	--
20	--	44	42.7
30	32	--	--
50	33	--	--
80	37	47	44.3
120	42	--	--
150	--	49	46.0
250	--	--	48.3
300	--	53	--
400	--	--	53.3
600	--	56	56.0
1000	--	60	56.3

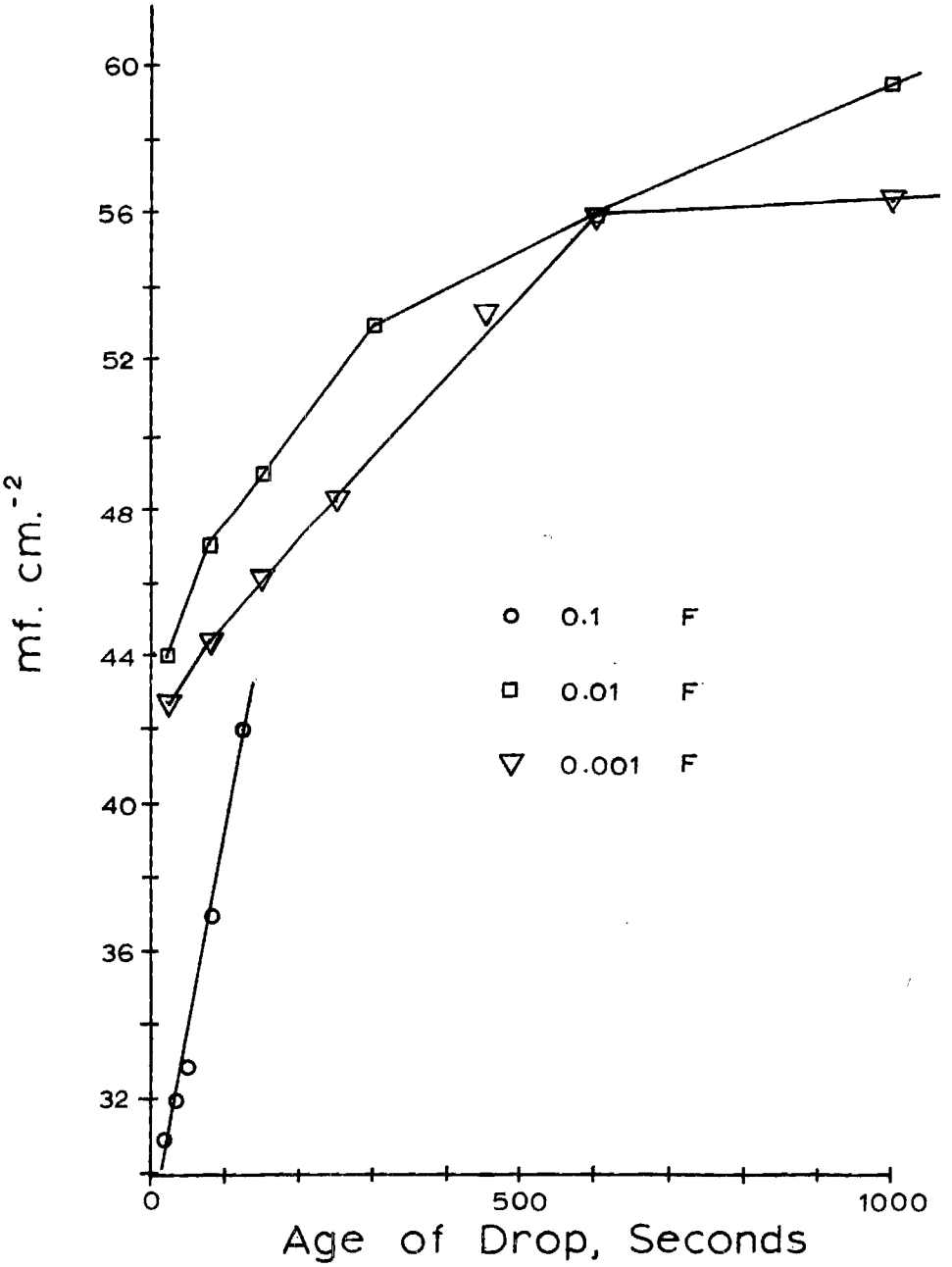

Figure 17. Capacity per Unit Area of a Hanging Mercury Drop Electrode as a Function of Pyrophosphate Concentration.

mercury ion present and those obtained in its absence. In addition, the order of magnitude of the time interval required for a certain decrease in slope about (300-500 seconds), was the same in each case.

Measurements for the series with mercury (II) present were first performed at constant ionic strength adjusted with potassium nitrate. An analagous series was then run in the absence of potassium nitrate in order to detect any effect of the nitrate ion. None was found.

As a concluding test, the differential capacities of a dropping mercury electrode in 1 F potassium nitrate solutions were determined at several potentials as a function of the sodium pyrophosphate concentration and the age of the drop. The results are given in Table 5. It can be seen that within each series the capacitance is either approximately constant or increases slightly with the drop age. If adsorption were occurring, it would be expected in this potential range, and would be indicated by a decrease in capacity with an increase in concentration. Clearly no such trend is indicated.

Thus it is concluded, from triangular sweep data, that no appreciable adsorption of any pyrophosphate species existing in alkaline solution takes place. It must be kept in mind that the accuracy of this method of capacity measurement is somewhat below that of other methods. The last set of data presented is the most reliable from the standpoint of experimental techniques. Larger oscilloscope deflections were used, and time measurement and step application were much more accurate and precise, respectively. The changes in capacity found in

Table 5. Capacitance per Unit Area in $\mu f.cm.^{-2}$ of a Hanging Drop Electrode at -1.30 Volts as a Function of Pyrophosphate Concentration and Electrode Age

Concentration of Pyrophosphate	Potential of Measurement, Volts	Drop Age, Seconds					
		0.142	0.365	0.96	1.60	2.40	3.55
0	-0.20	18.7	20.1	20.1	20.4	20.3	20.6
	-0.40	22.6	24.9	23.7	24.6	24.4	24.7
	-0.60	24.7	25.6	25.4	25.7	25.7	26.0
2 mF	-0.20	18.1	19.0	20.4	21.4	21.1	21.7
	-0.40	23.5	25.4	25.3	26.0	26.1	26.8
	-0.60	24.7	26.8	26.1	26.6	26.6	27.2
0.01 F	-0.20	20.5	22.5	22.1	22.7	22.6	22.8
	-0.40	27.1	28.9	28.6	28.1	28.4	28.6
	-0.60	27.1	28.6	27.4	27.5	27.5	27.8
0.10 F	-0.20	18.7	20.9	20.2	20.8	20.6	21.2
	-0.40	24.1	25.6	24.5	25.1	23.8	25.5
	-0.60	27.1	27.3	26.3	26.9	26.6	27.2

the earlier experiments are attributable to traces of adsorbable material, since no effort was made to rid the reagents and water of such materials. All measurements eventually employed in the interpretation of polarograms were made with dropping electrodes, within a few seconds after the drop begin to form. Data presented here indicate that, under such conditions, no adsorption effects are noticeable.

Electrocapillary Results

Electrocapillary Curves

Electrocapillary Maximum (ECM) Potentials. Although the drop-time method of determining electrocapillary curves does not allow accurate location of the ECM potential, certain other aspects of the curves may still be recognized. Large shifts of the ECM will be detected easily, and surface tension changes, corresponding to adsorption, will appear as long as the capillary is not moved or the mercury head disturbed.

An electrocapillary curve was obtained for 1 F potassium nitrate made alkaline to a pH of nine by the addition of potassium hydroxide. Then the solution was made 0.01 F in sodium pyrophosphate and another curve obtained. After making the solution 2 mF in Cu (II) a third curve was obtained. The results are presented in Figure 18. Comparison of curves a and b indicate that the pyrophosphate ion is not adsorbed. Curve c indicates that the copper(II)-pyrophosphate complex is also not adsorbed. If adsorption did occur, it would be most noticeable on the electrocapillary curve at potentials anodic to the reduction wave, but could also affect the curve at other potentials. Unfortunately, the

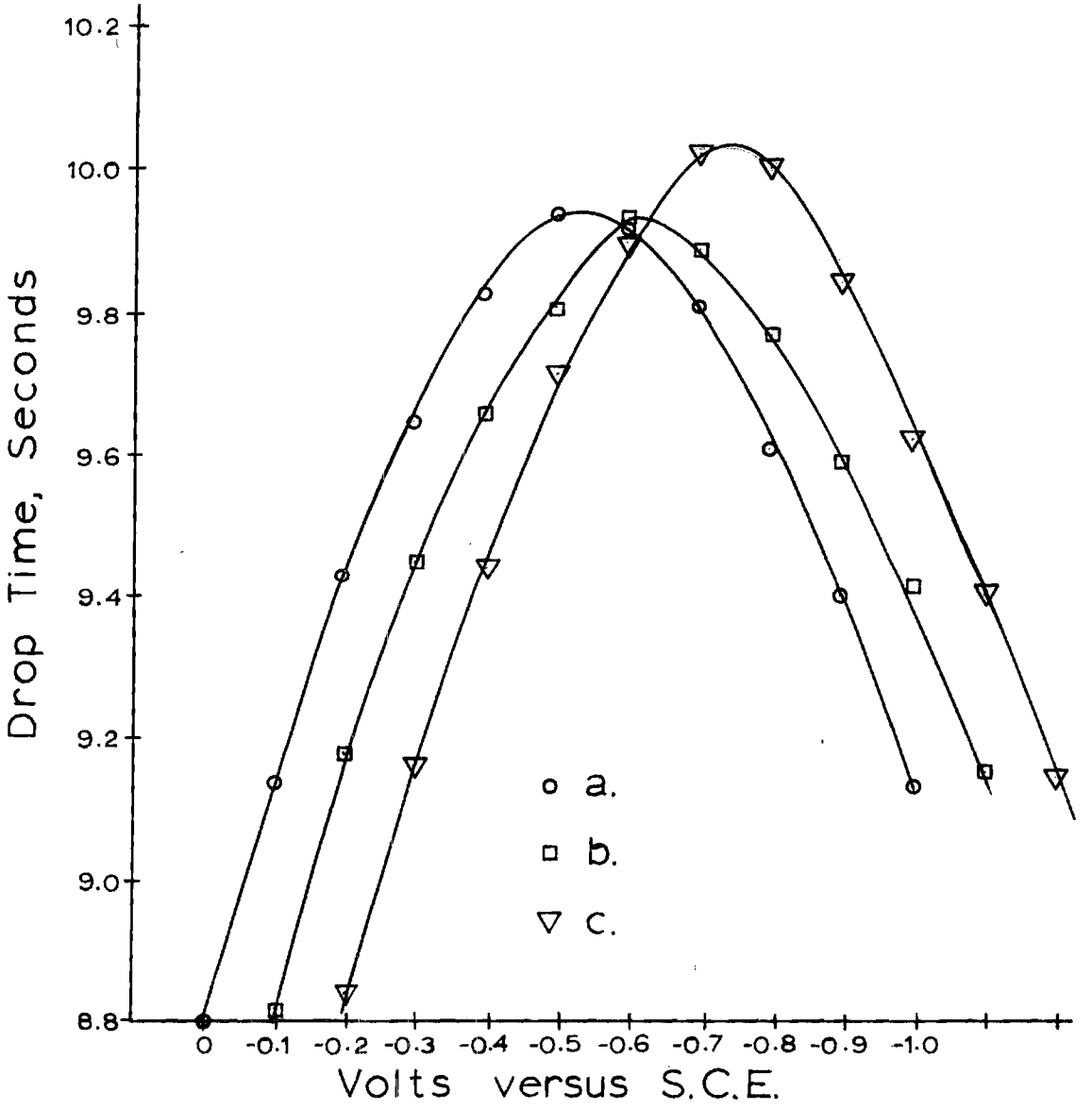

a. 1.11 F KNO_3

b. 1.0 F KNO_3 + 0.01 F Pyrophosphate; Shifted by -0.10 volt

c. 1.0 F KNO_3 + 0.01 F Pyrophosphate + 2.0 mF Cu(II); Shifted by -0.20 volts.

Figure 18. Electrocapillary Curves for Alkaline 1 F Potassium Nitrate.

potential range between the point anodic with respect to the first complex reduction wave and that cathodic to the oxidation of the electrode is rather small in the complexing pyrophosphate medium. For this reason, the electrocapillary curve was not measured at potentials more positive than zero. There is also no indication of adsorption of the negatively charged complex in the potential range within which there is both reduction and a positively charged electrode.

For 1 F potassium nitrate, the ECM potential obtained from each of the curves in Figure 18 is -0.54 ± 0.01 volts versus the S.C.E. The value obtained from another electrocapillary curve is -0.52_7 ± 0.01 volts. The value obtained from a measurement with the streaming mercury electrode in the absence of copper is -0.519 volts. The only value reported in the literature (39) for this quantity is -0.520 volts, the accuracy of which is somewhat doubtful. Nonetheless, there is fair agreement in the case of the values obtained from the electrocapillary curves, and good agreement in the case of the streaming electrode potential measurement. The latter value was reproducible to ± 0.4 millivolts, a fact which lends credibility thereunto.

A somewhat more accurate check of the measurement of ECM potentials is afforded in the case of 0.1 F potassium nitrate solution. The reported value (5) of the ECM potential of a mercury electrode in 0.1 F potassium nitrate solution is -0.478 volts. The streaming electrode value was -0.477 volts, an agreement within one millivolt. The electrocapillary curve yielded a value of -0.472 volts, within five millivolts of the reported value. These facts confirm the validity of the streaming electrode technique.

The difference between an ECM potential measured with the streaming electrode and one obtained from the drop-time electrocapillary curve is attributable to the electrocapillary curve. The shape of a curve is reproducible but the location of its maximum is somewhat uncertain, because points taken in that region scatter considerably. Since the dropping electrode is especially temperamental at the low mercury heights necessarily employed, it was found that the best way to avoid extreme scattering was to obtain all points within a reasonably short time. No part of the electrode assembly should be touched during the complete recording of all the curves in one series.

The value of the ECM potential to be expected in the absence of adsorption is -0.435 volts (11). This value was obtained employing solutions of sodium and potassium fluorides. The published values of ECM potentials had been measured against a 1 F calomel electrode and corrected for the liquid junction potential. The published values listed here are given versus the saturated calomel electrode, and are thus numerically 39 millivolts less than originally reported. The experimental values taken with the streaming electrode were not corrected for the liquid junction potential. Since the liquid junction potential is expected to increase as the concentrations on either side of the boundary become more nearly the same, a greater potential would be expected with the 1 F nitrate solution than with the 0.1 F one. The experimental streaming electrode potentials agree with the published values of the ECM within one millivolt, so that there appears to be no appreciable error arising from the liquid junction.

Electrocapillary curves were determined in the same manner with

a 0.1 F solution of sodium pyrophosphate alone and with the same solution made 2.0 mF in copper(II) ion. The results are given in Figure 19. The location of the ECM for the pyrophosphate is -0.428 volts and that for the pyrophosphate plus copper is -0.436 volts, a change of only eight millivolts. In the former case the potential is below that normally expected in the absence of adsorption. The ECM potential of 0.1 F sodium pyrophosphate as determined with the streaming electrode is -0.428 volts. This value agrees with that from the electrocapillary curve. The ECM measured in 0.2 F pyrophosphate solution was -0.427 volts. Cationic adsorption shifts the ECM to more positive values, and it might be that a slight amount of adsorption, either of potassium ion, or more likely of ion exchange resin, took place. There is also the possibility that a trace amount of reducible impurity was present. This would have also caused a slight anodic shift.

Electrode Charge. The charge on the electrode as a function of potential is given in Table 6 and is plotted in Figure 20 for different potassium nitrate concentrations. This charge, needed for the calculation of the potential drop across the diffuse double layer, was calculated from the slope of the electrocapillary curves at different potentials. The rational potential φ is the potential relative to the ECM potential of each solution. The curve agrees reasonably well with published ones (1). The slightly smaller value of the accumulated charge at a given φ for the 1 F solution indicates that there is some specific adsorption of nitrate. This is an expected result (see following section).

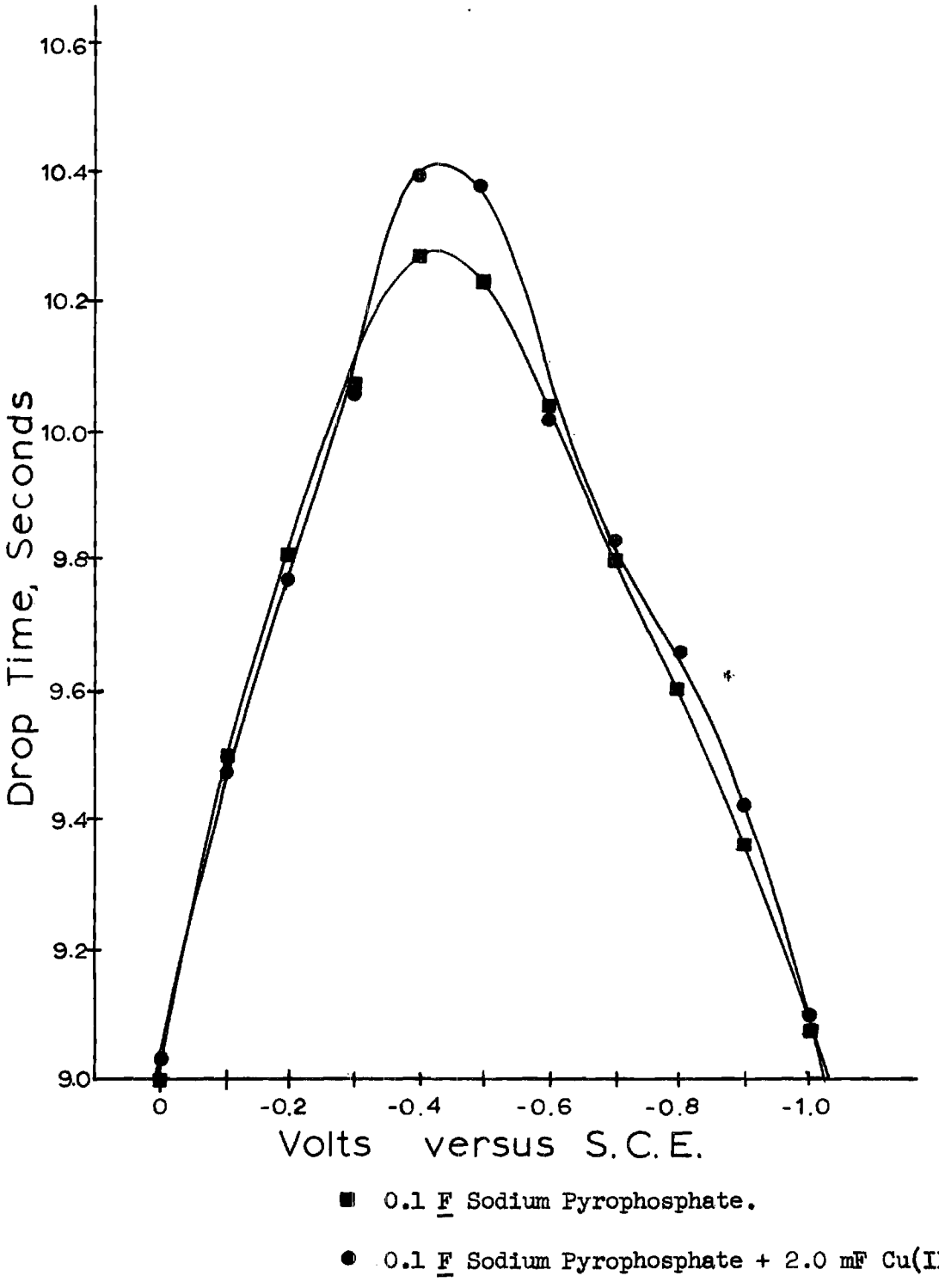

Figure 19. Electrocapillary Curves for Sodium Pyrophosphate.

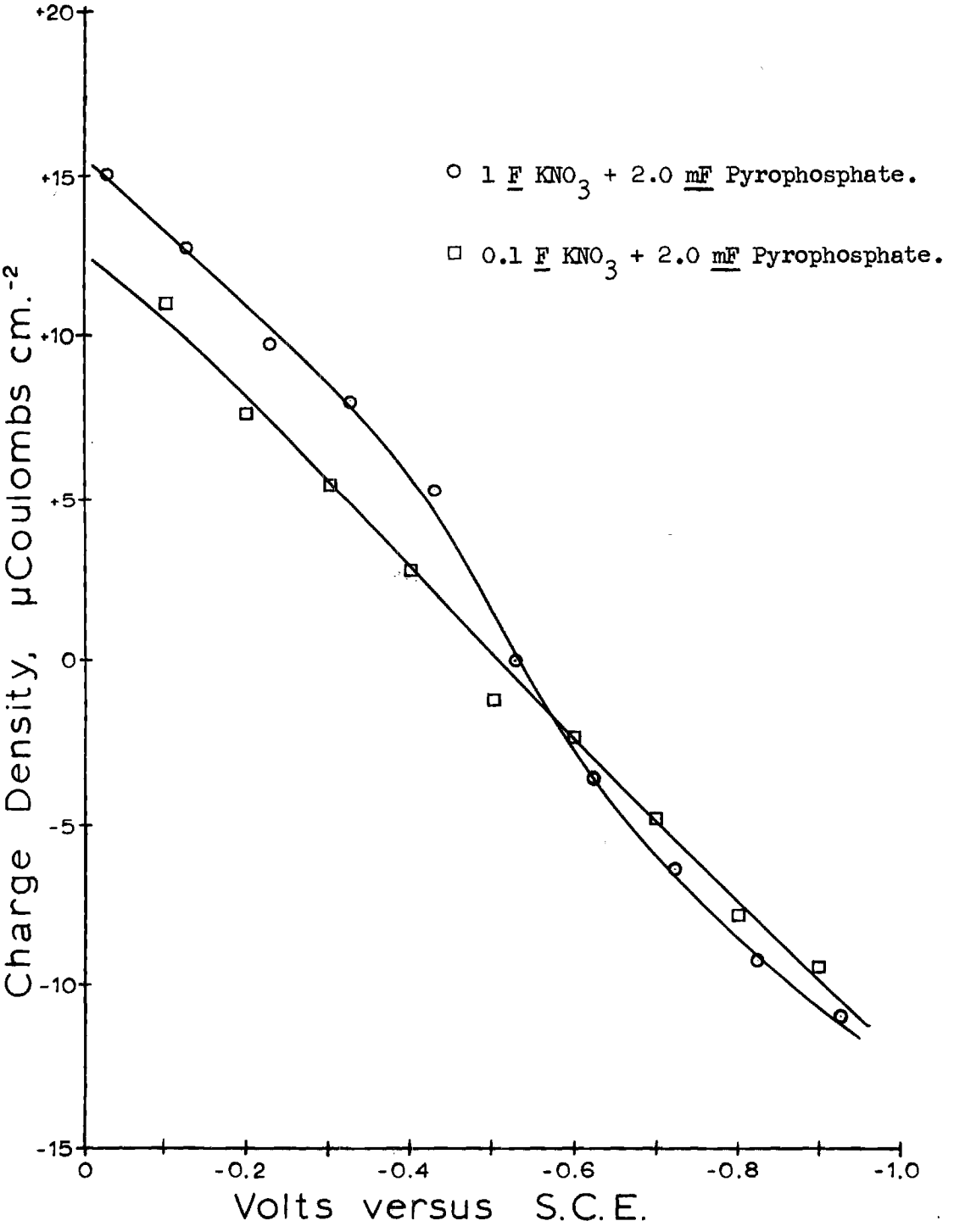

Figure 20. Charge Density Versus Electrode Potential for a Mercury Electrode in Aqueous Potassium Nitrate.

Table 6. Charge Density in μ Coulombs $cm.^{-2}$ on a Mercury Electrode in Potassium Nitrate Solution

1 F Nitrate			0.1 F Nitrate		
E vs SCE	Charge Density	φ	E vs SCE	Charge Density	φ
-0.027	15.03	0.500	-0.100	11.12	0.375
-0.127	12.80	0.400	-0.200	7.71	0.275
-0.227	9.80	0.300	-0.300	5.46	0.175
-0.327	8.11	0.200	-0.400	2.81	0.075
-0.427	5.28	0.100	-0.500	- 1.25	-0.025
-0.527	0	0	-0.600	- 2.34	-0.125
-0.627	- 3.59	-0.100	-0.700	- 4.87	-0.225
-0.727	- 6.88	-0.200	-0.800	- 7.83	-0.325
-0.827	- 9.21	-0.300	-0.900	- 9.46	-0.425
-0.927	-10.90	-0.400			

The Esin and Markov Effect

Sodium Pyrophosphate. The existence of the specific adsorption of an electrolyte at an electrode is indicated by the Esin and Markov effect. This effect is the shifting of the electrode potential with concentration, at any value of the electrode charge. The equation describing this behavior is

$$E_r = E \pm \frac{1}{zf} \ln a + \text{constant} \qquad (4\text{-}1)$$

where a is the activity of the electrolyte in question and the liquid junction potential is assumed to be constant. In this equation E represents the electrode potential in a cell without liquid junction. If concentration is assumed proportional to activity, a plot of ECM potential versus electrolyte concentration should yield a straight line.

The potential of the streaming mercury electrode (E_r in eq. 4-1) did not change with concentration of sodium pyrophosphate. In one approach sodium pyrophosphate was added to a 1 F solution of potassium nitrate and the potential was measured after each addition. In the other approach sodium pyrophosphate was added progressively to a dilute solution of pyrophosphate and the potential was measured. No shift of potential was observed with either approach. This is very strong evidence against the existence of specific adsorption of pyrophosphate. The test, applicable at any constant value of the electrode charge, is most reliable at or near the zero charge point (13).

Potassium Nitrate. The potential of a streaming electrode in potassium nitrate solution varies with the concentration. The results are shown in Figure 21. Since the potential shift is toward more cathodic values, specific adsorption of the nitrate ion is indicated. Recent evidence proving nitrate adsorption has been given by Payne (44).

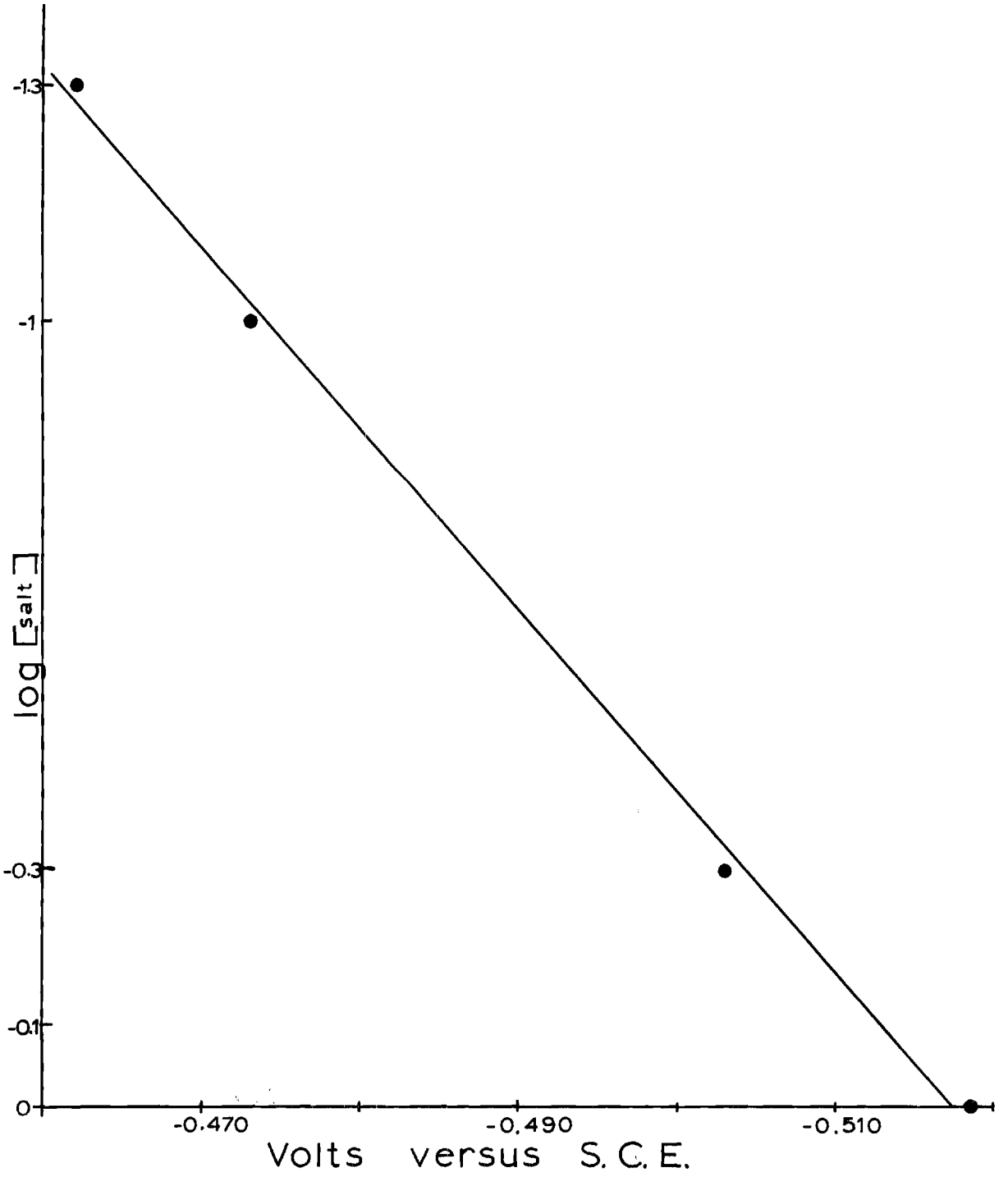

Figure 21. The Esin Markov Effect for Potassium Nitrate.

A plot of Payne's values of the specifically adsorbed charge q^1 versus concentration for q = 0 is given in Figure 22. For a 0.5 F solution, a value for q^1 of 9.85 μ coulombs $cm.^{-2}$ was read from this plot, since none was given by Payne. This value was included with the other q^1 values at q = 0 and the values were then plotted against the electrode potential. This plot, for q = 0 and for three other values of q, is given in Figure 23. The plot for q = 0 appears to be linear, although its $q^1 = 0$ intercept is 16 millivolts less than -0.435 volts, the value expected in the absence of adsorption. For each value of q the slope of the q^1 versus E plot is approximately constant, so that a reasonable prediction of the potential shift with concentration at a particular electrode charge may be made. Payne's results also indicate that, in concentrated solution, some nitrate adsorption occurs even when the electrode is negatively charged; however, the amount is relatively small except in 1 F solution, where q^1 is still about 2 μ coulombs $cm.^{-2}$ at q = - 10 μ coulombs $cm.^{-2}$.

It is therefore expected that the adsorption of nitrate affects the electrode reaction. The effect of this adsorption is probably different in nature on opposite sides of the ECM. This will be discussed in detail along with the Gierst analysis of polarograms. It is not thought, however, that reaction blocking occurs because of this adsorption. Whenever the electrical double layer exists there are at least two layers of adsorbed ions or dipoles at the electrode surface, in the Helmholtz planes. There is also a three-dimensional region around the electrode within which ions of one charge are predominantly accumulated. In the case of nitrate adsorption the adsorbed ions, present in the

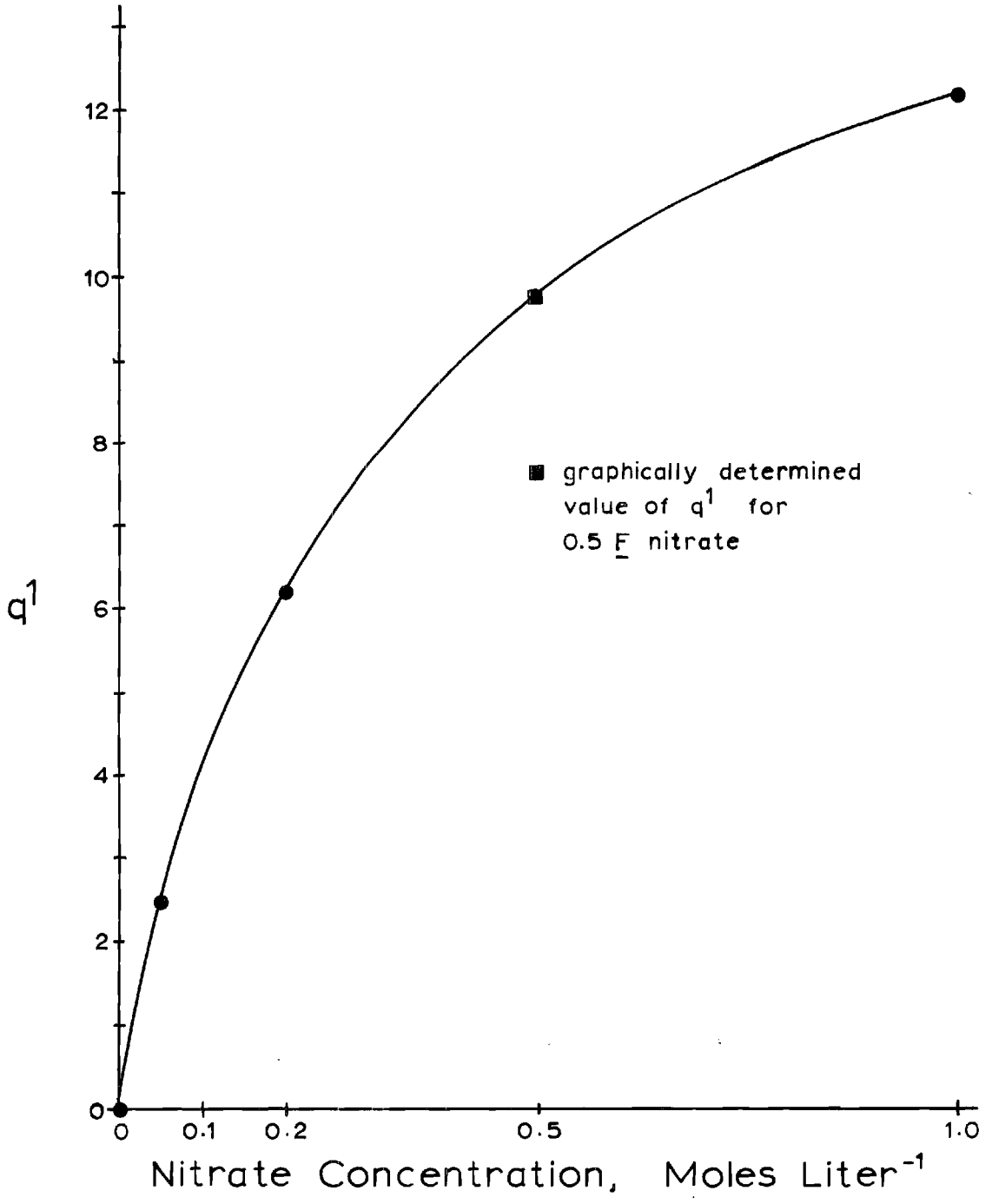

Figure 22. Specifically Adsorbed Charge q^1 Versus Nitrate at q = 0.

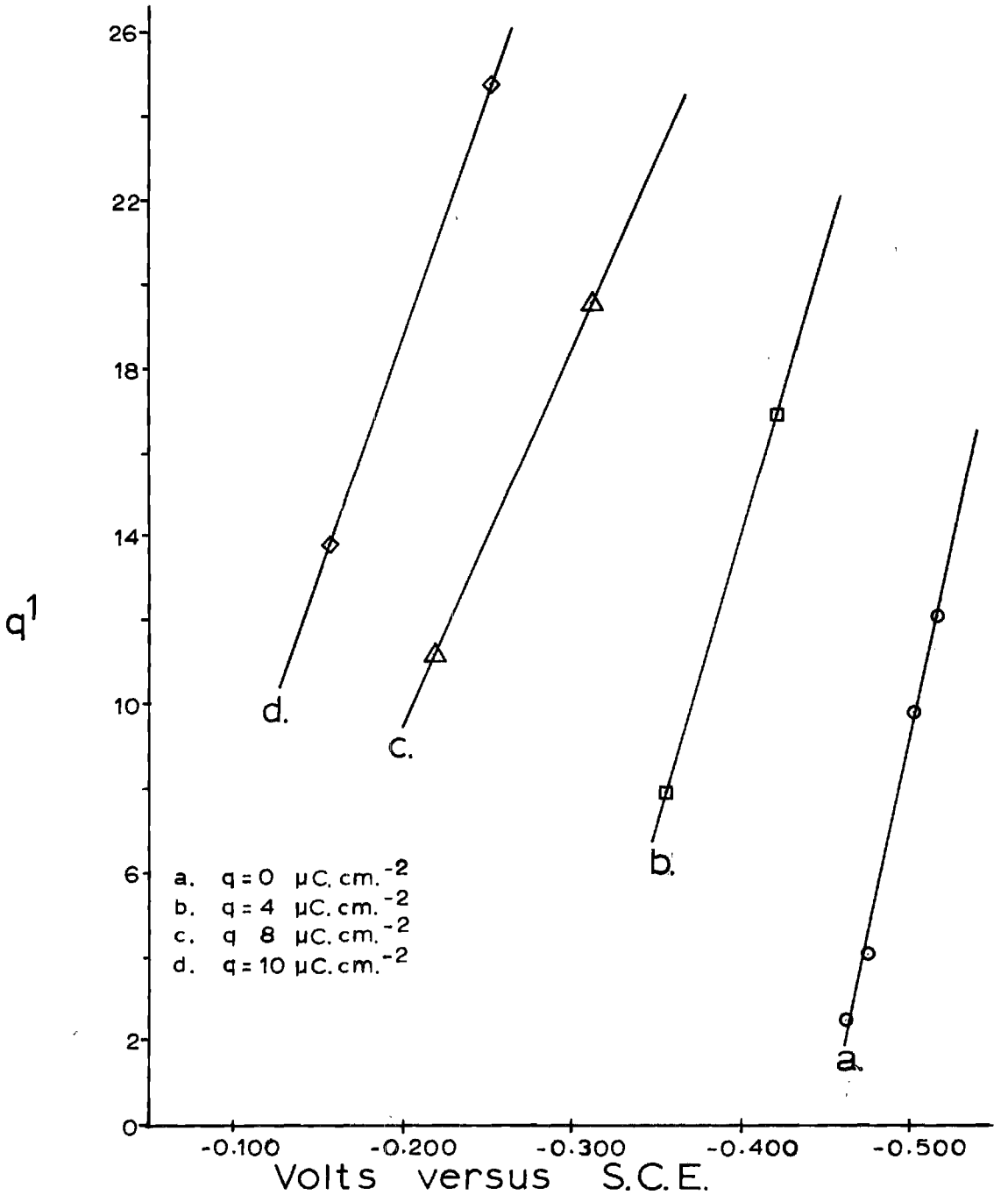

Figure 23. Specifically Adsorbed Charge q^1 Versus Potential at Constant q for 1 F Potassium Nitrate.

compact double layer, are independent of each other in terms of bonding, and there is even mutual repulsion by the like-charged ions in each Helmholtz plane. In order for reaction blocking to occur, there must be at least some interaction (46) in the solution phase between the adsorbed particles. Such interaction is more common with substances that act as surfactants, rather than with inorganic ions. Therefore the adsorbed nitrate ions effect the electrode reaction primarily through their effect on the electrical double layer.

Chronocoulometry

Double Layer Charging

The chronocoulometric technique is capable of detecting amounts of adsorbed electrochemical reactant or product corresponding to about 0.1 μ coulomb (1). For a two electron electrode reaction and an electrode area of 2×10^{-2} cm.^{2}, this means that the minimum amount of detectable adsorption, calculated employing the formula

$$Q = nFA\Gamma \qquad (4\text{-}2)$$

is about 2.5×10^{-11} Moles cm.$^{-2}$ under good experimental conditions. The error at this minimum amount may approach 50 per cent, but for larger quantities of adsorbed material it decreases rapidly to a tolerance of plus or minus the minimum value. Thus for a measured value of charge to indicate adsorption it must be at least somewhat larger than 0.1 μ coulomb. This is the criterion applied to chronocoulometric measurement of adsorption.

Inspection of Equation (4-2) leads to the conclusion that double

step chronocoulometry is very useful for the selective measurement of adsorption of electroactive reactant or product. Regardless of what non-electroactive species may additionally be adsorbed, assuming that the adsorption equilibrium is rapidly established, there is no net charge flow corresponding to adsorption and desorption of these electro-inactive species; all of the net charge flow will be due to the reduction or oxidation of an adsorbed reactant or product, respectively.

Experiments were initially performed with solutions 1 F in potassium nitrate and 2 mF in sodium pyrophosphate. The pH was adjusted by the addition of 1 F nitric acid. The potential of the electrode, initially at + 0.100 volts versus the S.C.E., was stepped by -0.400 volt at the desired instant. The results are given in Table 7 for double step chronocoulometry.

The value of charge required for charging of the double layer as obtained from the forward and reverse steps should be the same, since no electroactive material was present. The results for alkaline solution are reasonably reproducible, as seen by the fact that there is only 0.05 μ coulomb difference between the highest and lowest of the four values. The charging is not affected by a decrease in pH, as seen by the constancy of the values with varying pH.

The experiment was also performed at pH = 3.0, but it was not possible to use the same initial potential because oxidation of mercury occurs prior to step application, and this causes a reduction current to flow after the step is applied. Therefore the result is meaningless and is not listed.

Table 7. Number of Coulombs Required to Change the Potential of the Double Layer Between +0.100 and -0.300 Volts Versus S.C.E.

Forward Step	Reverse Step	pH
0.310 μC	0.280 μC	9.16
0.275 μC	0.262 μC	8.73
0.242 μC	0.260 μC	5.86

Test for Adsorption of Reactant with Double Step Chronocoulometry

Experimental Elimination of the Double Layer Charging. One of the chronocoulometric tests for adsorption consists of measuring the charge accumulated after the reverse potential step has been applied. Equation (2-33) gives the Q-t behavior as

$$Q(t > \tau) = \frac{2}{\pi^{1/2}} nFAC_{Ox} D^{1/2} [t^{1/2} - (t - \tau)^{1/2}] \quad (4-3)$$

No term is included for the normal double layer charging since the reverse step causes its cancellation. Therefore a plot of Q versus $[t^{1/2} - (t - \tau)^{1/2}]$ should have a zero intercept in the absence of adsorption. If adsorption does occur, a positive Q_i intercept will be obtained, that is related to the amount adsorbed by $Q_i = nFA\Gamma$. The only experimental condition that must be met is that the limiting slope of the Q-F(t) plot must have been attained, that is, the term K/λ of Equation (2-27) must be made independent of potential by having applied a sufficiently large potential step.

The method was applied to solutions 1 mF in copper(II), 2 mF in pyrophosphate, and 1 F in potassium nitrate. One series was performed with a constant potential step and varying the pH, and another with a constant, alkaline pH and varying the potential step. The results are presented in Table 8A. It must be remembered that there is an uncertainty of about ± 0.1 μ coulomb in the measurement, so that only Q intercepts appreciably larger than this value are indicative of adsorption.

Only in two cases is the absolute value of the intercept appreciably greater than 0.1 μ coulomb, and in these cases the values are not

Table 8. Values in Moles $cm.^{-2}$ of the Surface Excess of Reducible Species in the Copper(II)-Pyrophosphate System

A. $Q - [t^{1/2} - (t - \tau)^{1/2}]$ Intercept

B. Difference Between $Q - t^{1/2}$ and $Q - \theta$ Intercepts

Pyrophosphate	pH	E_i, volts	ΔE, volts	A Q_i	A $\Gamma \times 10^{10}$	B Q_i	B $\Gamma \times 10^{10}$
2 mF	8.98	0	-0.300	0.11	0.21	0.13	0.25
	5.66	0	-0.300	0.01	0.019	0.03	0.057
	2.96	+0.100	-0.300	-0.02	0.038	-0.10	0.19
	9.15	+0.100	-0.400	0.22	0.38	0.10	0.19
	5.88	0.100	-0.400	0.03	0.057	0.15	0.28
	3.26	0.100	-0.400	0.18	0.34	0	0
	9.21	-0.130(E_e)	-0.050	-0.22	-0.42	0.01	0.02
			-0.090	-0.26	-0.49	0.12	0.21
			-0.110	-0.22	-0.42	0.20	0.38
			-0.140	-0.22	-0.42	0.24	0.46
	8.98	-0.121(E_e)	-0.050	-0.14	-0.27	0.13	0.21
			-0.100	-0.12	-0.23	0.19	0.37
			-0.150	-0.11	-0.21	0.06	0.11
			-0.200	-0.078	-0.15	0.07	0.14
			-0.250	-0.070	-0.13	0.23	0.44
			-0.300	-0.058	-0.11	0.36	0.68
			-1.000	0.065	0.12		
5 mF	9.52	-0.189(E_e)	-0.100	0.106	0.20	0.02	0.038
			-0.300	0.113	0.21	0.06	0.12
			-0.600	0.182	0.34	0.13	0.254

reproducible. Using the maximum intercept, 0.265 μ coulomb, corresponding to at most 5.02×10^{-11} Moles $cm.^{-2}$ of an adsorbed species, has been attained. The latter value is more than an order of magnitude smaller than reported values corresponding to appreciable adsorption (41). From these results, it is concluded that there is no appreciable adsorption of either reactant or product at the electrode.

Graphical Elimination of the Double Layer Charge. In a double step experiment the value of Q, the charge following the first step, is plotted against $t^{1/2}$ according to Equation (2-31) and the curve is extrapolated to t = 0. Then the value of Q_τ, the charge accumulated following the second step, is plotted against $[\tau^{1/2} - (t-\tau)^{1/2} - t^{1/2}] = \theta$ according to Equation (2-36) and this curve is extrapolated to $\theta = 0$. The two zero-time intercepts should be equal in the absence of adsorption. Any difference in these intercepts is a measure of the amount of reactant adsorbed. The results from the same experiments discussed in the previous section, are presented in Table 8B.

Inspection of the table shows that the results are much the same as in the previous test. In three cases the value of Q_i appreciably exceeds the error of ± 0.1 μ coulomb. Two of these values are part of the same series, for which there seemed to be unusually large values of the $Q - t^{1/2}$ intercepts. The same value should have occurred at high overvoltage in the 5 mF pyrophosphate solution, but the value did not reoccur. If reactant adsorption were occurring, assuming the reactant is immediately reduced upon application of the step, a constant value of Γ should be obtained. The scattering of the data indicates that only a small amount, if any, is adsorbed and that the amount cannot

be more than 3×10^{-11} Moles $cm.^{-2}$. In any case such an amount is not enough to cause blocking of the electrode reaction, and moreover it would not be expected to be present when steady state reduction takes place.

Conclusions

Two observations so far not discussed were made in other experiments. In the potential step method, a comparatively large current excursion was observed in alkaline solutions of copper(II) pyrophosphate. This excursion lasted for about 0.2 millisecond and was followed by the expected current-time behavior. This effect was not noted in solutions of lower pH. Such behavior has been reported for cases where the reactant is adsorbed prior to current flow (54). Chronocoulometric experiments failed to confirm any appreciable reactant adsorption, and also indicated no adsorption differences between alkaline and acid solutions. The appearance of the current excursion was probably due to the fact that less reductant was available in the alkaline solution and thus, because the relative sensitivity of the readout was greater, the double layer charging component appeared to be greater. The magnitude of the time of duration of the excursion may be attributed to the risetime of the overall potentiostatic circuitry.

Survey work with chronopotentiometry gave a very slight indication of a wave preceding the first reduction step. This prewave could be taken as an indication of adsorption; however, since no definite wave could be confirmed, oxygen contamination was assumed as its cause.

Thus it can be stated that, of all the species in solution, only

nitrate, the anion of the supporting electrolyte, is appreciably adsorbed at the electrode surface. This adsorption, as already shown, is essentially limited to electrode potentials greater than the ECM potential. The effects of nitrate adsorption are seen in its influence on polarograms in the potential region below -0.5 volts and in the shift of the ECM potential. No degree or type of adsorption seems to occur that could block the electrode reaction or adversely affect its kinetics. Therefore adsorption is not a major factor in the interpretation of anomalous polarograms, although it does influence the results of some of the methods used for that purpose, as shall be seen in the following chapters.

CHAPTER V

ELECTROCHEMICAL PARAMETERS DETERMINED BY THE POTENTIAL STEP METHOD

Introduction

As was indicated in Chapter II, the electrochemical reaction may be characterized by the parameters i_a^o, k_a^o, and α. The quantity k_a^o is the apparent standard heterogeneous rate constant, and is a measure of the rate of reaction at the equilibrium potential. The units of k_a^o are cm sec^{-1}. The quantity k is the rate of reaction at any other potential, and is related to k_a^o by the expression

$$k = k_a^o \exp(-\alpha n f \eta) \qquad (5\text{-}1)$$

For overvoltages greater than about -0.1 volt k is so large that the rate of reaction is controlled by the rate of mass transfer to the electrode.

To study the kinetics of the electrochemical reaction, measurements must be made as close as possible to conditions of equilibrium, that is, when no net current flows at the electrode, and no concentration gradient exists.

Measurements made at potentials close to the formal equilibrium potential when employing the potential step method very nearly fulfill this requirement. Small potential steps (< 50 mv.) were used, and measurements were made within five milliseconds after application of the step.

In each case, the test solution was 1.0 mF in copper(II) and 2.0

mF in sodium pyrophosphate. Potassium nitrate was used as the supporting electrolyte. Its concentration was either 1.0 F, 0.5 F, 0.1 F, or 0.05 F. This variation was effected to allow a study of the influence of the double layer on the electrode reaction. The pH of each solution was adjusted by dropwise addition of either 1 F potassium hydroxide or 1 F nitric acid. The pH values selected were three, six, and nine. At pH 3, the copper(II) pyrophosphate complex is reversibly reduced. Schupp, et al., (53) have presented evidence that the reduction of $CuH(P_2O_7)_2^{5-}$ is at least partially irreversible. This species and $CuH_2(P_2O_7)_2^{4-}$ are almost equally abundant at pH 5.8. Above pH 9, the copper pyrophosphate exists nearly exclusively as $Cu(P_2O_7)_2^{6-}$. In this pH region the reduction is completely irreversible. The selection of the above values allowed a study of the reduction as it underwent the transition from being reversible to irreversible.

The above species exist when no alkali-metal cations are present. Foster (22) has presented evidence that in pyrophosphate solutions containing alkali-metal ions, at least one alkali metal ion will be associated with each pyrophosphate ion. The ligand written above as $P_2O_7^{4-}$ should then be $MP_2O_7^{3-}$, where M is either sodium or potassium. Foster merely states that the association with the alkali metal ions occurs, and that the rate determining step of the reduction reaction of the copper(II) pyrophosphate complex is the dissociation of a pyrophosphate ligand which, in the presence of a high concentration of alkali cations, is also associated with one of the latter ions. Evidence presented in this and the following chapter substantiates Foster's conclusions about this behavior. The type of bonding involved may be complexation,

ion-pairing, or some other undefined phenomenon. However, it has been shown (53) that alkali metal cations do indeed associate with the $Cu(P_2O_7)_2^{6-}$ complex species. Therefore, the conclusion is that an alkali metal cation is bound to each pyrophosphate ion, in addition to the complexation of the latter species with copper.

Direct Determination

The original theory of the method calls for a plot of the current versus the one-half power of time and an extrapolation of the resulting line to $t^{1/2} = 0$, according to 2-8. The zero time intercept, i_o, is then used with 2-15 to graphically determine the apparent exchange current density i_a^o. A series of experiments was performed with the solutions described in the introduction. The results are presented in Table 9.

The difficulty in using the procedure was that only a small number of the points on the $I - t^{1/2}$ plot fell on a straight line. This caused a large uncertainty in the values of i_o, particularly for alkaline solutions with high salt concentrations. In the case of such solutions the signal/noise ratio was often poor. This helped to obscure any straight line segment of the plot. Thus it was often difficult to determine where to draw the straight line of the $I - t^{1/2}$ plot. See Figure 26 for a representative plot of I versus $t^{1/2}$, including the points rejected because of supposed nonlinearity.

A plot of the i_a^o as determined by this simple method is given in Figure 24 as a function of pH for a 1 F salt solution. Because of the scattering of the points the choice of the relationship of i_a^o to pH was obtained at lower salt concentrations, as indicated by Figure 25.

Table 9. Graphical Results for the Apparent Electrochemical Parameters of the Reduction of the Copper(II)-Pyrophosphate Complex

Salt Concentration	pH	E_e, volts	$i_a^o \times 10^3$ amp cm^{-2}	$k_a^o \times 10^2$ cm sec^{-1}	α
1.0 F	9.34	-0.137	0.302	0.180	0.46
	8.24	-0.073	0.485	0.280	0.36
	5.82	-0.029	1.07	0.608	0.30
	* 5.78	-0.053	1.97	1.16	0.44
	* 3.02	+0.039	1.93	1.24	0.72
	2.99	+0.009	2.94	1.75	0.46
0.5 F	9.60	-0.150	0.189	0.109	0.36
	5.17	-0.021	1.61	0.899	0.32
	3.02	+0.006	2.60	1.57	0.50
0.1 F	9.78	-0.179	1.46	0.890	0.55
	5.84	-0.063	3.95	2.04	0.46
	2.98	+0.004	5.2	3.15	0.52
0.05 F	8.96	-0.143	0.612	0.369	0.50
	5.77	-0.056	1.03	0.620	0.50
	3.00	+0.021	1.25	0.753	0.51

*Believed less accurate.

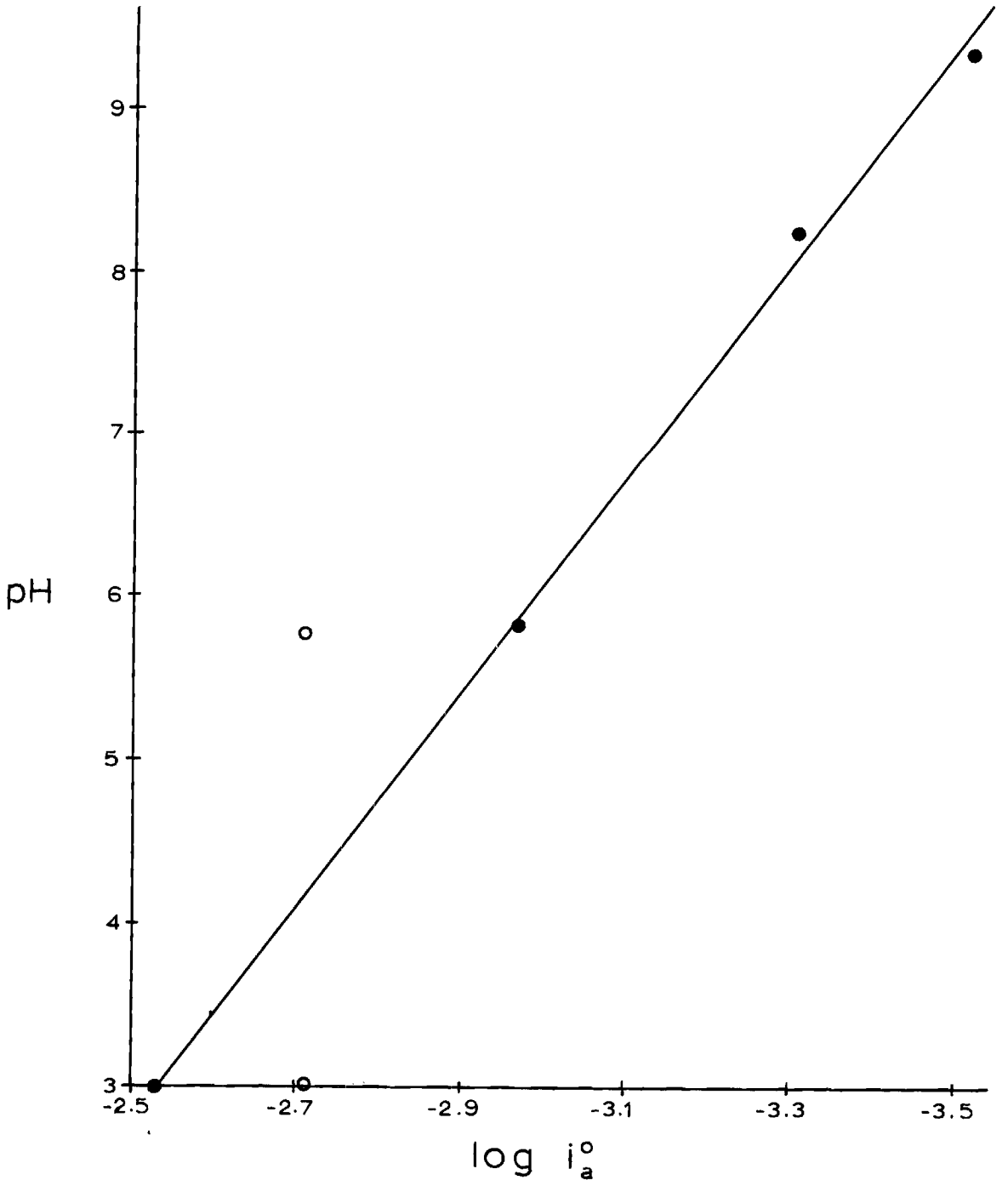

Figure 24. Plot of $1/(\partial \log i_a^o / \partial pH)$ for 1 F Potassium Nitrate.

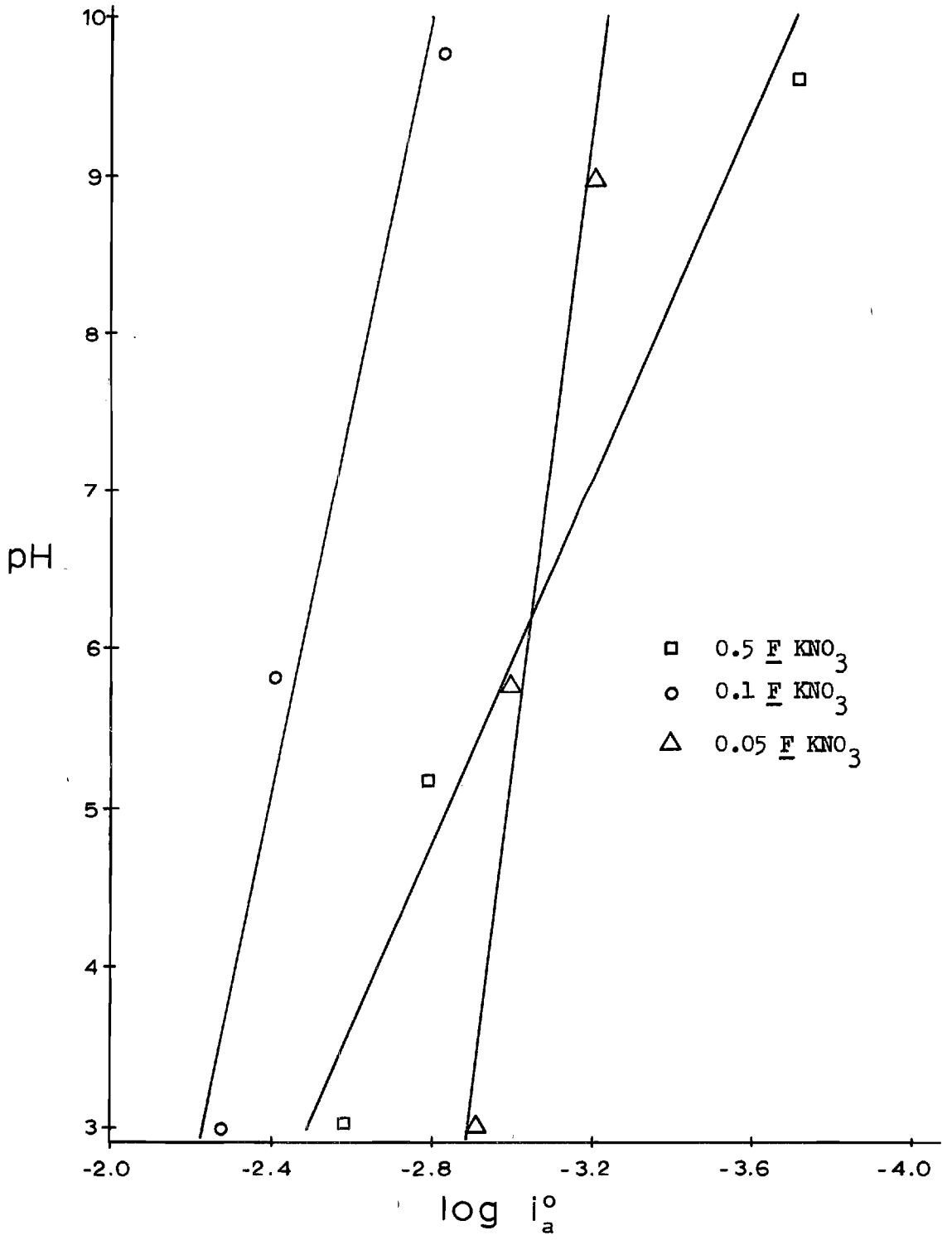

Figure 25. Plot of $1/(\partial \log i_a^o / \partial pH)$ for other Concentrations of Potassium Nitrate.

Computer Determination

Because of the ambiguous nature of the results obtained by using the direct method of intercept determination, a digital computer program to treat the current-time data was written in the ALGOL language. The program was written to accept data input in sets of current-time values for a specified overvoltage and electrode area. The square-root of each t value was calculated. The method of least squares was then used to calculate the best straight line through the $I - t^{1/2}$ points, and the $t^{1/2} = 0$ intercept was determined. The values of this intercept for several different over-voltages were used to calculate i_a^o and α. The method of linear least squares was applied to a plot according to Equation (2-15) Equation (2-18) was then used to calculate k_a^o.

The general appearance of the distribution of the $I - t^{1/2}$ points on the $I - t^{1/2}$ plots was known, since the plots had been constructed manually, as in the previous section. It was decided to discard points which were not even approximately on a straight line. The arbitrary time limit chosen was 3.50 milliseconds. The results from both discriminate and indiscriminate use of points are given in Table 10. The corresponding values of α are the same in each case. The values of i_a^o and k_a^o are slightly greater with discriminate use of the points. This is an expected result, since points which give a smaller slope to the best straight line have been deleted (see Figure 26). A plot of log i_a^o versus pH is given in Figure 27 for each salt concentration. The same uncertainties present in the results obtained by using the direct method of intercept determination are also present here.

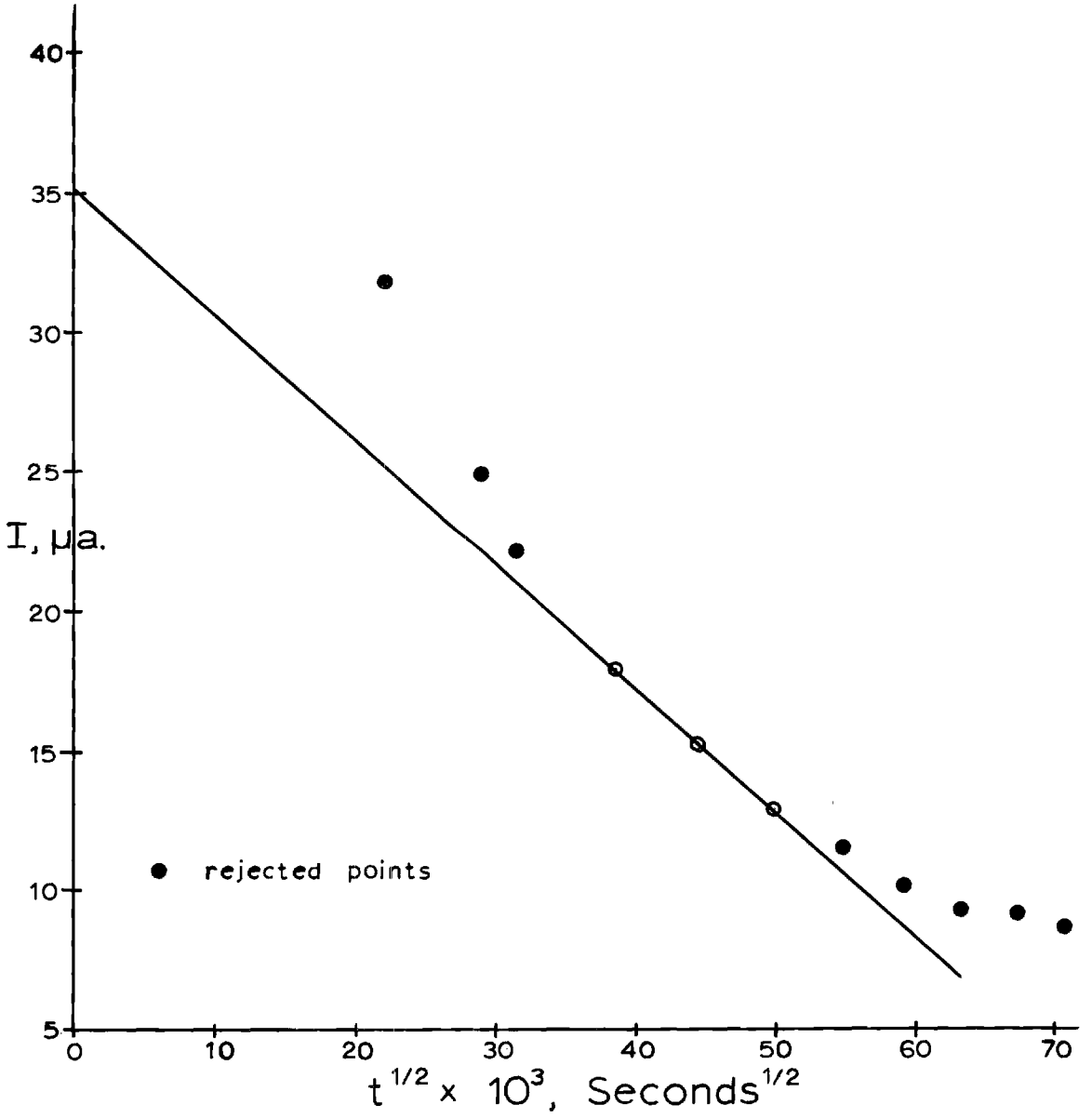

Figure 26. Representative I-$t^{1/2}$ Plot, Corresponding to 1 F Potassium Nitrate, 2.0 mF Pyrophosphate, and 1.0 mF Copper(II) at pH = 5.78.

Table 10. Computer Calculated Results for the Electrochemical Parameters of the Reduction of the Copper(II)-Pyrophosphate Complex

Salt Concentration Moles L^{-1}	pH	All Points Used $i_a^o \times 10^3$ amp cm^{-2}	All Points Used $k_a^o \times 10^2$ cm sec^{-1}	All Points Used α	Only Points Below t = 3.5 m sec. Used $i_a^o \times 10^3$ amp cm^{-2}	Only Points Below t = 3.5 m sec. Used $k_a^o \times 10^2$ cm sec^{-1}	Only Points Below t = 3.5 m sec. Used α
1.0	9.34	0.329	0.195	0.44	0.349	0.206	0.44
	8.24	0.590	0.333	0.28	0.630	0.354	0.26
	5.82	1.38	0.824	0.46	1.49	0.89	0.47
	5.78	1.82	1.04	0.34	2.00	1.15	0.33
	3.02	2.41	1.49	0.58	2.54	1.56	0.57
	2.99	3.27	1.92	0.40	3.53	2.06	0.40
0.5	9.60	0.214	0.123	0.34	0.236	0.134	0.31
	5.17	1.54	0.923	0.47	1.74	1.04	0.47
	3.02	3.01	1.78	0.44	3.22	1.88	0.40
0.1	9.78	1.79	1.05	0.39	1.98	1.15	0.38
	5.84	4.54	2.72	0.48	5.00	2.99	0.48
	2.98	5.64	3.38	0.48	5.88	3.52	0.48
0.05	8.96	0.69	0.412	0.47	0.726	0.433	0.47
	5.77	1.05	0.637	0.50	1.08	0.651	0.50
	3.00	1.27	0.767	0.50	1.28	0.772	0.50

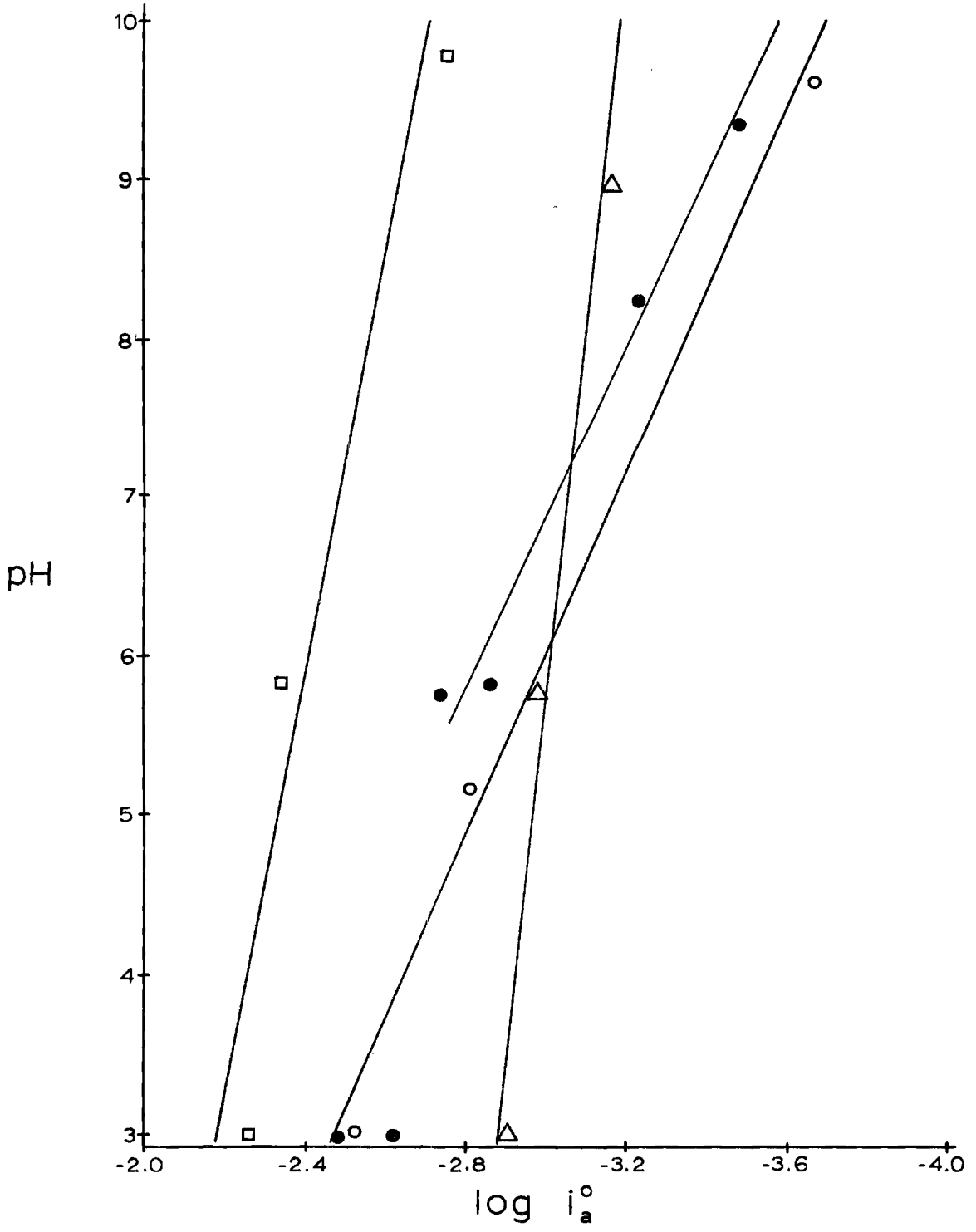

Figure 27. Plot of $1/(\partial \log i_a^o / \partial pH)$ for Indiscriminate Computer Treatment of Data.

Correct Determination of the Parameters

Shortly prior to this writing the method of Oldham and Osteryoung (42) for treatment of the current-time data from potential step experiments was published. As pointed out by these authors, if the smallest value of the current used to extrapolate the $I - t^{1/2}$ plot to $t^{1/2} = 0$ is less than 0.9 times that of the current at $t^{1/2} = 0$, the extrapolation is invalid. In Chapter II two methods of obviating this difficulty were presented. Both of these methods for calculation of the correct value of i_o were used in the present work, but only the results of the second method are presented here. The same conclusions were reached, and the second method is more accurate because of not having to transpose data points from the photographs of oscilloscopic traces.

Tangents were drawn at various points along each I - t curve, and the value of the ratio I/I_y was calculated for each point. The terms I_o and i_o were calculated from the value of I_y/I_o. The value of I_y/I_o was obtained from Figure 2. The kinetic parameters determined graphically employing Equation (2-17) are presented in Table 11. One set of values could not be calculated because when applying the criterion of Equation (2-13), the results contained no kinetic information. Another set at the same pH but different salt concentration gave a similar problem, except that the ratio I/I_y was just greater than two-thirds. The error in the corresponding region of Figure 2 is so large that a plausible result was not obtained. This set is indicated as not reliable.

As was expected, the values found in this calculation are more consistent than those of previous ones. Some of the values of i_o were found to be much larger than the former values mistakenly taken as i_o.

Table 11. Kinetic Parameters as Determined Graphically Using the Corrected Zero-Time Intercepts

Salt Concentration	pH	E_e Volts	$i_a^o \times 10^3$ amp cm^{-2}	$k_a^o \times 10^2$ cm sec^{-1}	α
1.0 F	9.34	-0.137	0.596	0.347	0.39
	8.24	-0.073	2.86	1.51	0.38
	5.82	-0.029	5.04	2.94	0.39
	5.78	-0.053	a	a	a
	3.02	+0.039	6.02	2.32[b]	0.14*
	2.99	+0.009	6.92	3.90	0.27
0.5 F	9.60	-0.150	0.339	0.187	0.20*
	5.17	-0.021	7.98	4.62	0.37
	3.02	+0.006	7.31	4.30	0.36
0.1 F	9.78	-0.179	4.28	2.37	0.22
	5.84	-0.063	18.5	----	0.74
	2.98	+0.004	7.39	4.41	0.48
0.05 F	8.96	-0.143	1.93	1.19	0.58
	5.77	-0.056	2.01	1.21	0.50
	3.00	+0.021	1.57	0.940	0.48

[a]Not calculable - see text.

[b]Possibly in error because of value of α used.

*Believed not reliable - see text.

The effect of this appeared in α as well as i_a^o. The pH dependence of the parameters can be clearly seen from these results. A plot of log i_a^o against pH is given in Figure 28a. At pH 3, the curve has a slope of only 0.022, indicating that the reaction is nearly independent of pH in that region. At pH 9.34, however, the slope is 0.97, about one. Using the equation

$$\frac{d \log i_a^o}{d\ pH} = P_{H^+} - \alpha P_{H^+} \qquad (5\text{-}2)$$

a reaction order, P, of two with respect to hydrogen for $\alpha = 0.5$ is obtained, indicating that two protons are participating in the overall reaction in some manner. The considerable difference in the shape of the corresponding curves in Figures 24 and 28a is due to the fact that the amount of scatter in Figure 24 belies the shape of the curve through the points.

The data for 0.5 F salt follow the same pattern. There are fewer points in this case but the shape of the curve is the same, as can be seen in Figure 28a. For 0.1 F salt solution there is an increase of i_a^o with decreasing pH, but the change is by a factor of two, as opposed to a factor of more than ten in the 1 F and 0.5 F solutions. In 0.05 F salt i_a^o is essentially independent of pH, and the values at each pH are not related to those at the higher salt concentrations in any regular manner. Whether or not the independence of i_a^o of pH in dilute solution is real or apparent can be decided by correcting for the influence of the double layer, as will be shown in the following section.

In acidic solution, there is essentially no change in i_a^o with

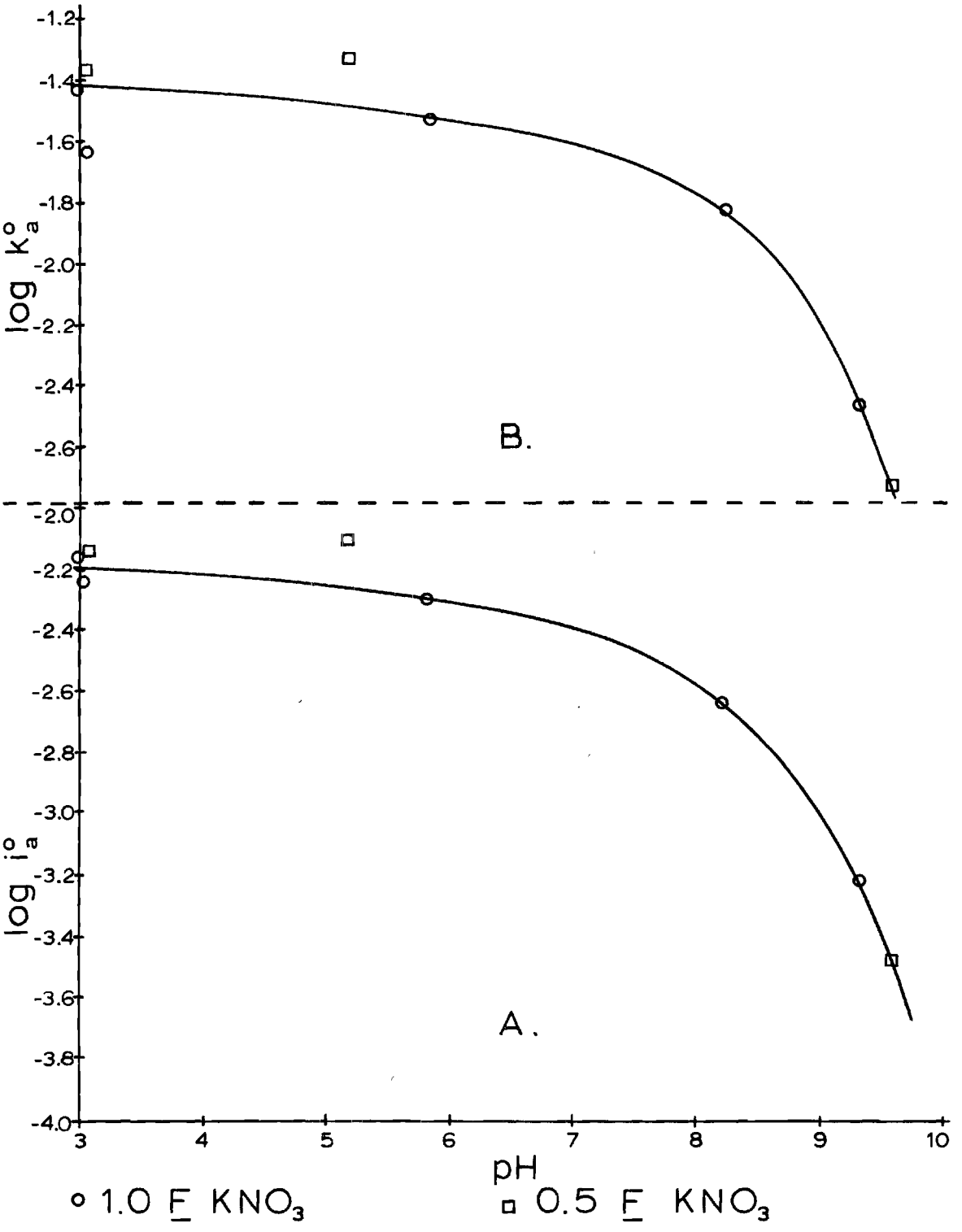

Figure 28. Apparent Electrochemical Parameters Versus pH.

salt concentration. In alkaline solution there is no regular variation of i_a^o with salt concentration, but all i_a^o values show some increase with decreasing salt concentration. There are interacting effects which complicate the interpretation of these facts. The adsorption of the nitrate ion may influence the behavior in one way, and the change in ψ_o, the potential across the diffuse double layer, may affect the behavior either in the same or opposite way. Present knowledge of these interactions is so limited that a better approach is to consider double layer effects as if adsorption did not occur, and then to modify the interpretation in terms of data from electrocapillary measurements of adsorption.

In 1 F salt solution the value of α is 0.4 at the two higher pH values, but in acidic solution it appears to be nearly 0.3. There is a high uncertainty associated with one of the determinations of α in acidic solution, but α is smaller in acidic solution. This may be due to adsorption of the nitrate ion. In 0.5 F solution α is about 0.36, and the value of 0.2 in pH 9 solution is probably in error. For 0.1 F solution, it is difficult to detect a trend in the variation of α with pH, but α appears to decrease with increasing pH. In 0.05 F solution α is apparently independent of pH. In alkaline solution α shows no regular variation with salt concentration. In acidic solution α apparently increases with decreasing salt concentration. The range of variation in the latter case is between 0.3 and 0.5.

Using Equation (2-18), k_a^o was calculated, and its pH dependence at the two higher salt concentrations is shown in Figure 28b. If α had not been nearly correct, the indicated agreement between both i_a^o and k_a^o as functions of pH would not have occurred. One value of k_a^o for 1 F

solution is out of line, and this one was calculated from an α value believed to be unreliable. However the calculation of k_a^o from i_a^o is relatively insensitive to changes in α as long as the concentrations are of comparable magnitude, since the concentration terms contain α and $1 - \alpha$ as exponents. The value of k_a^o in 0.5 F solution varies with pH in the same manner as in 1 F solution. In more dilute solutions, k_a^o becomes independent of pH, as does i_a^o.

The value of k_a^o for the reduction of copper(II) in 1 F potassium nitrate has been reported (45) to be 4.5×10^{-2} cm sec^{-1}. This value has been confirmed in a preliminary experiment with the technique and equipment described herein. The value of k_a^o for copper(II) pyrophosphate in an acidic solution of 1 F nitrate is nearly equal the value obtained when no pyrophosphate is present. Since reversible polarograms are obtained with copper(II) pyrophosphate under these conditions, this agreement is not unreasonable. The diminution of k_a^o in alkaline solution is due to the fact that the principal species present then is $Cu(P_2O_7)_2^{6-}$, which is not reduced as rapidly as the other species. The reduction of $Cu(P_2O_7)_2^{6-}$ is therefore irreversible by polarographic standards. The reduction of copper nitrate is known to be reversible. Since the decrease in the apparent standard heterogeneous rate constant is only about one and a half orders of magnitude, this irreversibility is a borderline case.

The Application of Double Layer Corrections

At a charged electrode in dilute electrolyte solution, there is an appreciable potential drop across the diffuse double layer (31). The

effect of this potential drop upon electrode reactions, although often neglected, can be profound (28). In this section double layer corrections are applied to the kinetic parameters of the electrode reaction. In the following chapter the treatment is extended to the entire reaction and to the complete polarization curve.

To apply the double layer corrections, Equation (2-16) is used in place of (2-15) to plot current versus overvoltage. The experimental curves of ψ_o versus φ and electrolyte concentration, as determined from the electrocapillary data in Chapter IV, are presented in Figure 29. Values of ψ_o taken from these curves were used in Equation (2-17), which may then be written as

$$B = 2.303 \log \frac{i_o}{1-e^{nf\eta}} = 2.303 \log i_t^o - zf\psi_o + \alpha nf(\psi_o - \eta) \qquad (5\text{-}3)$$

where B is the same quantity used previously in similar plots and i_t^o is the true value of the exchange current density, that is, the value corrected for the influence of the double layer. A plot of B versus $(\psi_o - \eta)$ at constant pH and salt concentration has a slope of αnf and an intercept of $2.303 \log i_t^o - zf\psi_o$.

In order to evaluate i_t^o, a value was needed for z, the ionic charge of the reducible species. Since i_t^o should be independent of salt concentration, Equation (5-3) may be written as

$$B' = B_o + zf\psi_o \qquad (5\text{-}4)$$

where B_o is the value of B at $(\psi_o - \eta) = 0$. The value of B_o was determined graphically. Since ψ_o is nearly constant for a given B_o, a

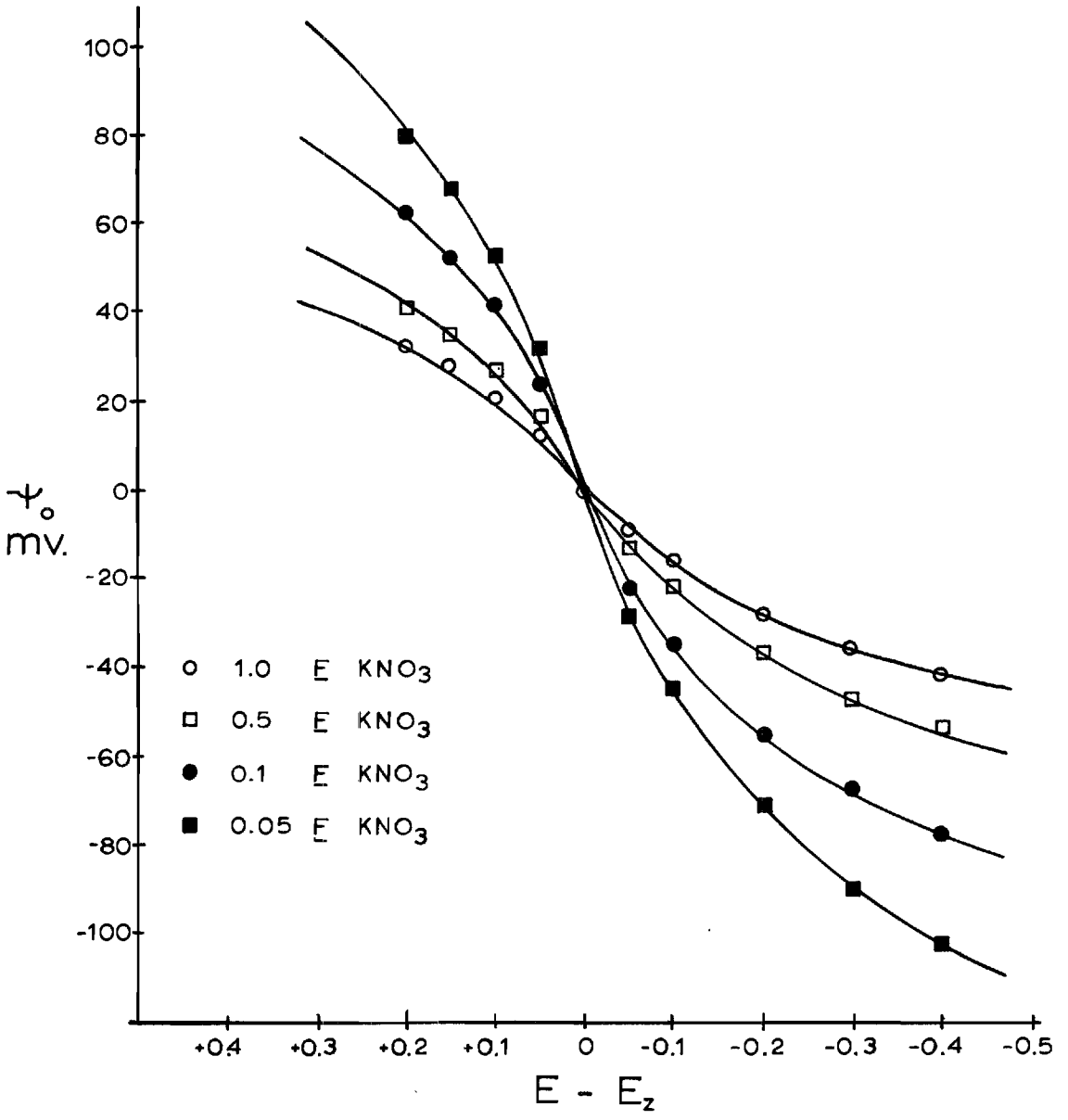

Figure 29. Plots of ψ_o Versus E - E_z for Various Salt Concentrations.

proper choice of an integral value for z should make B' constant. Recalling that z is the ionic charge on the reducible species, it was expected to have a negative sign in alkaline solution since the reducible species was the copper-pyrophosphate complex. From the Gierst analysis given in Chapter VI, it was strongly suspected that z = -2 in alkaline solution. For values of B_o at different salt concentrations different values of z between zero and minus five were used to calculate B', using Equation (5-4). Since no value of z gave a perfectly constant B', the statistical variance was calculated for the set of B' values at each z. These values are given in Table 12. The variance was calculated from the equation

$$V = \frac{QS}{N - 1} \tag{5-5}$$

where

$$QS = \Sigma x_i^2 - \frac{(\Sigma x_i)^2}{N} \tag{5-6}$$

The quantity x_i is the i^{th} value of a measurement, N is the number of measurements.

Sufficient data were available to allow the determination of the ionic charge of the reducible species at pH 9 and at pH 3. Since the value of B_o for 0.05 F salt solution was not consistent with the trend established by the other B_o values, its validity was questionable. Therefore two variances were calculated. The first variance, V_1, included the B' value from 0.05 F salt solution, and the second variance, V_2, omitted that B' value. All the variances are listed in Table 12.

Table 12. Values of B' as a Function of Salt Concentration for Different Trial Values of the Ionic Charge z.

pH	z	V_1	[Salt] 1 F	0.5 F	0.1 F	0.05 F	V_2
9+	0	2.095	- 9.39	- 9.04	- 6.87	-10.28	1.863
	-1	2.596	-11.337	-11.730	-10.02	-13.90	0.80
	-2	4.076	-13.284	-14.42	-13.17	-17.52	0.478
	-3	6.44	-15.231	-17.11	-16.32	-21.14	0.890
	-4		-17.178	-19.80	-19.47	-24.76	2.039
	-5		-19.125	-22.49	-22.62	-28.38	
3	3		- 0.60	----	----	----	
	2	0.884	- 2.74	- 0.900	- 0.67	- 1.76	1.29
	1	0.936	- 4.88	- 4.015	- 4.71	- 6.32	0.210
	0	3.26	- 7.02	- 7.13	- 8.75	-10.88	0.938
	-1	7.86	- 9.16	-10.245	-12.79	-15.44	3.477
	-2	15.25	-11.30	-13.360	-16.83	-20.00	
	-3		-13.44	-16.475	-20.87	-24.56	

In each case, V_1 does not show a minimum value, but rather increases continuously with decreasing z. However, V_2 does exhibit a minimum value. For pH 9 solutions the minimum occurs at z = -2, and for pH 3 solutions the minimum occurs at z = +1. This is an unexpected result in light of the fact that the complex species known to exist in alkali-free solution (57) at pH = 3 is $Cu(H_2P_2O_7)_2^{2-}$. It is also known (57) that at lower values of the pH, association of alkali cations with the copper pyrophosphate complex weakens the copper-ligand bond. As shown below, at a pH of 3, if one assumes z = + 1, the calculated value of the true exchange current density agrees with the published value for the reduction of copper(II) in 1 F nitrate. Thus it is concluded that the presence of the thousandfold excess of sodium ion weakens the complex to the extent that, at pH 3, appreciable amounts of uncomplexed copper(II) ion are present in the equilibrium mixture.

Assuming that z = -2 for the complex in alkaline solution, the resulting average value of B', not including the value from 0.05 F solution, is -13.6. Since $B' = 2.303 \log i_t^o$, the average B' at pH 9 gives the average i_t^o at that pH, and that was found to be

$$i_t^o = 1.21 \times 10^{-6} \text{ amp. cm.}^{-2} \text{ (pH 9)}$$

This is a radical departure from the uncorrected values at all salt concentrations, but the result is not surprising, since at the equilibrium potential the electrode has a fairly high positive charge density, and the species reduced from alkaline solution has a negative charge. Therefore the electrostatic attraction would be expected to favor an increase in the rate.

Assuming that z = +1 for the complex in solutions of pH = 3, the average value of the resulting B' is

$$B' = -4.02$$

again discarding the value for the 0.05 F solution. The resulting value of i_t^o at pH 3 is

$$i_t^o = 1.07 \times 10^{-2} \text{ amp.cm.}^{-2} \text{ (pH 3)}$$

This is very close to the reported value of $i^o = 9 \times 10^{-3}$ amp cm^{-2} for the reduction of copper(II) from 1 F nitrate solution. The pyrophosphate complexes with copper existing at this pH are weak complexes and they give reversible polarographic waves. In light of these facts, the agreement between these i^o values is not surprising. The individual corrected values of i_t^o are presented in Table 13.

Table 13. Experimental Values in amp cm^{-2} of i_t^o for Various Salt Concentrations and pH Values

pH	Salt 1 F	0.5 F	0.1 F	0.05 F
9	1.71×10^{-6}	5.48×10^{-7}	1.91×10^{-6}	2.47×10^{-8}
3	7.60×10^{-3}	1.81×10^{-2}	9.01×10^{-3}	1.80×10^{-3}

It is not possible to construct a plot of log i_t^o versus pH as was done previously, since corrected points are available for only two pH values. It is expected, however, that such a plot would have the

same appearance as the one of Figure 28, but would show more curvature because i_t^o has a greater pH dependence than does i_a^o. The change of i_t^o with pH was expected, because both the nature of the reducible species and the course of the overall reaction change with pH.

The true transfer coefficient may be different from the apparent value, in a manner analogous to the exchange current density. In the present case, however, the true values were usually the same as the apparent values. The true and apparent values are compared in Table 14. The only appreciable differences are between the values for 1 F salt solution. Since there is so great a variation of α, it can only be said that α is close to 0.4 in 1 F solution. Most of the divergent values are the result either of data of low precision, or of an insufficient number of data employed to construct a plot, or both. With every method of calculation, α becomes independent of pH in dilute salt solution, and approaches a value of 0.5.

A comparison of the kinetic parameters obtained by all methods is found, at the end of Chapter VI, in Table 15.

Values of k_t^o calculated from experimental i_t^o and α were found to be

$$k_t^o = 6.7 \times 10^{-6} \text{ cm.sec.}^{-1} \quad \text{(pH 9)}$$

and

$$k_t^o = 5.94 \times 10^{-2} \text{ cm.sec.}^{-1} \quad \text{(pH 3)}$$

Both values were calculated from Equation (2-18) assuming $\alpha = 0.2$. This assumption is probably erroneous at pH 3 but a wide range of

Table 14. True and Apparent Values of the Transfer Coefficient

	1.0 F Salt		0.5 F Salt		0.1 F Salt		0.05 F Salt	
pH	True	Apparent	True	Apparent	True	Apparent	True	Apparent
9.78					0.22	0.22		
9.60			0.21	0.20				
9.34	0.51	0.39						
8.96							0.53	0.58
8.24	0.38	0.38						
5.84					0.79	0.79		
5.82	0.34	0.39						
5.77							0.48	0.50
5.17			0.37	0.37				
3.02	0.13	0.14	0.35	0.36				
3.00							0.49	0.48
2.99	0.51	0.27						
2.98					0.46	0.48		

"true" values was found for α at this pH, and thus 0.2 was arbitrarily chosen. Since C_{Ox} and C_{Red} are similar, the difference is not so important, particularly in light of other errors.

Several sources of error contribute to the uncertainty of the values obtained by making double layer corrections. The Gouy-Chapman theory for the calculation of ψ_o potentials is not strictly applicable if adsorption takes place, and the treatment was applied although it had been shown that the nitrate ion is adsorbed. The ψ_o potentials used did not agree with the values determined by Grahame for sodium fluoride (31). This disagreement could, however, be explained by the fact that for the Copper(II)-pyrophosphate system the net ionic charge influencing the double layer was greater than unity, due to the presence of copper(II) and pyrophosphate ions. This effect is reflected in the fact that the experimental ψ_o potentials were larger than those expected for monovalent ions. The particular experimental method employed when determining the ψ_o potentials added considerably to the possible overall error.

CHAPTER VI

THE POLARIZATION CURVE

The Gierst Analysis

Separation of Components of Potential

The method proposed by Gierst (28) for the determination of the effect of each component of the electrode potential on the possible electrode reactions and their rates is employed below in the interpretation of polarograms of the alkaline copper(II)-pyrophosphate system. Solutions used for the polarographic experiments were always 2.0 mF in sodium pyrophosphate and 1.0 mF in copper(II). The concentration of supporting electrolyte (KNO_3) was varied between 1.0 F and 0.05 F. Adjustment of the pH was effected by addition of 1 F potassium hydroxide or 1 F nitric acid. Polarograms of solutions of pH 9 are given in Figure 30.

The rational electrode potential φ, defined as

$$\varphi = E - E_z \qquad (6\text{-}1)$$

consists of the components φ' and ψ_o. For the general case in which the apparent rate v^* is a function of both φ' and ψ_o, the Frumkin equation (24) gives the relationship between these potentials and v^* as

$$v^* = v^o [\exp(-\alpha n f \varphi')] \exp(-z f \psi_o) \qquad (6\text{-}2)$$

Equation (6-2) can be rearranged to give

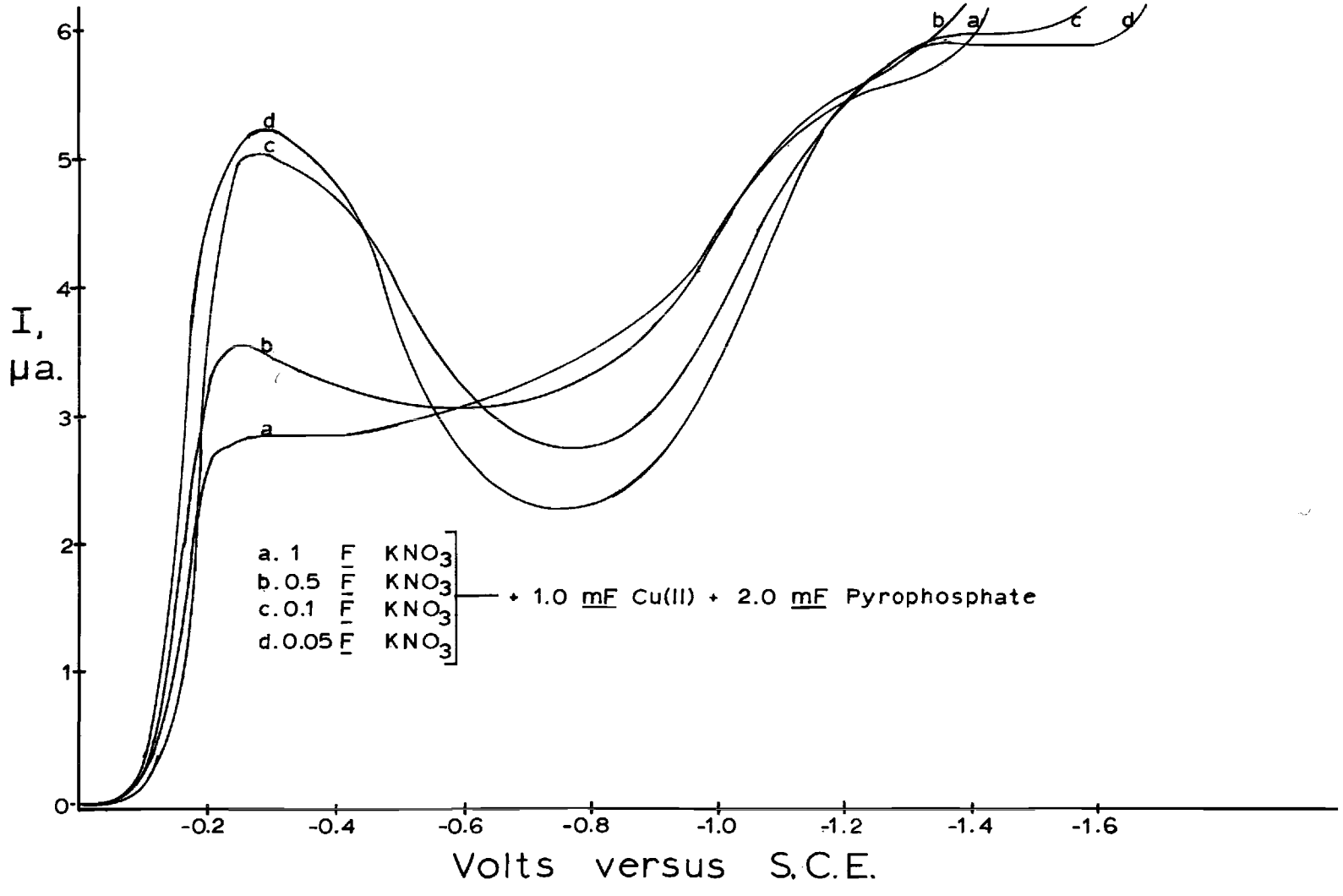

Figure 30. Polarograms of the Alkaline Copper-Pyrophosphate Systems Containing Different Concentrations of Supporting Electrolyte.

$$2.303/f \log v^* = 2.303/f \log v^o - \alpha n\varphi' - z\psi_o \qquad (6\text{-}3)$$

In light of Equation (6-3), some of the reasons for the existence of anomalous current-voltage curves are the magnitudes of α, z, and ψ_o. The relative magnitudes of these quantities affect the contributions of the last two terms on the right-hand side of Equation (6-3). If v^* for given conditions is not a function of φ' or ψ_o, then the value of the term containing that quantity in Equation (6-3) is zero. The Gierst analysis allows a graphical separation of the effects of each component of potential on the electrode reaction, and a determination of the kinetic parameters of the reaction. A plot of 2.303/f log v^* versus ψ_o at constant φ' will have a slope of -z. A plot of 2.303/f log v^* versus φ' with ψ_o constant will have a slope of $-\alpha n$. Once -z and $-\alpha n$ have been determined, v^o can be obtained.

Values of v^* were calculated from values of the ratio I/I_d and Equation (2-66), and then (2.303/f) log v^* was plotted versus φ. Values of ψ_o were computed from the charge density data given in Chapter IV. Plots of these values for alkaline copper(II)-pyrophosphate solutions are given in Figure 31, the 2.303/f log v^* data in the upper portion and the ψ_o data in the lower portion.

Graphical constructions on these plots allow determination of the kinetic parameters. At certain values of φ, vertical lines representing constant φ are drawn. From the points of intersection of these lines with the abscissa ($\psi_o = 0$), 45° lines corresponding to constant ϕ' are drawn to intersect with the curves $\psi_o = F(\varphi, C_S)$. The abscissa values of these points of intersection are then transposed to the corresponding

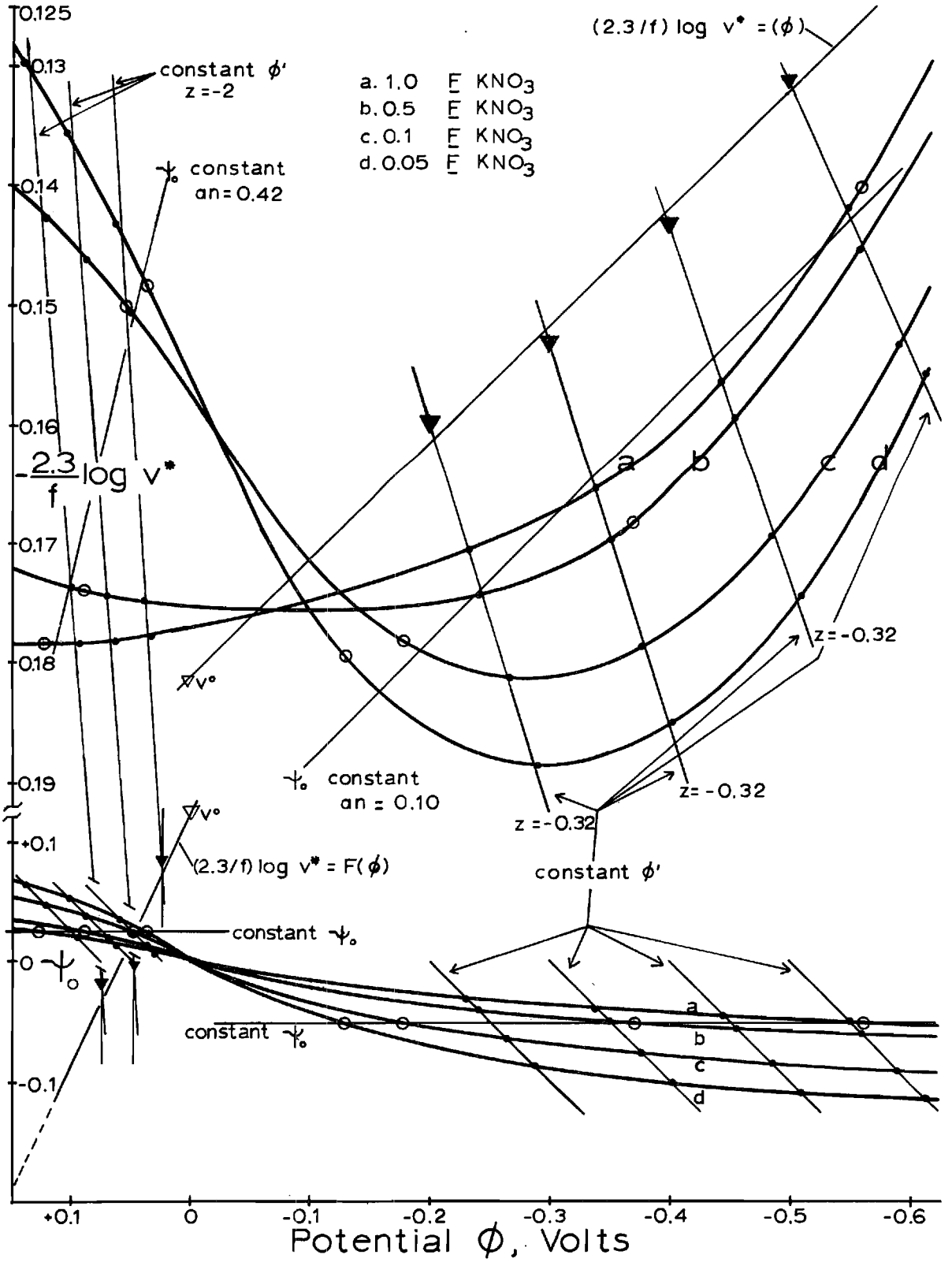

Figure 31. The Gierst Plot for Reduction of the Copper(II)-Pyrophosphate Complex in Alkaline Solution.

(2.303/f) log v^* curves, and a line is drawn through the points resulting and extrapolated until it intersects its corresponding φ = constant line. The locus of several of the latter intersects is the line (2.303/f) log $v^* = F(\varphi)$. Extrapolation of this line to $\varphi = 0$ yields the quantity v^o, the value of the apparent rate constant v^* in the absence of double layer effects. According to Equation (6-3), the slope of each φ' = constant line is -z, the charge on the reducible species existing in the bulk of the solution. The original contention by Gierst, that z is the charge on the reducible species at the outer Helmholtz plane, has been proven false by Frumkin et al. (24). The charge on a species produced by a preceding chemical reaction may still be determined, however. Although this restricts the usefulness of the method, it still allows some interpretations about the charge of the reducible species in the bulk solution, in terms of ion-pairing and similar phenomena, and this portion of the analysis is still useful for the present system.

A line representing constant ψ_o is intersected with the curves $\psi_o = F(\varphi, C_S)$. The abscissa values of these intersects are transposed to the corresponding v^* curves, and are connected by a line representing the condition of constant ψ_o. The slope of this line is -an.

Positively Charged Electrode

Results. The numerical values of the parameters for the reaction occurring in this potential region were obtained employing Figure 32, that uses an expanded abscissa scale.

For the charge z on the reducible species in the bulk solution the following values were obtained: -1.20, -1.25, -1.26, and -1.60, corresponding to decreasing anodic polarization. Determination of z,

using Figure 31, gave a value of approximately -2. The results obtained from Figure 32 are probably more reliable.

Extrapolation of the line (2.303/f) log v^* to $\varphi = 0$ gave a value for v^o of 7.97×10^{-4} cm sec^{-1}; construction of lines of constant ψ_o gave values for αn of 0.26 and 0.40, when using Figure 32. From Figure 31 a value of αn of 0.42 was obtained.

Discussion. Inspection of the $v^* = F(\varphi)$ curves in Figures 30 and 32 for 1 F and 0.5 F salt solutions shows that the current is almost constant for potentials in the region slightly less cathodic than +0.10 volt to approximately -0.20 volt versus S.C.E. This indicates that the current limiting process in this region is almost independent of φ'. Such behavior is characteristic of an electrode reaction limited by a preceding chemical process which in this case is believed to be the dissociation of the diligand complex to the monoligand complex and a pyrophosphate ion. With increasing cathodic potentials some other reaction begins to occur. This is thought to be direct reduction of the 2:1 complex $Cu(MP_2O_7)_2^{4-}$, containing a large negative charge.

The results for 1 F salt solution indicate that the reduction of the 2:1 complex is very irreversible, as can be deduced from the fact that the second rising portion of the polarogram is very drawn out. Because of the enhanced electrostatic attraction (i.e., greater double layer effect) for the complex species in more dilute solution, simple inspection of the polarograms for these solutions does not permit this conclusion. The foregoing observations combine to indicate that, within this potential range, v^* is a function of ψ_o. It is probably not a function of φ' within this region, but the test for this dependence is

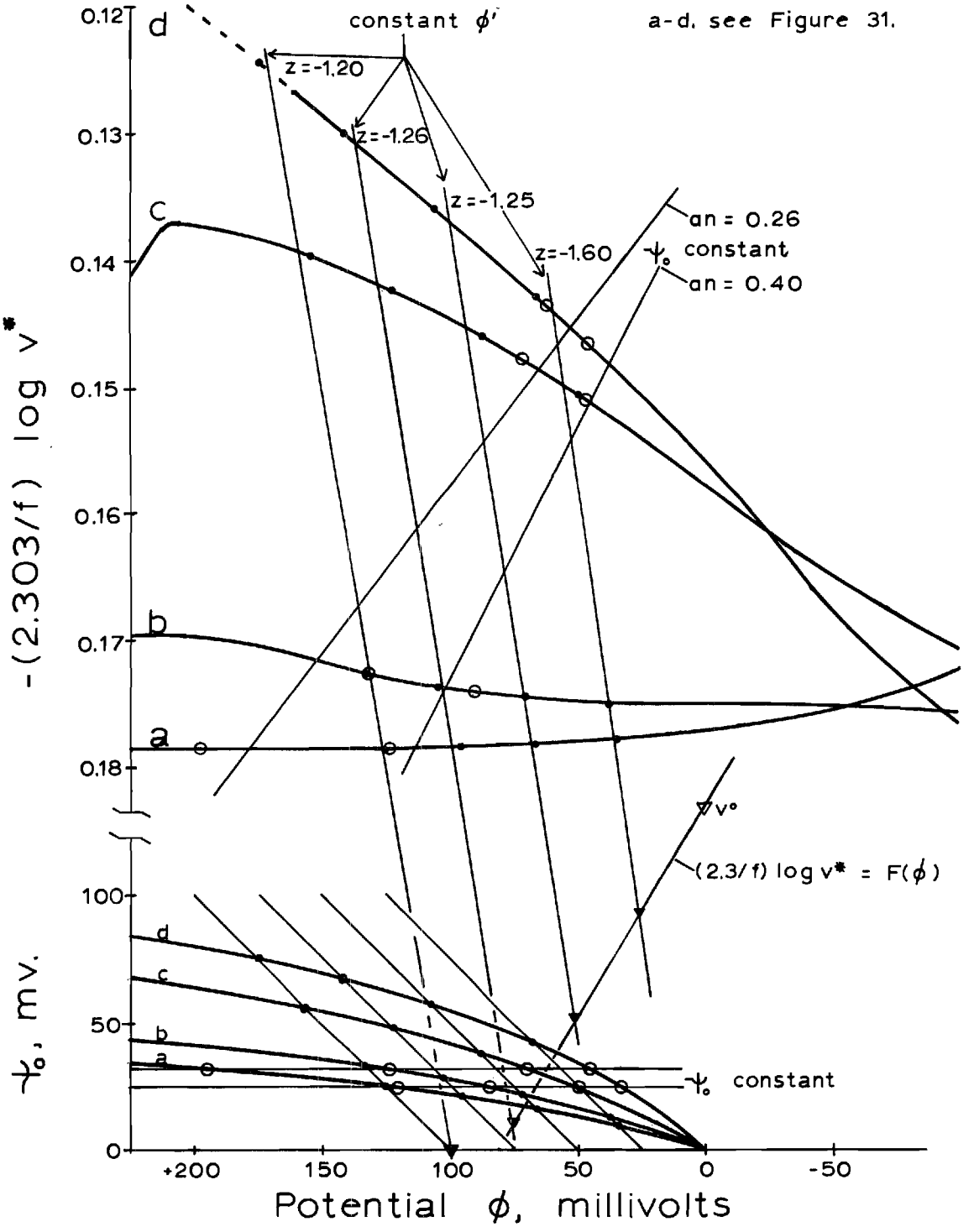

Figure 32. The Gierst Plot for Alkaline Copper(II)-Pyrophosphate. Potentials More Anodic Than the ECM.

not applicable to the data, that must be treated in the manner described in the discussion of the plot according to Equation (6-4) below. However, the polarogram of the system in 1 F salt solution shows that, within the region between about +0.25 and +0.05 volts, the current, and thus v^*, is approximately independent of φ. Therefore, it may reasonably be stated that the dissociation of the 2:1 complex is the rate determining step within this potential region. At more negative values of the potential, beginning somewhere around $\varphi = 0$, the total rate is a function of the reduction of both the 2:1 and 1:1 species.

For positive values of φ, as the concentration of the supporting electrolyte decreases, the electrostatic attraction for the negatively charged complex increases. This causes the increasingly large maximum in the potential region near $\varphi = 0.200$ volt. The fact that non-integral values of z were obtained from the curves in the potential region where it is thought that only the 1:1 complex is being reduced is indicative of two things. If only copper and pyrophosphate were present at this pH, the formula for the 1:1 complex would be $Cu(P_2O_7)^{2-}$. The addition of an alkali metal ion to each pyrophosphate ligand would result in a net z of -1. Since the measured z is between -1 and -2, it is probable that the average number of alkali metal ions bound to the 1:1 complex is less than one. If the net reduction of z is considered to be due to an ion-pair type of association, then the average reduction of about 0.7 units means that a majority of the 1:1 complex ions are ion-paired with alkali metal ions. However, regardless of which approach is taken, the important point is that not every 1:1 complex ion is associated with an alkali cation. The value of z shows an appreciable increase with

decreasing anodic polarization. This may be due either to the fact that reduction of the 2:1 complex is thought to begin at approximately $\varphi = 0$ volt, or to the distortions of the wave introduced by the variations in the specific adsorption of nitrate.

The values for α for $\varphi > 0$ obtained from Figures 31 and 32 are badly scattered. An agreement was expected between α found in this region from polarography and that found with the potential step method. Unfortunately, the corrected values from the latter method also are scattered (between 0.2 and 0.5). The corrected values from polarography are scattered between 0.13 and 0.31. However, considering both methods, more values are near 0.2, and 0.2 will thus be taken as the true value of the transfer coefficient for the reduction of copper(II)-pyrophosphate in alkaline solution. The hypothesis, that reduction of both complex species occurs, beyond a certain potential complicates the interpretation of the values of α obtained polarographically. Because of differences in size and charge, the values of α for the reduction of the two species would be expected to be different. However at the present time it is not possible to determine the kinetic parameters of two simultaneous electrode reactions. Since both chemical and electrochemical influences affect the total current flow, separation of the current into its components is impossible, and indirect approaches such as taken above have to be employed.

Extrapolation of the line $(2.303/f) \log v^* = F(\varphi)$, in Figure 32, to the equilibrium potential of -0.140 volts versus S.C.E. gives a value for $v^*_{E_e}$ of 6.43×10^{-6} cm sec^{-1}. At this potential the heterogeneous rate constant k of the electrode reaction attains its "standard" value

of k^o. The value of k_t^o found from measurements by the potential step method (given in Chapter V) is 6.7×10^{-6} cm sec^{-1}. This excellent agreement between the values of $v_{E_e}^*$ and k_t^o indicates not only the compatibility of the results obtained from the two methods, but more important, that the overall reaction occurring in each case is the same. If this were not true, then the values of $v_{E_e}^*$ and k_t^o would not be the same. The use of the two separate terms allows the consideration of separate possible reaction paths. Thus the initial assumption is that the two terms are not the same in the two separate methods, but they may be proven the same if the overall reaction is the same in each case. When several concurrent reaction paths are possible the rates are additive, and a single curve should define the potential dependence of the total rate provided the overall reaction is the same. This condition holds for the alkaline copper(II)-pyrophosphate system in the potential region where the electrode is positively charged. Thus the results obtained with the potential step method are consistent with those obtained with polarography.

Negatively Charged Electrode

Results. The numerical data presented here was obtained employing Figure 31.

For the charge z on the reacting particle, the following values were obtained for the four φ values: -0.32, -0.32, -0.32, -0.22, the last one corresponding to the most extreme cathodic potential.

Extrapolation of the $(2.303/f) \log v^* = F(\varphi)$ line to $\varphi = 0$ gave a value for v^o of 8.74×10^{-4} cm sec^{-1}.

Construction of a line representing a constant ψ_o gave a value

for αn of 0.10.

Discussion. When the electrode is negatively charged, electrostatic interaction with the negatively charged complex species causes their repulsion from the electrode, and the total current decreases. This effect can be seen in the polarograms of all solutions except those of high salt concentration ($\doteq$ 1 F). Both φ' and ψ_o affect the apparent rate. If the electrode processes are independent of φ', the second term on the right side of Equation (6-3) vanishes and, for constant v^*, a plot of ψ_o versus φ, according to

$$\psi_o = \frac{2.303}{(\alpha n - z)f} \log v^*/v^o + \left(\frac{\alpha n}{\alpha n - z}\right)\varphi \qquad (6\text{-}4)$$

yields a straight line of zero slope.

Figure 33 contains plots of ψ_o versus φ at several values of v^*. The points were obtained by drawing lines of constant v^* through the $2.303/f \log v^* = F(\varphi)$ curves for the various salt concentrations. The abscissa values of the intersects for each value of v^* gave the values of φ for one curve, and the transposition of these abscissa values to the corresponding $\psi_o = F(\varphi)$ curves gave a set of corresponding ψ_o values. The finite slopes of the plots in Figure 33 indicate that v^* is dependent upon φ'. The dependence of v^* on ψ_o may be established by plotting $2.303/f \log v^*$ versus ψ_o, according to

$$2.303/f \log v^* = 2.303/f \log v_o - \alpha n\varphi + (\alpha n - z)\psi_o \qquad (6\text{-}5)$$

Several of these plots are given in Figure 34 for various values of φ. The points were obtained by drawing lines of constant φ through both

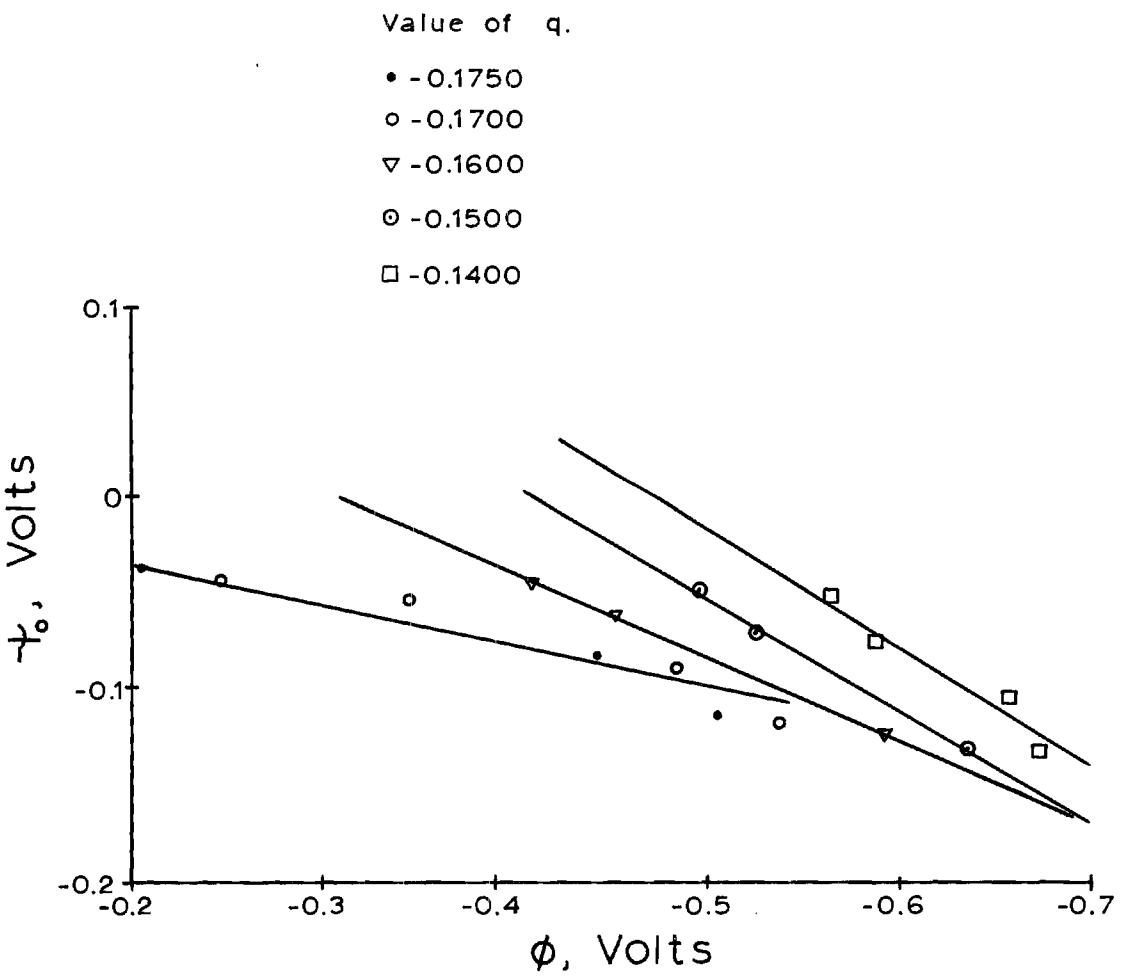

Figure 33. Plots of $\psi_o = F(\varphi)$ for Constant v^* and Negative q.

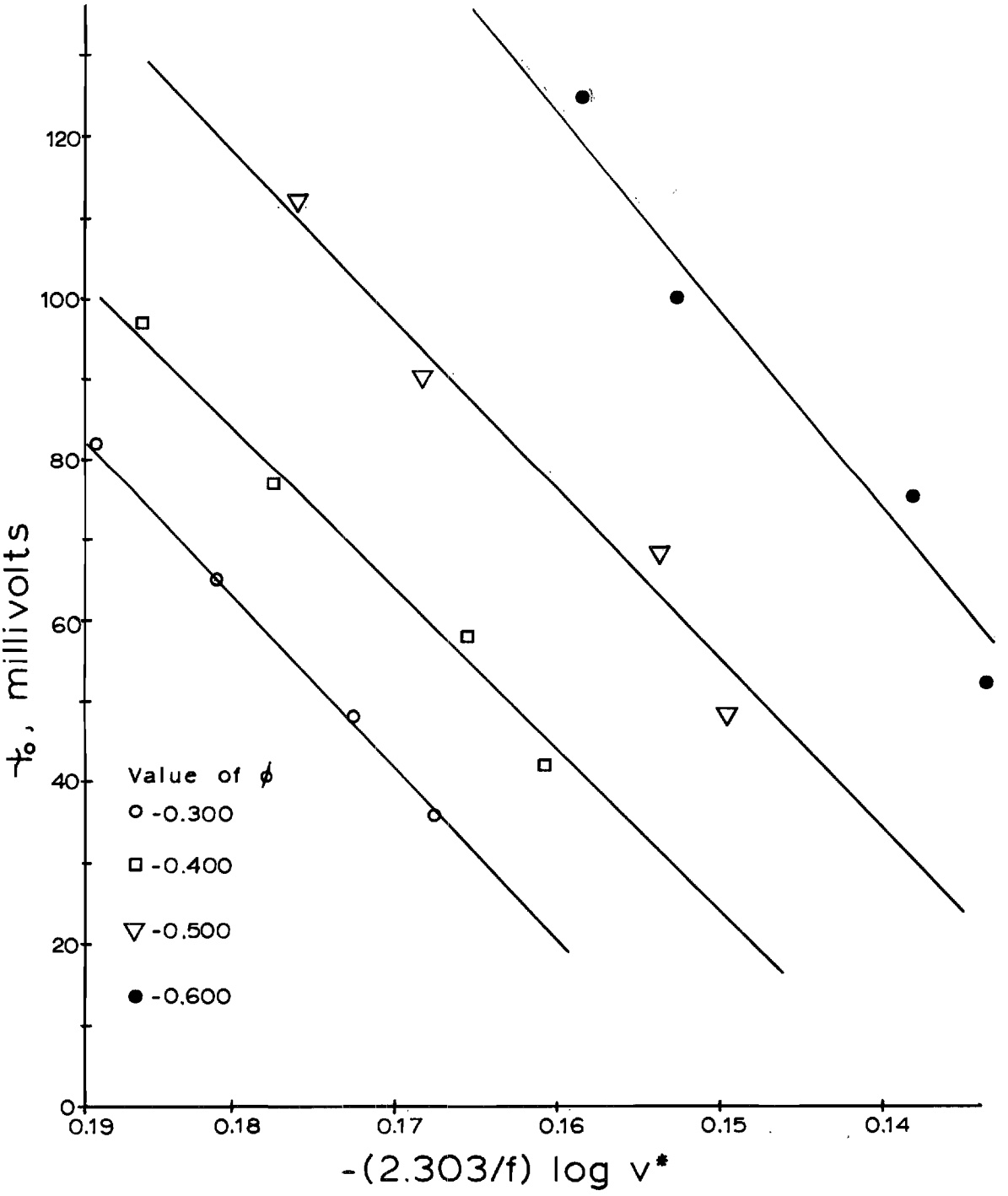

Figure 34. Plots of (2.303/f) log v^* = $F(\psi_o)$ for Constant φ and Negative q.

the 2.303/f log v^* = F(φ) and ψ_o = F(φ) curves. The respective abscissa values of the intersects were used as the points for each curve in Figure 34. The non-zero slopes for the plots in each figure indicate that in the potential region where the electrode is negatively charged the apparent rate v^* is a function of both φ' and ψ_o. At sufficiently cathodic values of φ, ψ_o becomes almost constant and normal reduction finally occurs because of the eventual predominance of the accelerating effect of the potential φ'.

The value for the ionic charge z is not consistent with that expected according to the complex species thought to be predominant in alkaline solution. Even in the presence of alkali metal cations the lowest ionic charge of any of the complex species is thought to be at least -1 in the bulk solution and this charge would be that of the 1:1 complex $[Cu(MP_2O_7)]^{-1}$. The complex $[Cu(MP_2O_7)_2]^{4-}$ has a much higher charge. However, at the point in the double layer at which reduction takes place, the profound influence of the electrostatic field of the double layer due to the negatively charged electrode is so great as to preclude reduction of the complex species thought to exist in the bulk solution. Moreover, because of the relatively high ionic charge of the copper(II) pyrophosphate species and the relative abundance of alkali metal ions, ion-pairing in excess of the complex association of an alkali metal ion with each pyrophosphate ligand is believed to occur. On the basis of the value obtained for z it is postulated, therefore, that ion-pairing of the copper(II) pyrophosphate complex with alkali cations occurs in the bulk solution, and that reduction of species which have undergone ion-pairing is favored. Such an assumption is not

unreasonable in light of the fact that a great excess of alkali metal ion is available for such reactions. This should not imply that these ion-pairing reactions are rate-determining, but rather that the relative abundance of species such as $[Cu(P_2O_7)_2M_{2x}]^{2x-6}$ with a net x greater than 1 is greater than that of those for which x equals 1.

The value of 0.10 obtained for αn in the potential region of a negatively charged electrode is appreciably smaller than that obtained for the potential region of a positively charged electrode. Since these values of α obtained by this method are supposedly the true values, the above result can only mean that, even allowing for a reasonable error (± 0.1 unit), α is quite small in this potential region. The significance of a small α is that the normally expected degree of influence of the potential ϕ' on v^* is considerably diminished, thus allowing the relative magnitude of the ψ_o effect to become proportionately more important. This behavior may be noted by examination of Equation (6-3). A small value of α would diminish the value of the term $\alpha nf\phi'$. The above conclusions are not contradictory to the hypothesis of simultaneous reduction of both the 2:1 and 1:1 complexes. The value of α obtained may be a composite one, and the general conclusions still hold.

The value for v^o obtained from data for the potential region of negative electrode charge agrees reasonably well with that obtained from data for the potential region of positive electrode charge. The former value is $v^o = 8.7 \times 10^{-4}$ cm sec^{-1} and the latter is $v^o = 8.0 \times 10^{-4}$ cm sec^{-1}. The slopes of the lines extrapolated to obtain these values are not the same because of the differences in α and in z in the two regions. The two values of v^o must, however, be related if there is not

to be a discontinuity in the dependence of v^* on φ. A further consequence of this requirement is that the actual dependence of v^* on φ in the region of $\varphi = 0$ is likely to be similar to that depicted by the dotted curve in Figure 31.

If a preceding chemical reaction takes place, the value of v^o by definition (29) is

$$v^o = [K \vec{v} D]^{1/2} \qquad (6\text{-}6)$$

where K and $\vec{v}$ are kinetic parameters of the chemical reaction assumed to be of the same type as Reaction 1-2a, and D is the diffusion coefficient of the electro-reducible species. Knowledge of $K \vec{v}$ allows the determination of $\vec{v}$, the rate of the chemical reaction. For this purpose the diffusion coefficient D of the copper(II)-pyrophosphate complex was calculated from the Ilkovic equation, employing the value of the final diffusion current from the polarogram of 1 F potassium nitrate.

Assuming that the two values of v^o represent the same entity, their average gives a value for $K \vec{v}$ of 0.10 for the dissociation of the complex according to the reaction

$$Cu(MP_2O_7)_2^{4-} \underset{\overleftarrow{v}}{\overset{\vec{v}}{\rightleftharpoons}} Cu(MP_2O_7)^{1-} + MP_2O_7^{3-} \qquad (6\text{-}7)$$

The value for the quantity $K' \vec{v}$, where $K' = K[z]$, and $\overleftarrow{v}' = \overleftarrow{v}$, is reported by Foster (57) to be 0.061. In the equation $K' = K[Z]$, $[Z]$ denotes the concentration of the pyrophosphate species that dissociates from the complex prior to reduction. Knowledge of the concentration of this species is required to order to calculate the individual values

of K', $\vec{v}$, and $\overleftarrow{v}$. In the present work the total concentration of pyrophosphate was only 2.0 mF, and in the presence of 1.0 mF copper(II) the amount of pyrophosphate not complexed with copper is small, and cannot accurately be calculated from dissociation constants, even if they were known. The values of the rate constants reported by Foster are independent of the pyrophosphate concentration, whereas the value for $K\vec{v}$ given above is a function of that concentration, and thus a direct comparison is not in order.

Sources of Error

The most serious difficulty in the application of the Gierst analysis to the present system arises from the specific adsorption of the nitrate ion. Under such conditions the Gouy-Chapman theory is not strictly applicable for the calculation of ψ_o', the potential at the outer Helmholtz plane. Since the amount of nitrate adsorbed at a given concentration is a function of potential, current-potential curves are not merely shifted but are distorted within the potential region where adsorption occurs.

An attempt was made to correct the log v^* curves for the effect of the adsorption. This was done in terms of Grahame's data for sodium fluoride (31). A calculation of the potential shift at each electrode charge and salt concentration yields results for log v^* which do not converge with those from the potential regions where nitrate ion is known not to be adsorbed. The difficulty is that the theoretical value of the ECM is different at each potential because of the varying amounts of nitrate adsorbed, even at constant bulk nitrate concentration. To calculate an additional correction to eliminate this influence would

introduce so great an error in the log v^* versus φ curves that application of the Gierst analysis would become meaningless. The rate of reduction of anions is retarded by specific adsorption of anions of the supporting electrolyte (15). As these anions are desorbed, the rate of reduction shows a corresponding increase, and an inevitable distortion of even the "corrected" current-voltage curve exists.

As already stated, use of the Gouy-Chapman theory to calculate ψ_o in the presence of adsorption is not strictly correct. No attempts were made to obtain data related to the surface excess of nitrate ion at particular potentials and concentrations. If the degree of adsorption is not too great, the Gouy-Chapman theory may be applied without causing too great an error. In nearly all ionic solutions specific adsorption is absent only at reasonably cathodic potentials, where the electrode is at a relatively high negative charge density. Some cations (Cs^+, Tl^+) are adsorbed in this potential region, but no adsorption has ever been reported for such speces as Na^+ and K^+. The only anion which has been unambiguously shown to be unadsorbed on a positively charged electrode is the fluoride ion. Thus adsorption actually occurs in most cases, but by a proper selection of conditions its effects can be minimized. The use of sodium fluoride as a supporting electrolyte was not feasible in the present work because of the desire to make studies in acid solution. Since studies also had to be made at both positively and negatively charged electrodes, the effects of nitrate adsorption had to be endured.

As already indicated in Chapter IV, the method (drop time method of electrocapillary curves) used to obtain charge data for the calculation

of ψ_o was subject to a moderate error of somewhat uncertain magnitude. Since this error was not strictly constant, its estimation was very difficult.

The normal uncertainty associated with polarographic measurements applies to those made here.

The determination of α from the variation of v^* with C_s has been shown by Frumkin (24) to give only approximate values in the presence of a strong ψ effect. This is due to the fact that an assumption must be made about the location of the reacting particle in the diffuse double layer. If it is located at the boundary of the double layer, that is, the outer Helmholtz plane, then the value of ψ affecting the reduction is ψ_o. In the present case, with both a preceding chemical reaction and a strong ψ effect due to a highly charged reacting species, this assumption about the location may be erroneous.

Chronocoulometry

Electrochemical Parameters

By assuming that, at times immediately after current control by mass transfer is established and at potentials not too cathodic of the equilibrium potential, the reduction reaction is the rate determining step, it is possible to calculate the parameters k_a^o and α from chronocoulometry. Equations (2-28) and (2-29) and the accompanying discussion apply to this calculation. A plot of log λ versus η according to Equation (2-29) is given in Figure 35. Values obtained from this plot are the following: $\alpha = 0.25$, $k_a^o = 3.45 \times 10^{-3}$ cm sec^{-1}.

The value of α of 0.25 is comparable to that obtained from the potential step and polarographic methods. The difference is not

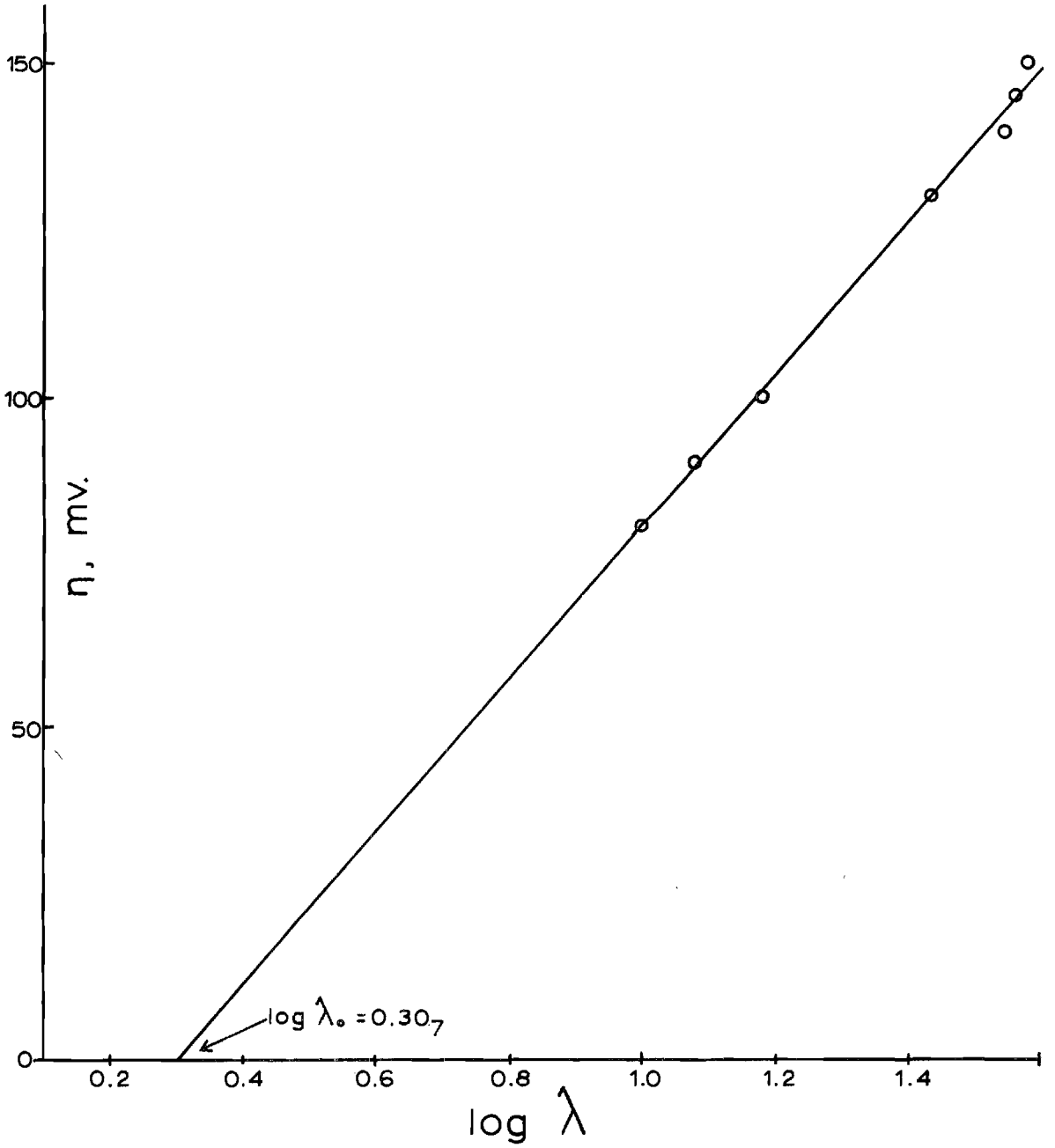

Figure 35. Chronocoulometric Determination of $\vec{v}K$.

unreasonably large in light of previous comments about the determination of α.

The value obtained for k_a^o is in excellent agreement with that of 3.47×10^{-3} cm sec^{-1} found from potential step experiments employing a comparable solution. The significance of this result is that the same overall reaction process is most probably occurring under the conditions of both the potential step and chronocoulometric experiments, and thus both sets of results have equal validity. It was thought that measurement of k_a^o at times at which mass transfer controls the current would give different results than measurements made at times at which the kinetics of a reaction control the current, especially in the case where a dissociation reaction precedes the reduction. The validity of the potential step results as a description of the reduction reaction has been established by the fact that all the data chosen to make calculations of kinetic parameters meet the criteria of Equations (2-11) and (2-12). The value for k_a^o derived from chronocoulometry contains no correction for double layer effects, and therefore does not approach the true value found with the potential step method.

Chemical Kinetic Parameters

The assumption that the electro-chemical reduction cannot be the rate determining step when the current flow at the electrode is limited by mass transfer, excludes the application of the chronocoulometric theory to the calculation of k_a^o. The following derivation was employed to obtain an expression for the product $K \vec{v}$. The derivation involves integrating the expression for the current which flows in a kinetically controlled reaction. The equation for this current has been given by

Delahay (20) as

$$I = B \exp y'''^2 \operatorname{erfc} y''' \tag{6-8}$$

where

$$B = nFA\, C_{Ox}\, D_{Ox}^{1/2}\, (\vec{v}\, K)^{1/2} \tag{6-9}$$

with

$$y''' = \lambda'''\, t^{1/2} \tag{6-10}$$

and

$$\lambda''' = (K\, \bar{v})^{1/2} \tag{6-11}$$

Integration of Equation (6-8), done in the same manner as with Equation (2-24), yields an expression for the intercept $t_i^{1/2}$ such that when the charge Q is plotted versus $t^{1/2}$ then

$$t_i^{1/2} = \frac{\pi^{1/2}}{2\lambda'''} \tag{6-12}$$

A single determination of λ_o, the value of λ at $\eta = 0$, yields the product $K\vec{v}$. Determination of λ_o at several concentrations allows the calculation of both $\vec{v}$ and K.

A plot of log λ versus η has already been given in Figure 35. Using the value of the $\eta = 0$ intercept, log $\lambda = 0.307$, gives a value for $K\vec{v}$ or 0.433. This value is approximately four times the value obtained by extrapolation from values nearly an order of magnitude larger, and its location is therefore somewhat uncertain. Since data were available at only one concentration of reactant (pyrophosphate) it was not

possible to individually determine $\vec{v}$ and K.

Even with the considerations already given, the result for $K\vec{v}$ should be closer to the value from polarography. The probable difficulty lies in the fact that diffusion control was not attained for the size of the potential steps used. In such a case, condition (2-26) is not achieved, and therefore a plot of Q versus $t^{1/2}$ is not in order. This same effect is probably the reason that the chronocoulometric results for k_a^o agree so well with those from the potential step method.

Table 15 brings together the kinetic parameters determined by all methods so that the various results may be readily compared.

Table 15. Comparison of Parameters Determined from the Various Methods. Units: $i^o \times 10^3$ amp.cm.$^{-2}$, $k_a^o \times 10^2$ cm.sec.$^{-1}$. Code: PSM, Potential Step Method; CC, Chronocoulometry; P, Polarography

Method	Salt	pH	i_a^o	i_t^o	k_a^o	k_t^o	α	true α	ν^o	$\vec{\nu}$ K	z
PSM	1.0	9.34	0.596		0.347		0.39	0.51			
		8.24	2.86		1.51		0.38	0.38			
		5.82	5.04		2.94		0.39	0.34			
		3.02	6.02		2.32		0.14	0.13			
		2.99	6.92		3.90		0.27	0.51			
	0.5	9.60	0.339		0.187		0.20	0.21			
		5.17	7.98		4.62		0.37	0.37			
		3.02	7.31		4.30		0.36	0.35			
	0.1	9.78	4.28		2.37		0.22	0.22			
		5.84	18.5		--		0.79	0.79			
		2.98	7.39		4.41		0.48	0.46			
	0.05	8.96	1.93		1.19		0.58	0.53			
		5.77	2.01		1.21		0.50	0.48			
		3.00	1.57		0.940		0.48	0.49			
	1.0	9+		1.7×10^{-3}		from manu-script					-2
	0.5			0.548×10^{-3}							
	0.1			1.91×10^{-3}							
	0.05			0.025×10^{-3}							
	1.0	3.0		7.60							+1
	0.5			18.1							
	0.1			9.01							
	0.05			1.80							
P	1.0	9+		Positive side			0.21	7.97×10^{-4}	0.10		-1.30
				Negative side			0.05	8.74×10^{-4}			-0.32
CC	1.0	9+			0.347		0.25			0.43	

APPENDIX I

Glossary of Symbols

A	Electrode area, cm^2 .
B	Parameter defined by $B = 2.303 \log \frac{i_o}{1 - e^{nf\eta}}$.
C	Concentration of Reactant, Moles cm^{-3}.
C_s	Salt concentration, Moles/Liter.
D	Diffusion coefficient of a species, cm^2 $sec.^{-1}$.
d	Density of mercury, gram cm^{-3}.
E	Electrode potential versus any reference, volts.
E_e	Formal equilibrium electrode potential versus any reference, determined by the particular concentrations of the two species of the electrochemical couple.
E_r	Electrode potential in a cell within liquid junction.
E_z	Potential of Zero Electrode charge.
erfc	Defined as 1 - erf, where $erf = \frac{2}{\pi} \int_o^y \exp(-z^2)dz$.
exp	Exponentiation operator.
F	Faraday constant.
f	Parameter defined by $f = \frac{F}{RT}$.
I	Current, amperes.
I_d	Diffusion limited current, amperes
i	Current density, amp. cm^{-2}.
i_o	Valid zero-time intercept of an i vs. F(t) plot.
i_x, i_y	Invalid zero-time intercept of an i vs. t(t) plot.
i_a^o	Apparent exchange current density, amp. cm^{-2}.

i_t^o	True exchange current density, corrected for double layer effects.
K	Equilibrium constant for a chemical reaction.
K	Integral Capacitance, farads.
k	Heterogeneous rate constant of an electrochemical reaction, cm $sec.^{-1}$
k_a^o	Apparent standard heterogeneous rate constant at $\dot{E}_e$.
k_t^o	True standard heterogeneous rate constant.
L	Differential double layer capacity, farads.
m	Flow rate of mercury, gram $sec.^{-1}$.
n	Number of electrons in an electrode reaction.
Ox	Electro-reducible species.
p_i or p_i'	Reaction order of the i^{th} species.
Q	Electrode charge, coulombs.
q	Electrode charge density, μ coulombs cm^{-2}.
q^1	Amount of adsorbed charge, μ coulombs cm^{-2}.
R	Gas Constant.
Red	A reduced species which may or may not be able to undergo oxidation.
T	Absolute temperature, °K.
t	Time, seconds.
v^*	Apparent overall rate constant, cm $sec.^{-1}$.
v^o	Value of v^* at $\varphi = 0$.
$\vec{v}, \overleftarrow{v}$	Chemical rate constants, either first or second order.
w	Potential sweep rate, volts sec^{-1}.
y	Argument of the function $\exp y^2$ erfc y, defined as $y = \lambda t^{1/2}$.
z	Ionic charge on a species.

α	Transfer coefficient of the reduction reaction.
Γ	Surface excess, moles cm^{-2}.
ν	Surface tension, dynes cm^{-1}.
ε	Dielectric constant.
η	Overvoltage in volts, defined as $\eta = E - E_e$.
θ	Function of time, defined by $\theta = [\tau^{1/2} + (t-\tau)^{1/2} - t^{1/2}]$, seconds $^{+1/2}$.
λ	Parameter containing kinetic terms, used in $y = \lambda t^{1/2}$, seconds $^{-1/2}$.
μ	Chemical potential of the i^{th} species.
τ	Time, relative to t, of reversal. The step reversal time of chronocoulometry; seconds.
φ	Electrode potential relative to the point of zero charge.
φ'	Potential drop between electrode and outer Helmholtz plane.
ψ	Potential at any point in the diffuse double layer.
ψ_o	Potential at the outer Helmholtz plane.

APPENDIX II

```
BEGIN COMMENT THEORETICAL PSI POTENTIAL CALCULATIONS;
INTEGER I,J,K,L,N;
REAL  C, CT, X;
ARRAY  Q[0:900], PHITWO[0:900];
FORMAT  FORM1 ("PHITWO VERSUS ELECTRODE CHARGE AS A FUNCTION
              OF CONCENTRATION CONSIDERING THE CONTRIBUTION OF
              REACTANTS",
        FORM2 (//, X15, "C", X15, "Q", X13, "PHI TWO" //),
        FORM3 (X9, E16.10, X8, R8.4, X8, R10.6),
        FORMX (///"PROCESSOR TIME = ", I3, X3, "I/O TIME = ",I3);
LIST    LIST3 (C, Q[N], PHI TWO [N]),
        LISTX (TIME(2)/60, TIME(3)/60);
        WRITE (PAPER, FORM1);
        FOR K ← 100,10,1 DO
BEGIN
        FOR I ← 10,5,2,1 DO
BEGIN
        C ← ((1.00 @ -03) ⊗ I ⊗ K)+0.01;
        CT ← C* 0.5;
        FOR L ← 1, -1  DO
BEGIN
        FOR N ← 1 STEP 1 UNTIL 150 DO
```

```
BEGIN
        Q[N] ← 0.1 ⊗N ⊗L;
        X ← Q[N]/(11.74 ⊗CT);
        PHITWO[N] ← (2/38.935) ⊗(LN(X+((X)*+1)*0.5));
END;
        WRITE (PAPER[PAGE]);
        WRITE (PAPER,FORM2);
        J ← N
        FOR N ← 1 STEP 1 UNTIL 5 DO
        WRITE (PAPER, FORM3, LIST3);
END; END; END;
        WRITE (PAPER, FORMX,LISTX);
END.
```

```
BEGIN COMMENT POTENTIAL STEP METHOD DATA TREATMENT;
INTEGER  G,H,J,K,L,N;
REAL M,B,IT,TT,V,A,ETAT,NF,AT,KZERO,R,C,IZERO,ALP,COX,CRED;
ARRAY T,I,THALF,CI[0:1020],BOA,EFF[0:1020],ETA[0:20],EFFCAL[0:100];
ALPHA ARRAY NM[0:13];
ALPHA TEST;
FORMAT  FORM1 (2R30.10,X14,A6),
        FORM2 (//"B=",E20.10,X5,"VARIANCE =",E20.10),
        FORM3 (4E25.10/),
        FORM4 (//X11,"T[K]",X21,"T1/2[K]",X17,"I[K]",X21,
              "I[K] CALCULATED"/),
        FORM5 (13A6),
        FORM7 (//"BOA=",E20.10,X5,"EFF=",E20.10),
        FORM8 (//"ALP=",R6.4,X13,"I ZERO=",E20.10),
        FORM9 (//X10,"ETA[L]",X15,EFF[L]",X15,"EFF[L]CALCULATED"/),
        FORM10 (E20.10,2R20.10),
        FORM11 (//X10,"KZERO=",E20.10//);
LIST    LIST1 (IT,TT,TEST),
        LIST2 (B,V),
        LIST3 (T[K],THALF[K],I[K],CI[K]),
        LIST5 (FOR J←0 STEP 1 UNTIL 12 DO NM[J]),
        LIST6 (A,ETAT,TEST),
        LIST7 (BOA[L],EFF[L]),
        LIST8 (ALP,IZERO),
        LIST10 (ETA[L],EFF[L],EFFCAL[L]),
        LIST11 (KZERO),
```

```
        LISTX (TIME(2)/60,TIME(3)/60);
LABEL L1,L2,EXIT;
PROCEDURE LSTSQ(X,Y,N,M,B,CY,V);
        VALUE N;
        ARRAY, X,Y,CY[0];
        INTEGER N;
        REAL M,B,V;
BEGIN
        REAL SUMX,SUMY,SUMXX,SUMYY,DEL;
        INTEGER I;
        SUMX←SUMY←SUMXX←SUMXY←0;
        FOR I←1 STEP 1 UNTIL N DO
BEGIN
        SUM[X]←SUM[X]+X[I];
        SUM[Y]←SUM[Y]+Y[I];
        SUM[XX]←SUM[XX]+X[I]*2;
        SUM[XY]←SUM[XY]+X[I] ⊗ Y[I];
END;
        DEL ← SUMX*2 - N ⊗ SUMXX
        M ← (SUMY ⊗ SUMX - N SUMXY)/DEL;
        B ← (SUMX ⊗ SUMXY - SUMY ⊗ SUMXX)/DEL;
        SUMX ← 0;
        FOR I ← 1 STEP 1 UNTIL N DO
BEGIN
        CY[I] ← X[I] ⊗ M + B;
        SUMX ← SUMX + CY[I]*2;
END;
```

```
        V ← SUMX/(N-2);
END     LSTSQ;
PROCEDURE SLOPE (X,Y,H,R,C,CY);
        VALUE H;
        ARRAY X,Y,CY[0];
        INTEGER H;
        REAL R,C;
BEGIN
        REAL SUMX,SUMY,SUMXX,SUMXY,DEL;
        INTEGER I;
        SUMX ← SUMY ← SUMXX ← SUMXY ← 0;
        FOR I ← 1 STEP 1 UNTIL H DO
BEGIN
        SUMX ← SUMX + X[I];
        SUMY ← SUMY + Y[I];
        SUMXX ← SUMXX + X[I]*2;
        SUMXY ← SUMXY + X[I] ⊗ Y[I];
END
        DEL ← SUMX*2 - H ⊗ SUMXX;
        R ← (SUMY ⊗ SUMX - H ⊗ SUMXY)/DEL;
        C ← (SUMX ⊗ SUMXY - SUMY ⊗ SUMXX)/DEL;
        SUMX ← 0;
        FOR I ← I STEP 1 UNTIL H DO
BEGIN
        CY[I] ← X[I] ⊗ R + C;
END;
```

```
END SLOPE;
        G ← 0;
BEGIN
        L ← 1;
BEGIN
        READ (CARDS,FORM5,LIST5)[EXIT];
        WRITE (PAPER[PAGE]);
        WRITE (PAPER,FORM5,LIST5);
        READ (CARDS,FORM1,LIST6);
        IF TEST ="SET" THEN GO TO L2;
        K ← 1;
BEGIN
        READ (CARDS,FORM1,LIST1)  [L1];
        IF TEST ="END" THEN GO TO  L1 ;
        T[K] ← TT ⊗ 0.001;
        I[K] ← IT ⊗ 1 @ =-6;
        THALF[K] ← SQRT(T[K]);
        K ← K+1;
END;
L1:     N ← K-1;
        LSTSQ (THALF,I,N,M,B,CI,V);
        WRITE (PAPER,FORM2,LIST2);
        BOA[L] ← B/(A ⊗ 1@ -2);
        ETA[L] ← ETAT ⊗ 1@ -3;
        NF ← 77.87
        EFF[L] ← LN(BOA[L])/1-EXP(NF ⊗ ETA[L])));
```

```
        WRITE (PAPER,FORM7,LIST7);
        L ← L+1;
        WRITE PAPER,FORM4);
        FOR K ← 1 STEP 1 UNTIL N DO
        WRITE (PAPER,FORM3,LIST3);
END;
L2:     H ← L-1;
        SLOPE(ETA,EFF,H,R,C,EFFCAL);
        IZERO ← EXP(C);
        ALP← - R/NF;
        WRITE (PAPER,FORM8,LIST8);
        COX ← 0.000001;              [experimental]
        CRED ← 0.000000739;          [experimental]
        KZERO ← IZERO/(1.93@ +5 ⊗ COX*(1-ALP) ⊗ CRED*ALP);
        WRITE (PAPER,FORM 11,LIST 11);
        WRITE (PAPER,FORM9);
        FOR L ← 1 STEP 1 UNTIL H DO
        WRITE (PAPER,FORM10,LIST 10);
        G ← G+1;
END;
EXIT:  WRITE (PAPER,FORMX,LISTX);
        END.
```

LITERATURE CITED*

(1) F. C. Anson, Anal. Chem., 38, 54 (1966).

(2) B. Breyer and H. H. Bauer, "Alternating Current Polarography and Tensammetry," Interscience, New York, 1963.

(3) D. L. Chapman, Phil. Mag., 25, 475 (1913).

(4) J. H. Christie, G. Lauer, and R. A. Osteryoung, J. Electroanal. Chem., 7, 60-72 (1964).

(5) B. E. Conway, "Electrochemical Data," Elsevier, Amsterdam, 1952, p. 221.

(6) P. Carbusier and L. Gierst, Anal. Chim Acta, 15, 254 (1956).

(7) P. Delahay, "New Instrumental Methods in Electrochemistry," Interscience, New York, 1954, Chapter 6.

(8) P. Delahay, ibid., Chapter 5.

(9) P. Delahay, "Advances in Electrochemistry and Electrochemical Engineering," Vol. I, edited by P. Delahay, Interscience, New York, 1961, p. 247.

(10) P. Delahay, "Double Layer and Electrode Kinetics," Interscience, New York, 1965, p. 53.

(11) P. Delahay, ibid., p. 23.

(12) P. Delahay, ibid., p. 35.

(13) P. Delahay, ibid., p. 41.

(14) P. Delahay, ibid., p. 201.

(15) P. Delahay, ibid., p. 206.

(16) P. Delahay, reference 7, Chapter 4.

(17) P. Delahay, J. Phys. Chem., 70, 2373 (1966).

---

*Title abbreviations used here are all according to the standard ACS listing given in the decennial index of Chemical Abstracts.

(18) P. Delahay and I. Trachtenberg, J. Am. Chem. Soc., 79, 2355 (1957).

(19) E. G. Enke, L. Ramaley, and R. L. Brubaker, Anal. Chem., 35, 1088 (1963).

(20) C. G. Enke and R. A. Baxter, J. Chem. Ed., 41, 202 (1964).

(21) O. A. Esin and B. F. Markov, Acta Physiochem., U.R.S.S., 10, 353 (1939).

(22) J. N. Foster, Thesis, California Institute of Technology (1965).

(23) A. Furlani and A. M. Guiliani, Lincei-Rend. Sc. Fis. Mat. e Nat., Vol. XXXVII, 297 (1964).

(24) A. N. Frumkin, O. A. Petry, and N. V. Nicolaeva-Fedorovich, Electrochim. Acta, 8, 177 (1963).

(25) Z. Galus, H. Y. Lee, and R. N. Adams, Triangular Wave Cyclic Voltammetry, Unpublished Review.

(26) H. Gerischer, Z. Electrokhem., 64, 29 (1960).

(27) H. Gerischer and N. Vielstich, Z. Physik. Chem. (Frankfurt), 3, 16 (1955).

(28) L. Gierst, "Transactions of the Symposium on Electrode Processes," E. Yeager, Editor, John Wiley and Sons, New York, 1961, pp. 109-138.

(29) L. Gierst and H. Hurwitz, Z. fur Electrochem., 64, 36 (1960).

(30) G. Gouy, Compt. Rend., 149, 654 (1910).

(31) D. C. Grahame, Chem. Rev., 41, 441 (1947).

(32) D. C. Grahame, J. Am. Chem. Soc., 79 2978 (1949).

(33) T. Kambara, Bull. Chem. Soc., Japan, 27, 527 (1954).

(34) I. M. Kolthoff and J. I. Watters, J. Am. Chem. Soc., 70, 2455 (1948).

(35) J. Koutecky, Chem. Liste, 47, 323 (1953).

(36) H. A. Laitinen and E. J. Onstott, J. Am. Chem. Soc., 72, 4729 (1950).

(37) S. M. Lambert and J. I. Watters, ibid., 79, 4262 (1957).

(38) J. J. Lingane, ibid., 68, 2 448 (1946).

(39) L. Meites, "Handbook of Analytical Chemistry," McGraw-Hill, New York, 1963, Chapter 5.

(40) L. Meites, "Polarographic Techniques," Interscience, New York, 1955, p. 21.

(41) R. N. Murray and D. J. Gross, Anal. Chem., 38, 392 (1966).

(42) K. B. Oldham and R. A. Osteryoung, J. Electroanal. Chem., 11, 397 (1966).

(43) R. Parsons and F. Zobel, ibid., 9, 333 (1965).

(44) R. Payne, J. Phys. Chem., 69, 4113 (1965).

(45) J. E. B. Randles and K. W. Somerton, Trans. Faraday Soc., 48, 951 (1952).

(46) C. N. Reilley in "Progress in Polarography," P. Zuman, ed., Interscience, New York, 1962, p. 81.

(47) C. N. Reilley in "Treatise on Analytical Chemistry," Part I, Vol. 4, Chapter 42, edited by I. M. Kolthoff and P. J. Elving, John Wiley and Sons, New York, 1963, p. 2123.

(48) C. N. Reilley and R. N. Schmid, J. Am. Chem. Soc., 80, 2087 (1958).

(49) N. H. Reinmuth, L. B. Rogers, and L. E. J. Hummelstedt, ibid., 81, 2947 (1959).

(50) L. B. Rogers and C. A. Reynolds, ibid., 71, 2081 (1949).

(51) H. Rose, Liebig's Ann. Chem., 76, 2 (1850).

(52) C. D. Russell, J. Electroanal. Chem., 6, 486 (1963).

(53) O. E. Schupp, P. E. Sturrock, and J. I. Watters, Inorg. Chem., 2, 106 (1963).

(54) N. M. Schwartz and I. Shain, J. Phys. Chem., 69, 30 (1965).

(55) A. Sevcik, Czechoslov. Chem. Communs., 13, 349 (1954).

(56) O. Stern, Z. Electrochem., 30, 508 (1924).

(57) P. E. Sturrock, Dissertation, Ohio State University, 1960.

(58) N. L. Underkofler and I. Shain, Anal. Chem., 35, 1778 (1963)

(59) J. I. Watters and R. Simonaitis, Talanta, 11, 247 (1964).

(60) A. Wilson, private communication.

VITA

Gibson Watley Higgins was born May 28, 1940 in Birmingham, Alabama to John Todd Higgins and Sara Gibbons Higgins. He attended Ensley High School, graduating in June, 1958. He then entered Birmingham Southern College, Birmingham, Alabama, and was graduated with a B.S. in Chemistry in June, 1962.

In September, 1962, he entered the Graduate School of the Georgia Institute of Technology, Atlanta, Georgia, and was appointed a Graduate Teaching Assistant, School of Chemistry. In December, 1963, he was appointed Graduate Research Assistant.